PHASE TRANSFORMATION IN $AlPO_4$:Fe^3 AND QUARTZ

BY ELECTRON PARAMAGNETIC RESONANCE

A STUDY OF THE α-β PHASE TRANSFORMATION

IN $AlPO_4:Fe^{3+}$ AND QUARTZ BY ELECTRON

PARAMAGNETIC RESONANCE

by

ROBERT LANG, B.Sc., M.Sc.

A Thesis

Submitted to the Faculty of Graduate Studies

in Partial Fulfilment of the Requirements

for the Degree

Doctor of Philosophy

McMaster University

October 1971

DOCTOR OF PHILOSOPHY (1971)　　　　　　　McMASTER UNIVERSITY
(Physics)　　　　　　　　　　　　　　　　　Hamilton,　Ontario.

TITLE:　　　　　A Study of the α-β Phase Transformation in
　　　　　　　　$AlPO_4$:Fe^{3+} and Quartz by Electron Paramagnetic
　　　　　　　　Resonance

AUTHOR:　　　　Robert Lang, B.Sc. (McMaster University)
　　　　　　　　　　　　　　　M.Sc. (McMaster University)

SUPERVISORS:　Dr. C. Calvo and Dr. W. R. Datars

NUMBER OF PAGES:　ix ,138

SCOPE AND CONTENTS:

The α-β phase transformation was studied in hydro-
thermally grown crystals of $AlPO_4$ by measuring the spin-
Hamiltonian parameters of Fe^{3+} as a function of temperature.

The theory of the Blume-Orbach mechanism for the
zero-field splitting of S-state ions was generalized and
used to calculate the D-tensor of the spin-Hamiltonian. The
experimentally observed temperature variation of the spin-
Hamiltonian was interpreted in terms of a temperature-dependent
point-multipole model of the charge distribution in the crystal
lattice.

A similar study of the α-β phase transformation in
quartz was attempted but E.P.R. measurements could only be
taken up to 450°C (123°C below the transformation temperature)
because of the instability of the Fe^{3+} center at higher
temperatures.

ACKNOWLEDGEMENTS

TABLE OF CONTENTS

LIST OF FIGURES

LIST OF TABLES

CHAPTER I

INTRODUCTION

The α-β phase transformation in quartz is one of
the more extensively studied structural phase transfor-
mations in solids. It has been approached both in terms
of lattice dynamics (Kleinman and Spitzer, 1962; Shapiro,
O'Shea, and Cummins, 1967; Scott, 1968; Axe and Shirane,
1970) and x-ray crystallography (Young, 1962; Arnold, 1965;
Ishida and Honjo, 1969; Brumberger et al, 1969). However,
the detailed nature of the transformation mechanism still
remains unresolved. There is considerable experimental
evidence which suggests that the transformation results from
the instability of a normal lattice vibrational mode, simi-
lar to the mechanism which has been proposed for several
ferroelectric phase transformations (Cochran, 1960). These
results indicate that the atoms are displaced continuously
up to the transformation temperature T_o. At T_o a dis-
continuous change occurs so that the transformation is ulti-
mately of first order but T_o is close to the critical
temperature.

A second model, discussed by Wannier (1959), employs
the concept of an order-disorder mechanism. Each atom may
occupy either one of two positions which are symmetrically

1

located on either side of the high symmetry β-phase site.
These sites correspond to the two Dauphiné twin configura-
tions of α-quartz. The high symmetry β-phase corresponds
to a random, equal molar mixture of the two Dauphiné twin
configurations.   In the α-phase the composition of the
mixture is unequal and temperature-dependent. This model
presupposes that the two Dauphiné twin configurations remain
distinct in the β-phase whereas in the previous "soft mode"
model the distinction between the two twin configurations
is lost, as the atoms have moved to positions midway between
two twin-related sites. Except for the x-ray results of
Arnold (1965) and the light scattering results of Shapiro
and Cummins (1968) all currently available results are con-
sistent with the "soft mode" model.

The technique of electron paramagnetic resonance
has been shown to be a valuable tool in the study of phase
transformations in crystalline solids. It was first used by
Chambers, Datars, and Calvo (1964) to determine the point
group symmetries of cation sites of the various phases of
$Zn_2P_2O_7$:Mn and $Zn_2P_2O_7$:Cu. More recently E.P.R. has been
used to measure the rotation of octahedral groups about tetra-
gonal or trigonal axes in certain perovskites (Mueller et al,
1968).

In the present case an E.P.R. study of the α-β phase

transformation in quartz was approached with some reluctance because suitable paramagnetic impurities require charge compensation when introduced into the host lattice. It was expected that the distribution of these imperfections would show temperature dependences which were likely to obscure the changes associated with the phase transformation.

One of the polymorphs of $AlPO_4$ (Berlinite) is known to show both the α- and β-quartz structures, with the cations occupying alternate Si-sites. In this system the α-β phase transformation occurs at 581°C as compared to 573°C in quartz (Corbridge et al, 1966). This compound therefore provides an alternative system in which the α-β phase transformation can be studied. Moreover, in the case of iron-doped crystals of $AlPO_4$ the Fe^{3+} ions were expected to enter the Al-site substitutionally in which case there is no need for charge compensation. Thus, E.P.R. measurements were taken in $AlPO_4$ as well as in quartz. Due to the instability of the Fe^{3+} center in quartz, temperature-dependent studies in quartz could only be made up to approximately 450°C. Measurements in $AlPO_4$ were taken up to temperatures exceeding the phase transformation temperature.

When the S-state ion Fe^{3+} is introduced into the crystal lattice the sixfold degeneracy of the free-ion ground state $^6S_{5/2}$ is partially removed. This splitting of the energy levels

in the absence of an applied magnetic field, which is commonly
referred to as zero-field splitting, is typically of the order
of a fraction of a wave number. It is therefore easily mea-
sured by E.P.R. It is clear that the zero-field splitting
is due to the interaction of the paramagnetic ion with the
crystalline environment. However, the relationship between
the zero-field splitting and the crystalline electric field
at the site of the paramagnetic ion is extremely complex and
only poorly understood. Nevertheless it was the primary ob-
jective of this study to interpret the temperature-dependent
size and symmetry of the zero-field splitting of Fe^{3+} in $AlPO_4$
in terms of the structural changes associated with the $\alpha-\beta$
phase transformation. It is believed that the zero-field
splitting of an S-state ion which is surrounded by a predomi-
nantly cubic crystalline environment is primarily due to the
Blume-Orbach mechanism. This has been concluded by Sharma,
Das and Orbach (1966) who also presented the theory of the
Blume-Orbach mechanism and derived expressions for the orthor-
hombic spin-Hamiltonian parameters D and E. These expressions
are valid if the crystalline axes of the cubic and orthorhombic
field coincide. This requires that the point symmetry of
the lattice site in question must be at least D_2. The point
symmetry at the Al-site in $\alpha-AlPO_4$, however, is only C_2. It
was therefore necessary to generalize the above theory of the
Blume-Orbach mechanism and derive expressions for each com-

ponent of the D-tensor, which replaces the parameters D and E if the point symmetry is lower than D_2. This theory was used to provide the link between the zero-field splitting and the crystalline electric field.

The crystalline electric field was calculated on the basis of a temperature-dependent point-multipole model which represented the charge distribution in the crystal lattice. This model included the monopoles of all the atoms as well as the induced electric dipoles and the thermally generated quadrupoles of the oxygen atoms. The temperature dependence was introduced into the point-multipole model by changing the positions of the atoms as well as the size and orientation of the thermal quadrupoles and the size of the unit cell in accordance with the results of extensive temperature-dependent x-ray measurements in quartz by Young (1962).

Point-multipole calculations of the zero-field splitting are often regarded with a great deal of skepticism. This applies particularly to the part of the zero-field splitting calculations which deal with the computation of the crystalline electric field. In the case of $AlPO_4$, however, it was possible to treat effects due to higher order multipoles in a quantitative way by making use of previous results as well as a computing method due to Schwarzenbach (1966). As far as the mechanism of the zero-field splitting is concerned, the skepticism is often justified. Because of the large number of mechanisms which contribute to the zero-field splitting of

S-state ions, one can never be certain whether all the relevant mechanisms have been taken into account. Quite often two important mechanisms give rise to contributions of nearly equal size but of opposite sign. In this case their combined effect becomes quite small and the contribution of a less significant mechanism may become predominant. The present study provides an opportunity to compare the magnitude and the temperature dependence of the calculated zero-field splitting with experiment. It is very desirable to have this additional check because order of magnitude agreement between measured and calculated values of the zero-field splitting can be fortuitous. The purpose of the zero-field splitting calculations was therefore twofold: If the calculated zero-field splitting responds to the temperature-dependent changes of the point-multipole model in such a way as to reproduce satisfactorily the experimental temperature dependence, one may conclude that the zero-field splitting mechanism under consideration is indeed a predominant one and that point-multipole calculations of this type do have some merit. Secondly, if the point-multipole model is valid, one may conclude that the temperature-dependent changes of the model represent at least an approximation of the phase transformation mechanism in the real crystal.

CHAPTER II

THE α-β PHASE TRANSFORMATION

1. Crystal Structures of Quartz and $AlPO_4$

The molecular unit which comprises all forms of silica is SiO_2. The best known crystalline forms of silica are quartz, tridymite, and crystobalite. Each of these share a common structural unit consisting of a tetrahedron that is made up of a silicon atom which is tetrahedrally surrounded by oxygen atoms. In the case of quartz, successive tetrahedra are linked together to form helical chains which run parallel to the crystalline c-axis. The tetrahedra which make up these chains are related by the operation of a three-fold screw axis parallel to $\vec{c}$ such that the structure repeats after every six molecular units of SiO_2.

For each of the above crystalline silica phases there exists an analogous $AlPO_4$ structure (Corbridge et al,1966). In the polymorph of $AlPO_4$ which corresponds to quartz, alternate silicon atoms in the helical chains parallel to $\vec{c}$ are replaced by an aluminium and a phosphorous atom respectively. This results in a doubling of the unit cell size along the c-axis.

The quartz structure exists in two modifications; α- or low quartz which is stable up to 573°C and β - or high

7

quartz which is stable from 573° to 867°C. For the analogous $AlPO_4$ structures the temperatures are 581° and 705°C respectively. Alpha quartz has the space groups $P3_221$ or $P3_121$ depending on whether the helix is left-handed or right-handed. The two fold axis is perpendicular to $\vec{c}$ and passes through a silicon atom.

The structure of quartz is specified in terms of four parameters which define the positions of a silicon and an oxygen atom. Since the silicon atom lies on a twofold axis, only one parameter u, denoting its distance from the threefold screw axis, is needed to specify its position. The other three parameters, x, y, and z specify the fractional coordinates of an oxygen atom. The coordinates are referred to an axis triplet $\vec{a}_1$, $\vec{a}_2$, and $\vec{c}$, where $\vec{a}_1$ and $\vec{a}_2$ are parallel to a twofold axis each and $\vec{c}$ is parallel to the triad screw axis. The positions of all other atoms in the unit cell are obtained by symmetry operations. The atomic positions and the values of the positional parameters are according to Smith and Alexander (1963):

Si-sites at: $\bar{u}$, $\bar{u}$, $\frac{1}{3}$;   u, 0, 0;   0, u, $\frac{2}{3}$;

O-sites at: x, y, z;   y-x, $\bar{x}$, z + $\frac{1}{3}$ $\bar{y}$, x-y, z + $\frac{1}{3}$;

       x-y, $\bar{y}$, $\bar{z}$; y, x, $\frac{2}{3}$ - z $\bar{x}$, y-x, $\frac{1}{3}$ - z;

where u = 0.4698, x = 0.4145, y = 0.2662, z = 0.1189;

The lattice parameters at 25°C are:

$$a = 4.9039 \text{ Å}$$

$$c = 5.3943 \text{ Å} \; .$$

The structure of the α-quartz modification of $AlPO_4$ requires twice as many positional parameters as quartz because there are two types of cations and two crystallographically inequivalent oxygen atoms. According to Schwarzenbach (1966) the atomic positions and the values of the positional parameters for $AlPO_4$ are:

Al-sites at: $u, 0, \frac{1}{3}$; $0, u, \frac{2}{3}$; $\bar{u}, \bar{u}, 0$;

where $u = 0.4664$

P-sites at: $u, 0, \frac{5}{6}$; $0, u, \frac{1}{6}$; $\bar{u}, \bar{u}, \frac{1}{2}$;

where $u = 0.4669$

O-sites at: x, y, z ; $\bar{y}, x-y, \frac{1}{3}+z$; $y-x, \bar{x}, \frac{2}{3}+z$;

$y, x, \bar{z}$; $\bar{x}, y-x, \frac{1}{3}-z$; $x-y, \bar{y}, \frac{2}{3}-z$;

where $x = 0.4165$, $y = 0.2918$, and $z = 0.3982$

for oxygens of type I

and $x = 0.4169$, $y = 0.2569$, and $z = 0.8833$

for oxygens of type II.

The lattice parameters at 25°C are:

$$a = 4.9429 \text{ Å}$$

$$c = 10.9476 \text{ Å}$$

A better understanding of the structure of β-quartz can be gained by first considering the twinning properties of α-quartz.

As mentioned above, quartz occurs in two so-called enantiomorphic forms with space groups $P3_121$ and $P3_221$. The names right-handed and left-handed quartz describe the direction of rotation of the plane of polarization when light travels along the c-axis. Given the optical activity of quartz, this property enables one to determine readily the type of structure at hand by examining the crystal between crossed polaroids. The simultaneous presence of these two structures in one crystal is referred to as optical or Brazilian twinning.

Another type of twinning, which is more relevant to the present discussion, is the Dauphiné or electrical twinning. It describes the simultaneous presence of two structures which are related by 180° rotation about the c-axis. Since quartz is piezo-electric the sign of the piezo-electric effect, when measured along any direction perpendicular to $\vec{c}$, will be opposite for the two structures. To identify the particular type of twin it is necessary to study the surfaces of properly edged crystals (Cady, 1946). However, this technique only reveals domains that extend to the surface whereas electrical measurements are sensitive to the bulk properties of the crystal and will show a decrease of the piezo-electric effect if Dauphiné twinning is present in the crystal.

The two Dauphiné configurations are denoted by α_1 and α_2. Their projections onto the basal plane are shown in Fig. (II-1).

Figure II-1

Projection of quartz structures onto plane
perpendicular to $\vec{c}$. The numbers indicate the
fractional z-coordinates.

	α_1	α_2	β
Si	▽	☐	○
O	▼	▬	●

α_1

α_2

β
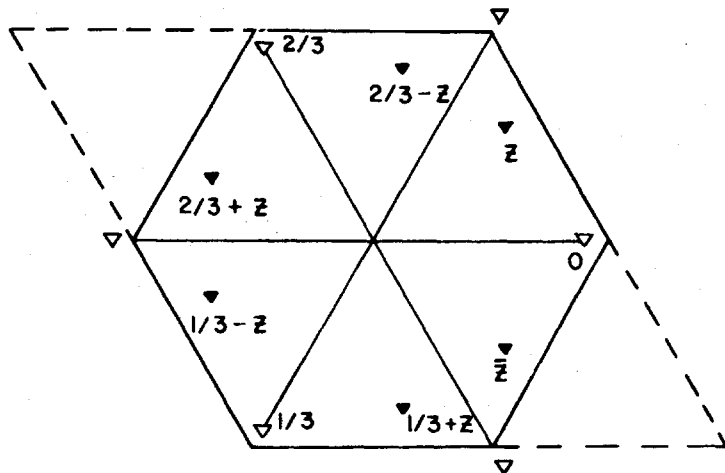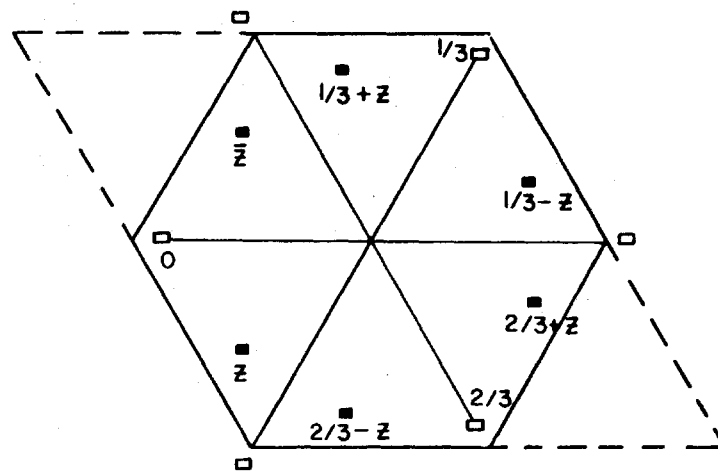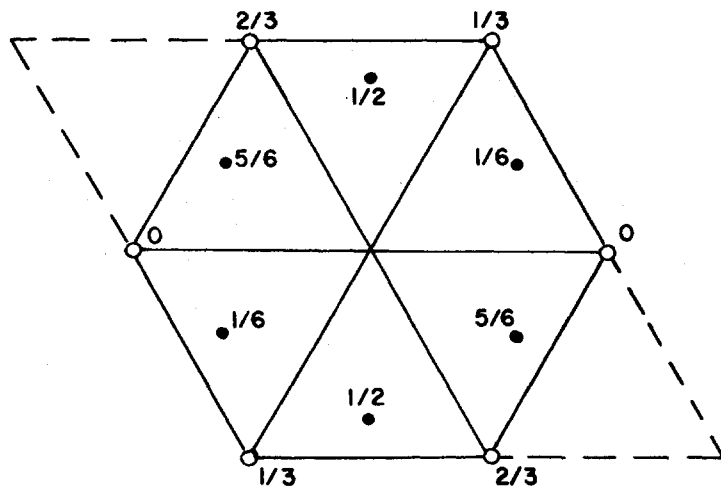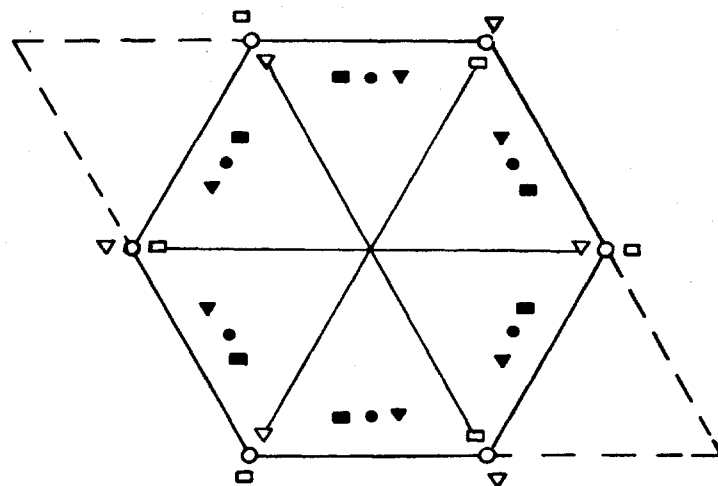
$\alpha_1 + \alpha_2 + \beta$

It is seen that the atomic displacements by which the two configurations differ are relatively small and in the case of the O-atoms are nearly perpendicular to the Si-O-Si plane. The fact that the bond lengths remain nearly unchanged may account for the relative ease with which such displacements occur. In particular, small, externally applied mechanical shock can result in considerable Dauphiné twinning the extent of which can also be influenced by the rate of cooling from the high temperature β-phase (Frondel, 1945). The "average atomic positions" in the β-phase lie midway between and along the line joining two corresponding atoms in the α_1 and α_2 configurations (Young, 1962). The term "average atomic position" is used in order to allow for the possibility of an order-disorder model for the β-phase structure. This model is based on the hypothesis of a statistical distribution of the atoms among Dauphiné twin-related sites. The space groups of the two enantiomorphic forms of β-quartz are $P6_222$ and $P6_422$. The helicity or handedness of the α-quartz structure is preserved across the transition. The existence of the sixfold screw axis implies that the Si-atoms have moved to the vertices of the hexagonal unit cell, as shown in Fig. (II-1), whereas the oxygens have moved to positions equidistant from the silicon atoms. The new twofold axis is normal to the $(1\bar{1}00)$ plane. In α-quartz the Si-atoms occupy sites of C_2 symmetry and all the oxygen atoms are symmetry related although

they occupy sites of only trivial symmetry. In the β-phase, the Si-atoms occupy sites having point group symmetry 222 and the O-atoms occupy sites of C_2 symmetry. In both the α- and β-phases there are interstitial sites with the same point group symmetry as have the Si-sites.

The twinning properties of $AlPO_4$ are topologically equivalent to the Brazilian and Dauphiné type twinning found in quartz. The β-phase of $AlPO_4$ has the same space group as quartz. Each of the Al- and P-atoms occupy sites of point group symmetry 222, at least on the average. The oxygen atoms however do not lie at sites of C_2 symmetry as in quartz but lie at a site of only trivial symmetry. Both in the α- and β-phase of $AlPO_4$ there are interstitial sites with the same point group symmetry as have the Al- and P-sites.

The fact that the atoms in the α-phase may occupy sites which are displaced in one of two directions from the high symmetry β-phase sites implies that all atoms move in double minimum potentials centered about the β-phase sites. Since the crystal as a whole is equally likely to be in either one of the two Dauphiné twin configurations this double potential minimum, insofar as it describes the configurational potential energy of the whole crystal, is symmetric about the β-phase site. However, for an individual atom the double wells are strongly asymmetric due to the cooperative inter-action so that all atoms tend to be on the same side of the

Figure II-2

      Conceptual sketch of the α-phase potential
energy for a quartz crystal as a whole (solid curve)
and for an individual atom in the crystal lattice
(dashed curve).
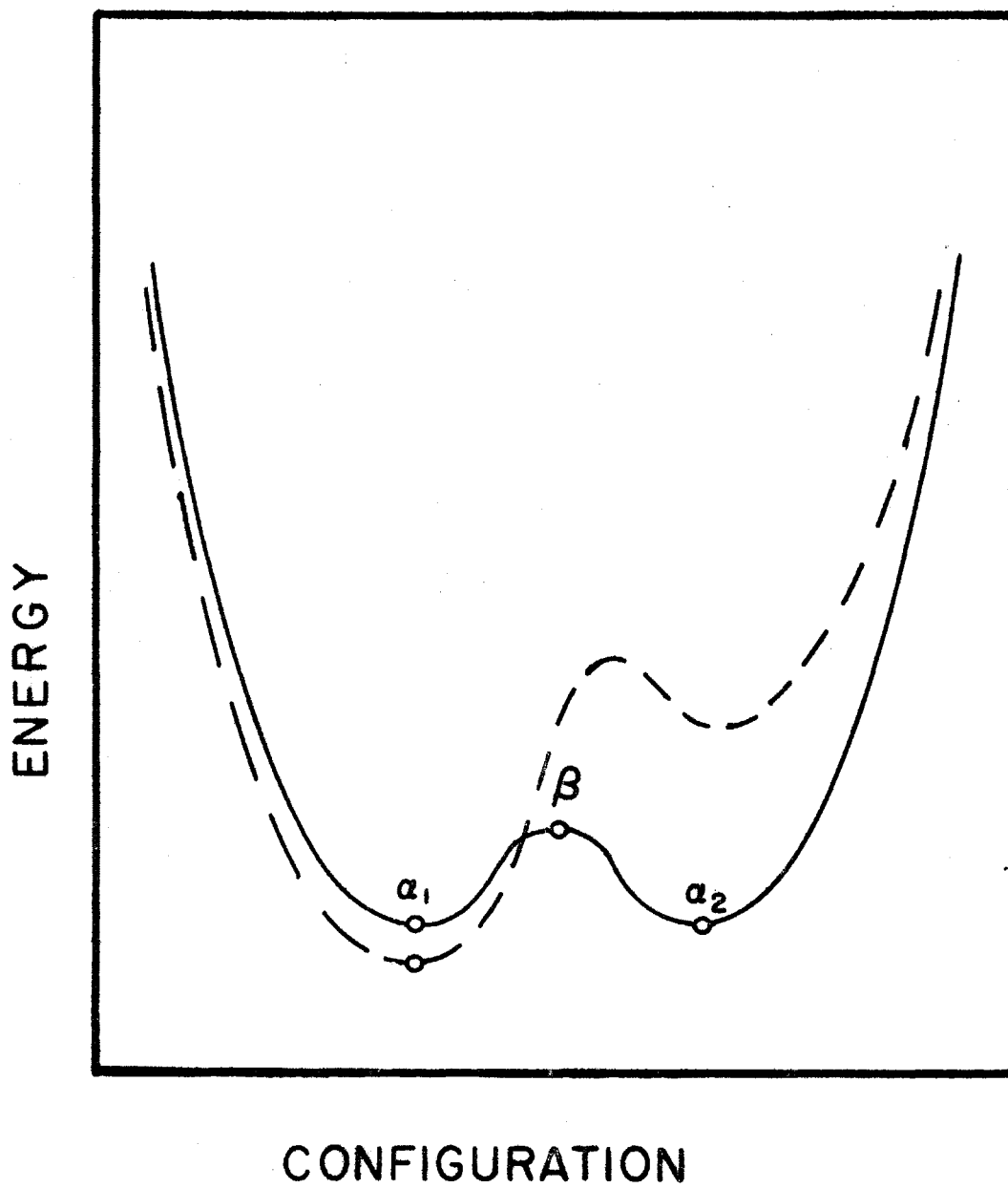
double well. A conceptual sketch of the α-phase potential

of the crystal as a whole and for an individual atom is

shown in Fig. (II-2).

2. Theoretical Aspects of Phase Transformations

Displacive-type phase transformations can be qualita-

tively discussed in terms of Landau's phenomenological theory

of second order phase transformations (Landau and Lifshitz,

1958). This theory also lends itself for a description of

first order transformations provided that the atomic displace-

ments are small (O'Leary and Wheeler, 1970). The assumption

is made that, near the transition temperature T_c the Gibbs free

energy can be expanded in a Taylor's series in terms of the

order parameter η as follows:

$$\Phi(T,\eta) = \Phi_o + \alpha\eta + A(T)\eta^2 + B(T)\eta^3 + C(T)\eta^4 + \dots \quad \text{(II-1)}$$

where the order parameter η is a generalized coordinate describing

the amplitude of the mean displacements of the atoms from

their high-symmetry lattice sites. The value of η at a

particular temperature can be obtained by requiring that the

free energy $\Phi(T,\eta)$ be a minimum. Clearly the linear term in

(II-1) must vanish identically for such a minimum to exist

at all temperatures. Similarly, for the minimum in the high

symmetry phase to occur at η = 0 it is necessary that A(T)>0

in the high-symmetry phase. In the low-symmetry phase, on the

other hand, the minimum of Φ must occur for a finite value of η and this requires that $A(T)<0$ in that phase. Since second order phase transitions involve, by definition, a continuous change of η across the transition the free energy must also be continuous. For this reason $A(T_c)$ and $B(T_c)$ must vanish. Furthermore, for $\Phi(T_c)$ to be a stable minimum it is necessary that $C(T_c)>0$. If it is assumed that the high-symmetry phase coincides with the high-temperature phase, these conditions can be summarized as follows:

$$A(T) > 0 \quad \text{for} \quad T > T_c$$
$$A(T) < 0 \quad \text{for} \quad T < T_c$$
$$A(T_c) = 0$$

and $B(T) = 0$ and $C(T)>0$ for T in the immediate vicinity of T_c. Minimization of Φ with respect to η leads to

$$\eta^2 = 0 \quad \text{for } T > T_c$$
$$\text{and} \quad \eta^2 = -\frac{A}{2C} \quad \text{for } T < T_c \quad .$$

The assumption is made that, to first order, the coefficient A is given by

$$A(T) = a(T-T_c)$$

where a is a constant. This leads to the following temperature dependence of the order parameter:

$$\eta = \pm \frac{a|T-T_c|^{\frac{1}{2}}}{2C} \quad . \tag{II-2}$$

This relationship, however, does not, in general, agree with experiments (Heller, 1967). Moreover, the Landau theory predicts the same critical exponents (i.e. the power according to which various physical quantities diverge to infinity or converge to zero as T approaches T_c) for all phase transitions, in contradiction with experiment. It has been shown that this difficulty can be overcome by using a more general form of the free energy expansion (Amit, 1970).

The order parameter which describes the static displacement of the atoms from their high-symmetry positions can be expressed as a linear combination of the phonon eigenfunctions of the high symmetry phase provided that these displacements are small. In particular, if the distortion can be described in terms of a single phonon eigenfunction, then the static displacement of the n'th atom in the ℓ'th unit cell is given by

$$\vec{u}(\ell,n) = \vec{e}(n;\vec{k},j) \frac{<Q(\vec{k},j)>}{(NM_n)^{\frac{1}{2}}} \exp[2\pi i \vec{k} \cdot X(\ell)] \qquad (II-3)$$

(O'Leary and Wheeler, 1970), where $Q(\vec{k},j)$ is the normal coordinate of wave vector $\vec{k}$ and branch label j and $\vec{e}(n;\vec{k},j)$ is the relative displacement vector of the n'th atom of mass M_n when only the (k,j)th mode is excited. Since $\frac{<Q(\vec{k},j)>}{(NM_n)^{\frac{1}{2}}}$ is a measure of the mean amplitude of the distortion it will serve as the order parameter $\eta(\vec{k},j)$. A normal mode analysis in quartz by Kleinman and Spitzer (1962) shows that there is one Raman-active mode of symmetry A_1 which corresponds very

closely to the atomic displacements in the α-β transformation, indicating that a description by a single phonon eigenfunction is appropriate.

Further insight into the lattice dynamical aspect of phase transformations can be gained by making use of a result derived by Cowley (1965). It states that the distortion (II-3) makes an extra contribution to the harmonic term of the free energy and is given by

$$\Delta F = \omega^2(\vec{k},j)\eta^2(\vec{k},j) \qquad (II-4)$$

where $\omega(\vec{k},j)$ is the frequency of the high-symmetry normal mode which is used in (II-3) to describe the distortion. By comparing (II-4) with (II-1) one can identify $\omega^2(\vec{k},j)$ with Landau's coefficient A(T) and the conditions for a second order phase transformation can be seen to imply that the frequency of a high-symmetry normal mode must vanish as T_c is approached from above. Furthermore, the continuous change of the order parameter across the phase transition leads to a continuous change of the dynamical matrix elements and hence the eigenvalues of the dynamical matrix are continuous across T_c. This implies that there must also be at least one mode in the low-symmetry phase which has a frequency that vanishes as T_c is approached from below. For this reason displacive-type phase transitions are often called "soft mode transitions". Measurements of the temperature dependence of the frequency of a Raman-active A_1 mode in quartz (Shapiro, O'Shea, and

Cummins, 1967) and in $AlPO_4$ (Scott, 1970) show that there is a marked shift toward lower frequencies as the transition is approached. In the β-phase there is still no conclusive evidence of an unstable excitation although experimental results have been reported which are consistent with a soft zone-center optical mode in the β-phase (Ishida and Hanjo, 1969; Axe and Shirane, 1970).

Landau's theory can also be applied to first order phase transformations in which both Φ and $\frac{\partial \Phi}{\partial T}$ have a discontinuity at T_c. In this case the coefficient B must be finite at $T = T_c$ and the expression for the free energy becomes

$$\Phi(\eta) = A\eta^2 + B\eta^3 + C\eta^4 + \ldots$$

The condition that $\frac{\partial \Phi}{\partial \eta} = 0$ yields two solutions for the order parameter:

$$\eta = 0$$

and

$$\eta = -3B \pm [(9B^2 - 32AC)/8C]^{\frac{1}{2}} .$$

Since the coefficients A, B, and C are functions of temperature one can define the transition temperature T_c as the temperature at which the quantity $9B^2 - 32AC$ becomes positive and hence a finite, real value of η is obtained. Recalling the above interpretation of the coefficient A as the square of the frequency of a particular normal mode, it becomes evident that, even for a first order transition, a decrease

in frequency of some normal mode is required to make the quantity $9B^2 - 32AC$ positive, provided C is positive, which is usually the case.

A major shortcoming of Landau's theory, which is a mean field theory, is the neglect of time-dependent fluctuations of the order parameter. In a region close to the transition temperature these fluctuations will become larger than the mean value of the order parameter. Hence the free energy expansion (II-1) in powers of the mean atomic displacements is only valid outside this region, which is known as the critical region. The width of the critical region varies greatly for different second order phase transitions. Ginzburg (1960) was able to describe the significance of fluctuations in different second order phase transformations in terms of a single parameter. This parameter essentially expresses the ratio of volume to correlation energies in the Hamiltonian of a system. If this ratio is small the fluctuation effects will be limited to an extremely narrow region around T_c and Landau's theory adequately describes the transition. Experimentally, the size of the critical region can be determined by specific heat measurements which reflect any singular behaviour of the free energy at the transition temperature. In the case of quartz a pronounced anomaly (a λ-point) has been observed (Mosesman and Pitzer, 1941; Sinel'nikov, 1953) which consists of an unlimited increase of the specific heat on either side of the transition

temperature.

3. The α-β Phase Transformation in Quartz

The α-β phase transformation in quartz takes place at 573°C. At this temperature the crystal undergoes a change in symmetry from the trigonal α-phase with space group $P3_121$ to the hexagonal β-phase with space group $P6_222$.

On the microscopic scale three different situations may exist with regard to the β-phase structure:

1. The atoms may be distributed among Dauphiné twin-related sites. This implies that the double minimum of the α-phase configurational potential energy persists in the β-phase. The potential barrier separating the two minima may be sufficiently high to constrain the atoms to vibrate primarily on one side of the double well. In this case the α-β phase transformation is of an order-disorder type and the disorder is static.

2. The atoms may be statistically distributed but possess sufficient thermal energy to vibrate between the two minima. In this case the transition is still of an order-disorder type but the disorder is dynamic.

3. The equilibrium positions of the atoms may lie midway between two Dauphiné twin-related sites. In this case the α-β phase transformation is of the displacive type.

Various experimental studies have been undertaken to determine

Figure II-3

       Temperature dependence of the magnitude of
the normalized vectors $\vec{\delta}$ and $\vec{\gamma}$ in quartz (after
Young, 1962). The β-phase values which were used in
the temperature-dependent point-multipole model are
represented by the dashed curve.
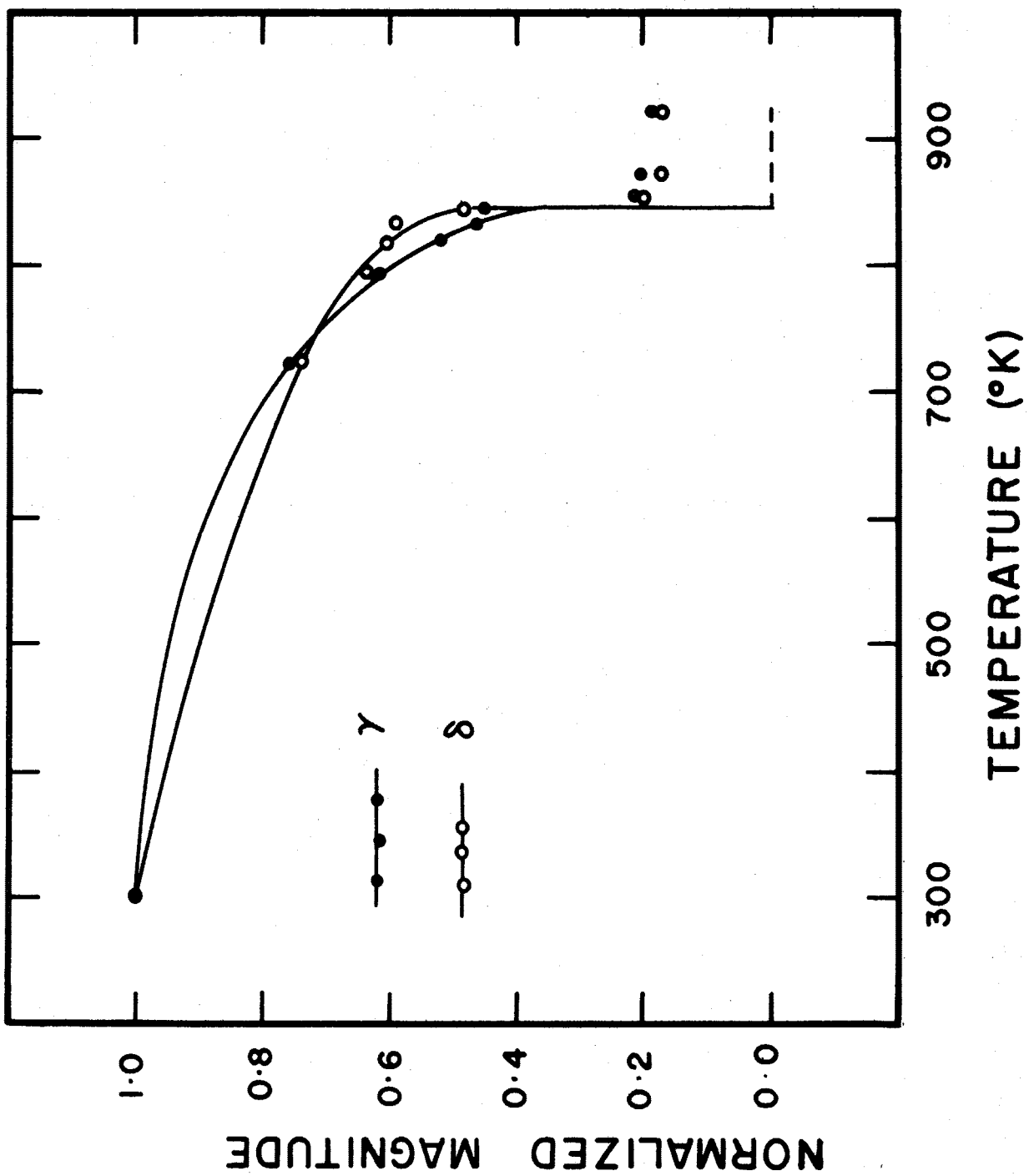
the detailed mechanism of the α-β phase transformation.
The most important of these include crystallographic studies
by x-ray diffraction as well as lattice vibrational studies
by Raman-, Brillouin-, and inelastic neutron scattering.

By far the most extensive x-ray study was carried
out by Young (1962). It is perhaps appropriate to discuss
Young's work in some detail as it provides the basis for
the temperature-dependent point-multipole model which is used
in this work to calculate the spin-Hamiltonian parameters as
a function of temperature.

As pointed out above, the average atomic positions
in the β-phase lie midway between two Dauphiné twin-related
sites. Young has defined two vectors $\vec{\delta}$ and $\vec{\gamma}$ such that $\vec{\delta}$
extends from the midpoint between two Dauphiné related oxygen
sites to the oxygen position in the α_1 configuration. The
vector $\vec{\gamma}$ is analogously defined for the case of the silicon
atom. From the results of a least squares refinement carried
out for eight different temperatures ranging from 450° to 650°C
and using anisotropic temperature factors, Young obtained a
temperature dependence for the magnitudes of the vectors $\vec{\delta}$ and
$\vec{\gamma}$ as well as for the size and orientation of the thermal el-
lipsoids. The magnitudes of the vectors $\vec{\delta}$ and $\vec{\gamma}$ play the role
of the order parameter η in Landau's theory. Their tempera-
ture dependences are shown in Fig. (II-3). The temperature
variations of the r.m.s. vibrational amplitudes along the three

Figure II-4

　　　Temperature dependence of the r.m.s. ampli-
tudes of the lattice vibrations of the oxygen atoms
in quartz along the three principal axes, p, q and r
of the thermal ellipsoid (after Young, 1962). The
dashed lines represent the extrapolations which were
used in the temperature-dependent point-multipole
model.
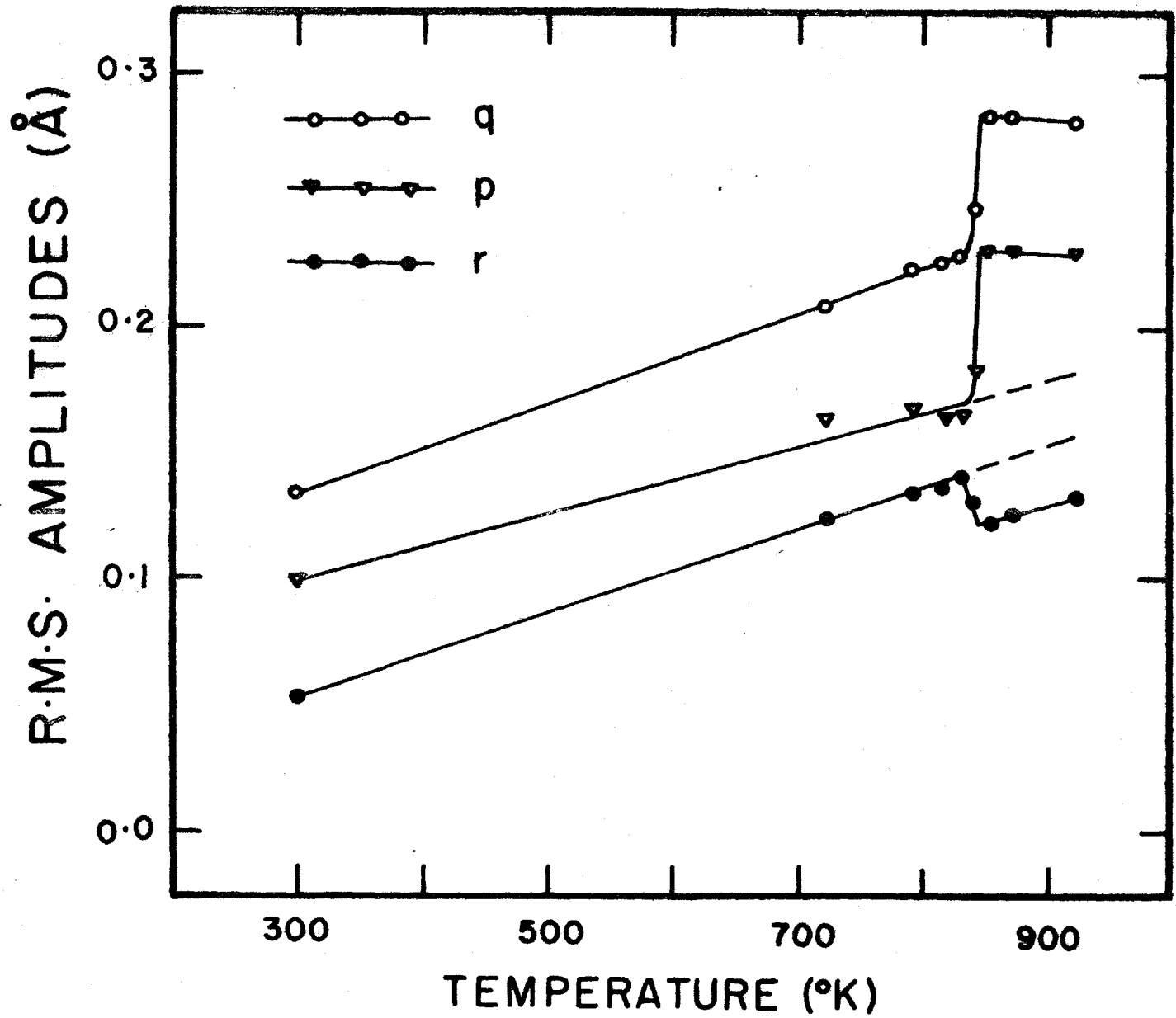
principal axes, p, q and r of the thermal ellipsoid are shown in Fig. (II-4). The direction of $\vec{q}$ is perpendicular to the Si-O-Si bonding plane, and $\vec{r}$ is parallel to the line joining the two Si-atoms in the Si-O-Si plane, and $\vec{p}$ is perpendicular to $\vec{q}$ and $\vec{r}$.

On the basis of least squares refinement procedures alone Young was not able to distinguish between the single and double minimum case in the β-phase. However, by studying individual reflection intensities as a function of temperature it was possible to rule out the double minimum model for the β-phase structure. In addition, Young concludes that the α-β phase transformation in quartz is thermodynamically of first order. In most of the specimens investigated by Young, the transformation proper was preceded by complete small scale Daulphiné twinning such that at a few degrees below the transition there were equal volumes of the crystal in either type of Dauphiné configuration.

Due to effects of "parameter interaction" in the least squares refinement of the x-ray data, the results shown in Figures (II-3) and (II-4) must be regarded with some caution. Young points out that in any least squares parameter fit the parameters are only uncoupled if the assumed correlation function, i.e. the square of the theoretical structure factor, has the functional form of the actual correlations present in the signal. However, since the assumed correlation function

is based on harmonic vibrations only, one would expect

that parameter interaction is particularly severe near the

transition temperature. Thus the non-zero values of $|\vec{\delta}|$ and

$|\vec{\gamma}|$ in the β-phase are most likely due to parameter interaction

which indicates that some anharmonic character persists in

the β-phase. Furthermore, the temperature variation of the

r.m.s. amplitudes along $\vec{p}$ and $\vec{r}$ near the transition tempera-

ture is difficult to reconcile with the results of a normal

mode analysis of quartz (Kleinman and Spitzer, 1962) and the

measured temperature variation of the normal mode frequencies

by Raman spectroscopy (Shapiro, 1969). A very simple,

physically intuitive picture emerges from the normal mode

analysis as far as the motions of the O-atoms are concerned.

If the Si-O-Si bonding plane is viewed as a separate unit one

would expect the highest frequency vibration to involve a

motion along the r-direction because this motion stretches

and compresses the Si-O bonds more than any other type of

motion. Similarly, the lowest frequency vibration should

involve primarily a motion along $\vec{q}$ which nearly preserves the

bond lengths. The motion along $\vec{p}$, on the other hand, involves

mainly a bending of the Si-O-Si bond angle and its frequency

would be expected to be intermediate between the previous two.

These qualitative considerations are borne out by the normal

mode analysis which includes stretching and bending forces

within the Si-O-Si unit. In particular, the O-motions along

$\vec{p}$, $\vec{q}$ and $\vec{r}$ correspond to three of the four A_1 vibrational modes of α-quartz. Their room temperature frequencies are 466, 207, and 1081 cm^{-1} respectively. Of these only the 207 mode shows a marked shift toward lower frequencies as the transition temperature is approached. Furthermore, the configuration of the 207 normal mode is in remarkable agreement with the atomic displacements of the α-β phase transformation, whereas none of the other modes show any such resemblance. It has therefore been suggested that the 207 mode plays the role of a "soft mode" in the α-β phase transformation. The lack of any temperature variation of the 1081 and 466 modes (Shapiro, 1969) in the vicinity of the phase transition implies that the generalized restoring forces for the p- and r-type motions do not change significantly. The sharp increase of the r.m.s. amplitude obtained by Young for vibrations along $\vec{p}$, however, should be accompanied by a decrease in frequency of the p-type normal mode. One might therefore be inclined to believe that the temperature variation of the r.m.s. amplitudes along $\vec{p}$ and $\vec{r}$ is occasioned by parameter interaction. Young himself points out that the reliability of his least squares refinement is very doubtful in the vicinity of the transition, especially for the 570°C measurements. For the purpose of calculating the crystal field coefficients as a function of temperature, it was assumed that only the r.m.s. amplitude along $\vec{q}$ had the temperature dependence as shown in Fig. (II-4). The values for the p and r amplitudes were taken to be straight

line extrapolations of their low temperature values. The
above arguments for justifying this procedure are by no means
conclusive since virtually all modes, including the accous-
tical branches enter the r.m.s. amplitudes and not just the
zone-center A_1 modes.

4. The α-β Phase Transformation in $AlPO_4$

There have been few previous studies which are rele-
vant to the problem of the microscopic mechanism of the α-β
phase transformation in $AlPO_4$. Most of the previous work
deals with the measurement of microscopic physical quantities
such as the thermal coefficient of expansion (Shafer and Roy,
1957) and the temperature dependence of the lattice constants
(Troccaz et al, 1967). The latter authors have also measured
a discontinuity in the specific heat across the transition.
They point out that this discontinuity is of the same order of
magnitude as the one observed in quartz.

It was the publication of preliminary results of the
present work which inspired the temperature-dependent Raman
study in $AlPO_4$ (Scott, 1970). Raman scattering experiments
which were carried out between room temperature and the
transition point revealed a striking similarity of the spectra
in $AlPO_4$ and quartz. The room temperature frequencies of
the A_1 soft optic mode as well as the frequency band of the
two-phonon state which interacts with the A_1 mode are virtually
the same in both systems. The fact that the frequencies of

the soft modes in $AlPO_4$ and quartz do not intersect $\omega=0$
at the transition temperature indicates that both systems
behave as if they were undergoing a phase transformation
of the second kind but undergo a first order phase transfor-
mation at a temperature T_o before the critical temperature
is reached.   This view is confirmed by the temperature-
dependent measurements of the lattice constants "a" and "c"
which show a discontinuity at the transition temperature.

The only previous E.P.R. work in $AlPO_4$ consisted
of a study of Cr^{3+}-doped $AlPO_4$ which was carried out at liquid
helium temperatures. (Henning et al, 1967).

CHAPTER III

THEORY

In the present chapter, the origin of the zero-field splitting is discussed and a relationship between the spin-Hamiltonian parameters D and E and the crystal field is worked out. This is followed by the presentation of a method for calculating the crystal field coefficients using a point-multipole model which includes effects due to thermal vibrations of the lattice.

1. Zero-Field Splitting by the Blume-Orbach Mechanism.

In view of the multitude of mechanisms which can contribute to the zero-field splitting of a paramagnetic S-state ion in a crystal, it would be impractical here to consider each one individually. However, by considering the most important mechanisms, Sharma, Das, and Orbach (1966, 1967, 1968) have shown that one predominant mechanism, the Blume-Orbach mechanism, can be singled out, provided that the magnetic ion is surrounded by a predominantly cubic environment. To appreciate the problem of the zero-field splitting of S-state ions, it is perhaps useful to recall that any ion with a half-filled shell configuration, such as $3d^5$, will have an orbital singlet, i.e. and S-state, as its ground state. For

Figure III-1

The quartet states of the free Fe^{3+} ion are indicated on the left. The energies are in units of 10^3 cm^{-1} (after Moore, 1962). The energy levels on the right are the Γ_4 levels appropriate in the presence of a cubic crystalline field.
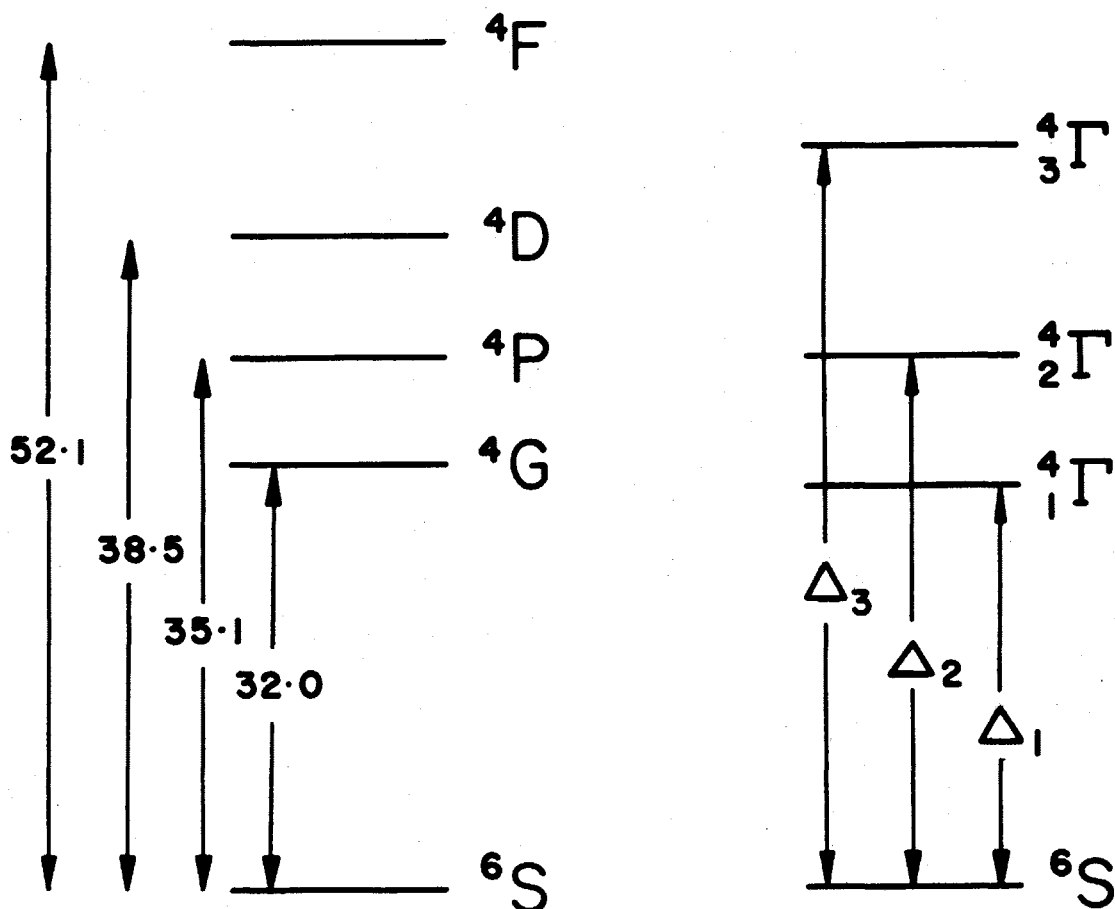
SCHEMATIC OF LEVEL
SPLITTINGS FOR Fe^{3+}

this reason, any orbital operator, such as the crystalline potential, cannot by itself remove the spin-degeneracy. It is the spin-orbit coupling which provides a link via which the spin can interact with the diamagnetic crystalline environment. In the language of perturbation theory, one can use this interaction to admix into the ground state higher lying excited states of finite orbital angular momentum which, in turn, will interact with the crystalline field. The best estimate of the free ion energy levels of Fe^{3+}, which are not very accurately known (Moore, 1962), are shown in Figure (III-1). Because of the triangle selection rule, only the $|^4P>$ excited state will be admixed into the $|^6S>$ ground state by the spin-orbit coupling. The subsequent action of the crystalline potential V_c on the perturbed ground state depends therefore on the matrix element $<^4P|V_c|^4P>$. This matrix element, however, vanishes on account of the half-filled shell theorem (Watanabe, 1966) which states that matrix elements of one-electron operators, such as the Laplace expansion of the crystalline potential, vanish between states of the same Russel-Saunders multiplet. This fact has led to the proposal of mechanisms involving perturbation terms of higher order than second and, consequently, smaller contributions to the zero-field splitting. However, Blume and Orbach (1962) have proposed that diagonalization of the excited quartets with respect to the cubic field is necessary in order to obtain realistic zero order wave

functions prior to any perturbation treatment. This is evident because the cubic splitting parameter $10D_q$ is typically of order of 10^4 cm^{-1} for 3d electrons and therefore comparable in magnitude to the free ion splittings. Furthermore, this procedure ensures that other multiplets such as $|^4G>$ and $|^4F>$ are admixed into the ground state leading to non-vanishing matrix elements of the axial and rhombic crystal-line field potentials.

Symbolically, the contribution of the Blume-Orbach mechanism to the axial and rhombic zero-field splitting para-meters D and E can therefore be written

$$D_{BO}, \; E_{BO} \propto \frac{<^6S|H_{SO}|^4\Gamma_4><^4\Gamma_4|V_c'|^4\Gamma_4><^4\Gamma_4|H_{SO}|^6S>}{[E(^4\Gamma_4) - E(^6S)]^2} \qquad (III-1)$$

where H_{SO} is the spin-orbit interaction, V_c' is the unbalanced axial component of the crystal field, as defined below, and $|^4\Gamma_4>$ are the basis states of the Γ_4 irreducible represen-tation of the O_h cubic group. Fortunately, other irreducible representations of the O_h cubic group need not be considered since H_{SO} transforms as Γ_4. Hence only wave functions of Γ_4 character are admixed into the $|^6S>$ ground state which trans-forms as the identity representation Γ_1. Strictly speaking, one should use the tetrahedral group T_d instead of O_h when dealing with the Al-site in AlPO$_4$, but, since only 3d wave functions of even parity are involved, the wave functions are invariant under the action of the inversion operator. Clearly

the above process yields a larger contribution to the zero-field splitting than conventional perturbation treatments of the cubic field which would have resulted in an extra factor of $\dfrac{H_{cubic}}{E(^4G)-E(^6S)}$ in (III-1).

2. The Electrostatic Potential in the Crystal Field Approximation.

According to electrostatic theory the potential at a point $\vec{r}$ due to charges at points $\vec{r}_i$ is given by

$$V(\vec{r}) = \sum_{\ell=0} \sum_{m=0}^{\ell} C_{\ell m} r^{\ell} [Y_{\ell m}(\theta,\phi) + Y_{\ell m}^*(\theta,\phi)] \qquad \text{(III-2)}$$

where

$$C_{\ell m} = \sqrt{\frac{4}{2\ell+1}} \sum_i \frac{|e|}{2a_o^{\ell+1}} \left[\frac{q_i}{r_i^{\ell+1}} (Y_{\ell m}(\theta_i,\phi_i) + Y_{\ell m}^*(\theta_i,\phi_i))\right] \qquad \text{(III-3)}$$

e is the electronic charge, q_i is the ith charge in units of $|e|$, r_i is in units of the Bohr radius a_o, and all $r_i > r$. The crystalline potential energy operator for a many-electron system becomes therefore

$$V_c = - |e| \sum_k V(\vec{r}_k)$$

$$= - \sum_k \sum_{\ell=0}^{\infty} \sum_{m=0}^{\ell} B_{\ell m} r_k^{\ell} (Y_{\ell m}(\theta_k,\phi_k) + Y_{\ell m}^*(\theta_k,\phi_k)) \qquad \text{(III-4)}$$

where

$$B_{\ell m} = \sqrt{\frac{4}{2\ell+1}} \sum_i \left[\frac{q_i}{r_i^{\ell+1}} (Y_{\ell m}(\theta_i,\phi_i) + Y_{\ell m}^*(\theta_i,\phi_i))\right] \qquad \text{(III-5)}$$

and $B_{\ell m}$ is in units of $\dfrac{|e|^2}{2a_0^{\ell+1}}$ which yields V_c in units of Rydbergs ($\dfrac{|e|^2}{2a_0}$). The summation $\sum\limits_{k}$ extends over all electrons in the unfilled shell of the paramagnetic ion. For this expression to be valid, one must assume that the charge distribution can be represented by point charges which are all situated outside a sphere of radius r. However, this model does not assume spherically symmetric charge distributions of the ions at the lattice sites, since actual charge distributions can be approximated by the superposition of point-multipoles.

The number of terms in the crystal field expansion can often be considerably reduced by considerations of symmetry. In particular, when dealing with quantum states which are strictly derived from the $3d^5$-configuration, it is possible to omit all odd spherical harmonics and to terminate the expansion at $\ell = 4$, because any other spherical harmonics have vanishing matrix elements. Furthermore, if the symmetry at the magnetic ion's site consists of a twofold axis parallel to the z-axis, then the values of m are restricted to even integers. The crystalline field operator can therefore be written as

$$V_c = V_{20} + V_{22} + V_{40} + V_{42} + V_{44} \,. \qquad \text{(III-6)}$$

In anticipation of its future application, it is advantageous to express V_c in a coordinate system which coincides with the orthogonal axis triplet defined by the cubic component of the

crystalline field. If λ_{22} and λ_{42} are used to denote the angles of the extrema or "lobes" of V_{22} and V_{42} then the final expressions for the transformed crystal field components V_{22} and V_{42} become, using $Y_{\ell m}^{*} = Y_{\ell -m}$ for m even

$$V_{22} = -B_{22} \sqrt{\frac{4\pi}{5}} \sum_{k} r_k^2 (Y_{22} e^{-2i\lambda_{22}} + Y_{2-2} e^{+2i\lambda_{22}}) \quad \text{(III-7)}$$

$$V_{42} = -B_{42} \sqrt{\frac{4\pi}{9}} \sum_{k} r_k^4 (Y_{42} e^{-2i\lambda_{42}} + Y_{4-2} e^{+2i\lambda_{42}}) \quad \text{(III-8)}$$

Finally, since the magnetic ion is surrounded by a nearly cubic field it is desirable to split off the cubic component of the crystalline potential because the effect of the residual rhombic and axial components will be treated by perturbation methods.

In perfect cubic symmetry the crystal field coefficients B_{40} and B_{44} are related as follows

$$B_{40} = \sqrt{\frac{14}{5}} B_{44} \quad \text{(III-9)}$$

The cubic potential is therefore

$$V_{cubic} = \sqrt{\frac{4\pi}{9}} [\sum_{k} \sqrt{\frac{14}{5}} B_{44} r_k^4 Y_{40} + \sum_{k} B_{44} r_k^4 (Y_{44} + Y_{4-4})] \quad \text{(III-10)}$$

The residual crystal potential then becomes

$$V_{c} = V_{20} + V_{22} + V_{40}' + V_{42} \quad \text{(III-11)}$$

where the crystal field coefficient of V_{40}' is

$$B_{40}' = B_{40} - \sqrt{\frac{14}{5}} B_{44} \quad \text{(III-12)}$$

3. Effect of Tetrahedral Potential on Excited Quartets.

The problem of obtaining the proper zero order wave functions of an ion which resides in a lattice site of a certain symmetry is greatly simplified by symmetry considerations. In particular, by employing group theory to obtain wave functions of the correct symmetry one can considerably reduce the number of off-diagonal matrix element and hence the size of the secular determinant.

As pointed out earlier, only wave functions of $\Gamma_4(O_h)$ symmetry can be admixed into the ^6S ground state by the spin-orbit interaction. It is therefore appropriate to project out the Γ_4 components contained in the excited quartets shown in Figure (III-1). Let $|^4P\Gamma_4M_\Gamma>$, $|^4F\Gamma_4M_\Gamma>$ and $|^4G\Gamma_4M_\Gamma>$ denote the Γ_4 components contained in the ^4P, ^4F and ^4G wave functions respectively, where M_Γ can take the values 1, 0, -1 to distinguish the three subvectors of the Γ_4 representation. Therefore the wave functions with proper symmetry become:

$$|^4P\Gamma_4 1> = |^4P1>$$

$$|^4F\Gamma_4 1> = \sqrt{\frac{3}{8}}\,|^4F1> + \sqrt{\frac{5}{8}}\,|^4F-3>$$

$$|^4G\Gamma_4 1> = -\sqrt{\frac{7}{8}}\,|^4G1> - \sqrt{\frac{1}{8}}\,|^4G-3>$$

$$|^4P\Gamma_4 0> = |^4P0>$$

$$|^4F\Gamma_4 0> = |^4F0>$$

$$|^4G\Gamma_4 0> = -\sqrt{\frac{1}{2}}\,|^4G4> + \sqrt{\frac{1}{2}}\,|^4G-4>$$

$$|4P\Gamma_4 -1> = |^4P-1>$$

$$|^4F\Gamma_4 -1> = \sqrt{\frac{5}{8}} \, |^4F3> + \sqrt{\frac{3}{8}} \, |^4F-1>$$

$$|^4G\Gamma_4 -1> = \sqrt{\frac{1}{8}} \, |^4G3> + \sqrt{\frac{7}{8}} \, |^4G-1> \qquad \text{(III-13)}$$

where all wave functions are 5-dimensional Slater determinants made up of single electron (3d) wave functions. $|^4D>$ does not appear because it contains no Γ_4 component.

The problem of obtaining the eigenfunctions and energy eigenvalues under the action of the tetrahedral potential is now reduced to solving a 3 × 3 secular determinant resulting from the remaining non-zero off-diagonal matrix elements. These were found to be

	$|^4P\Gamma_4 1>$	$|^4F\Gamma_4 1>$	$|^4G\Gamma_4 1>$
$<^4P\Gamma_4 1|$	35100	0	$-4\sqrt{5}D_q$
$<^4F\Gamma_4 1|$	0	52100	$2\sqrt{5}D_q$
$<^4G\Gamma_4 1|$	$-4\sqrt{5}D_q$	$2\sqrt{5}D_q$	32000

(III-14)

where $D_q = \dfrac{B_{40}<r^4>}{14\sqrt{\pi}}$, and $<r^4>$ is the expectation value of r^4 with respect to the radial part of the 3d-orbital. For the diagonal elements of the matrix (III-14) the following free ion Fe^{3+} splittings were used (Moore, 1962):

$$E(^4P) - E(^6S) = 35100 \text{ cm}^{-1}$$

$$E(^4F) - E(^6S) = 52100 \text{ cm}^{-1} \qquad \text{(III-15)}$$

$$E(^4G) - E(^6S) = 32000 \text{ cm}^{-1} .$$

The three eigenvectors of the cubic field are denoted by

$$|^4_i\Gamma_4 M_\Gamma> = \alpha_i |^4P\Gamma_4 M_\Gamma> + \beta_i |^4F\Gamma_4 M_\Gamma>$$

$$+ \gamma_i |^4G\Gamma_4 M_\Gamma> \qquad \text{(III-16)}$$

where i = 1, 2, 3 and $[\alpha_i, \beta_i, \gamma_i]$ are the eigenvectors of the matrix (III-14).

It is perhaps appropriate to point out that the value for D_q for tetrahedral coordination is negative and generally about half as large as the corresponding D_q for octahedral coordination. In particular, if only nearest neighbour point charges are considered, the D_q's are related by

$$D_q(T_d) = - \frac{4}{9} D_q(O_h) \qquad \text{(III-17)}$$

where the coordinations are four and six respectively. In the case of the Al-site in $AlPO_4$ the deviations from a regular tetrahedron are substantial. In spite of the crude approximations, the relationship (III-17) is generally borne out by experiment. For the purposes of this work, D_q was taken to be of negative sign but its magnitude was left as an adjustable parameter.

4. Perturbation Treatment of the Spin-Orbit Interaction

The spin-orbit interaction can be written as

$$H_{SO} = \sum_{i=1}^{5} \xi(r_i)\, \vec{\ell}(i) \cdot \vec{s}(i)$$

$$\simeq \sum_{i=1}^{5} \lambda [\ell_x(i) s_x(i) + \ell_y(i) s_y(i) + \ell_z(i) s_z(i)] \qquad \text{(III-18)}$$

where the summation extends over the five electrons in the $3d$ shell and λ is the spin-orbit coupling constant. The effect of the spin-orbit coupling is to admix the excited cubic eigenstates (III-16) into the $|{}^6S\rangle$ ground state. In view of later applications, it is expedient to split the spin-orbit interaction into its three cartesian components:

$$\lambda \sum_i \ell_x(i) s_x(i) \quad , \quad \lambda \sum_i \ell_y(i) s_y(i) \quad , \quad \lambda \sum_i \ell_z(i) s_z(i) \; .$$

Under the action of the three components of the spin-orbit coupling the perturbed wave functions are to first order:

$$|{}^6SM_s\rangle'_{\ell_x s_x} = |{}^6SM_s\rangle - \sum_{i=1}^{3} \frac{\alpha_i}{\Delta_i} \lambda \Big[\frac{a(M_s)}{2} |{}^4_i\Gamma_4 1, M_s-1\rangle$$

$$+ \frac{b(M_s)}{2} |{}^4_i\Gamma_4 -1, M_s+1\rangle + \frac{d(M_s)}{2} |{}^4_i\Gamma_4 1, M_s+1)\rangle + \frac{e(M_s)}{2} |{}^4_i\Gamma_4 -1, M_s-1\rangle \qquad \text{(III-19)}$$

$$|{}^6SM_s\rangle'_{\ell_y s_y} = |{}^6SM_s\rangle - \sum_{i=1}^{3} \frac{\alpha_i}{\Delta_i} \lambda \Big[\frac{a(M_s)}{2} |{}^4_i\Gamma_4 1, M_s-1\rangle$$

$$+ \frac{b(M_s)}{2} |{}^4_i\Gamma_4 -1, M_s+1\rangle - \frac{d(M_s)}{2} |{}^4_i\Gamma_4 1, M_s+1\rangle$$

$$- \frac{e(M_s)}{2} |{}^4_i\Gamma_4 -1, M_s-1\rangle] \qquad \text{(III-20)}$$

$$|^6SM_s>'_{\ell_z s_z} = |^6SM_s> - \sum_{i=1}^{3} \frac{\alpha_i}{\Delta_i} \lambda \ c(M_s) |^4_i\Gamma_4 0,M_s> \qquad \text{(III-21)}$$

where

$$|^4_i\Gamma_4 M_\Gamma,M_s> = |_i\Gamma_4 M_\Gamma> \cdot |\tfrac{3}{2}M_s>$$

and the Δ_i are the eigenvalues of (III-14)

and

$$a(M_s) = \tfrac{1}{2}<^4P1,M_s-1|\sum_i \ell^+(i)s^-(i)|^6SM_s>$$

$$b(M_s) = \tfrac{1}{2}<^4P-1,M_s+1|\sum_i \ell^-(i)s^+(i)|^6SM_s>$$

$$c(M_s) = <^4P0,M_s|\sum_i \ell_z(i)s_z(i)|^6SM_s> \qquad \text{(III-22)}$$

$$d(M_s) = \tfrac{1}{2}<^4P1,M_s+1|\sum_i \ell^+(i)s^+(i)|^6SM_s>$$

$$e(M_s) = \tfrac{1}{2}<^4P-1,M_s-1|\sum_i \ell^-(i)s^-(i)|^6SM_s>$$

and $\ell^+ = \ell_x + i\ell_y$; $s^+ = s_x + is_y$;

$$\ell^- = \ell_x - i\ell_y \quad ; \quad s^- = s_x - is_y \quad ; \qquad \text{(III-23)}$$

The values of the quantities (III-22) are listed in Table (III-1)

M_s	5/2	3/2	1/2	-1/2	-3/2	-5/2
$a(M_s)$	$\sqrt{5}$	$\sqrt{3}$	$\tfrac{1}{2}\sqrt{6}$	$\tfrac{1}{2}\sqrt{2}$	0	0
$b(M_s)$	0	0	$\tfrac{1}{2}\sqrt{2}$	$\tfrac{1}{2}\sqrt{6}$	$\sqrt{3}$	$\sqrt{5}$
$c(M_s)$	0	$-\sqrt{2}$	$\sqrt{3}$	$\sqrt{3}$	$\sqrt{2}$	0
$d(M_s)$	0	0	$-\tfrac{1}{2}\sqrt{2}$	$-\tfrac{1}{2}\sqrt{6}$	$-\sqrt{3}$	$-\sqrt{5}$
$e(M_s)$	$-\sqrt{5}$	$-\sqrt{3}$	$-\tfrac{1}{2}\sqrt{6}$	$-\tfrac{1}{2}\sqrt{2}$	0	0

Table (III-1): List of values of a (M_s), b(M_s) c(M_s), d(M_s), e(M_s).

5. Calculation of the (D_{ij})-Tensor.

The effect of the axial and rhombic crystalline field components upon the spin-orbit-perturbed ^6S ground state is to remove the 6-fold spin degeneracy by splitting the various M_s-levels by amounts $\Delta E(M_s) = '<^6SM_s|V_c|^6SM_s>'$, thereby giving rise to a zero-field splitting. It is customary in E.P.R. work to describe the magnetic energy levels by the use of an effective spin-Hamiltonian. In particular, the orthorhombic part of the effective spin-Hamiltonian is given by

$$H = (S_x, S_y, S_z) \begin{pmatrix} D_{xx} & D_{xy} & D_{xz} \\ D_{yx} & D_{yy} & D_{yz} \\ D_{zx} & D_{zy} & D_{zz} \end{pmatrix} \begin{pmatrix} S_x \\ S_y \\ S_z \end{pmatrix} \qquad \text{(III-24)}$$

where (D_{ij}) is a positive definite, real symmetric tensor whose principal axes are commonly referred to as the magnetic axes.

Since both the effective spin-Hamiltonian, a phenomenological treatment, and the Blume-Orbach mechanism, a theoretical treatment, describe the zero-field splitting, it is desirable to establish a relationship between the two approaches and thereby arrive at expressions of the components D_{ij} in terms of more fundamental quantities. The problem is somewhat simplified by the fact that Fe^{3+} in $AlPO_4$ occupies a site of twofold symmetry and hence, by designating this direction as the z-axis, the D-tensor is already partially diagonalized since D_{xz}, D_{zx}, D_{yz} and D_{zy} vanish in this coordinate system. Therefore, the remaining

problem is to find expressions for $\begin{pmatrix} D_{xx} & D_{xy} \\ D_{yx} & D_{yy} \end{pmatrix}$ and to diagonalize

this submatrix in order to obtain the directions of the remaining

two magnetic axes in the plane perpendicular to the z-axis.

Expression (III-1) can be decomposed into parts which are

quadratic in the cartesian components of the single electron spin

operator and each individual part is proportional to matrix elements

which are quadratic in the corresponding components of the total

spin operator. It is clear that the constants of proportionality

can then be identified with the corresponding components of the

D-tensor. Specifically the following identifications can be made:

$$\langle^{6}SM_{s}+1|D_{xx}S_{x}^{2}|^{6}SM_{s}-1\rangle = \ell_{x}s_{x}'\langle^{6}SM_{s}+1|V_{40}+V_{42}|^{6}SM_{s}-1\rangle\ell_{x}s_{x}'$$

$$\langle^{6}SM_{s}+1|D_{yy}S_{y}^{2}|^{6}SM_{s}-1\rangle = \ell_{y}s_{y}'\langle^{6}SM_{s}+1|V_{40}+V_{42}|^{6}SM_{s}-1\rangle\ell_{y}s_{y}'$$

$$\langle^{6}SM_{s}|D_{zz}S_{z}^{2}|^{6}SM_{s}\rangle = \ell_{z}s_{z}'\langle^{6}SM_{s}|V_{40}+V_{42}|^{6}SM_{s}\rangle\ell_{z}s_{z}'$$

$$\langle^{6}SM_{s}+1|D_{xy}S_{xy}|^{6}SM_{s}-1\rangle = \ell_{x}s_{x}'\langle^{6}SM_{s}+1|V_{40}+V_{42}|^{6}SM_{s}-1\rangle\ell_{y}s_{y}' \quad \text{(III-25)}$$

where each relationship is independent of M_{s} and the crystal field

components V_{20} and V_{22} have been dropped on account of their

vanishing elements.

By substituting the crystalline potential (III-11) and the

perturbed ground state wave functions (III-19), (III-20), and

(III-21) into (III-25) the following expressions are obtained for

the components of the D-tensor:

$$D_{xx} = - \frac{<r^4>\lambda^2 p_{\alpha\gamma}[2p_{\alpha\alpha}-p_{\alpha\beta}]}{6} \left[\frac{\sqrt{5}}{2} B'_{40} + \sqrt{2} B_{42} \cos2\lambda_{42}\right] \quad (\text{III-26})$$

$$D_{yy} = - \frac{<r^4>\lambda^2 p_{\alpha\gamma}[2p_{\alpha\alpha}-p_{\alpha\beta}]}{6} \left[\frac{\sqrt{5}}{2} B'_{40} - \sqrt{2} B_{42} \cos2\lambda_{42}\right] \quad (\text{III-27})$$

$$D_{yx} = D_{xy} = - \frac{\sqrt{2}}{3} <r^4>\lambda^2 p_{\alpha\gamma}[2p_{\alpha\alpha}-p_{\alpha\beta}]B_{42} \sin2\lambda_{42} \quad (\text{III-28})$$

$$D_{zz} = 0 \quad (\text{III-29})$$

where

$$p_{\alpha\alpha} = \sum_{i=1}^{3} \frac{\alpha_i^2}{\Delta_i} \; ; \quad p_{\alpha\beta} = \sum_{i=1}^{3} \frac{\alpha_i \beta_i}{\Delta_i} \; ;$$

$$p_{\alpha\gamma} = \sum_{i=1}^{3} \frac{\alpha_i \gamma_i}{\Delta_i} \; ; \quad (\text{III-30})$$

These components are related to the spin-Hamiltonian parameters b_2^0 and b_2^2 or, the more conventional parameters D and E as follows:

$$b_2^0 = D = D_{zz} - \frac{1}{2}(D'_{xx} + D'_{yy}) \quad (\text{III-31})$$

$$b_2^2 = 3E = \frac{3}{2}(D'_{xx} - D'_{yy}) \quad (\text{III-32})$$

where D'_{xx} and D'_{yy} are the eigenvalues of the submatrix $\begin{pmatrix} D_{xx} & D_{xy} \\ D_{yx} & D_{yy} \end{pmatrix}$.

6. Dipolar Contributions to the Crystal Field.

Before the spin-Hamiltonian parameters D and E can be evaluated it is necessary to calculate the crystal field coefficients B_{40}, B_{42} and B_{44} as well as the orientation of the cubic and orthorhombic potential in the plane perpendicular

to the z-axis, the (xy)-plane.

Crystalline electric field calculations in $AlPO_4$ have been carried out by Schwarzenbach (1966) who obtained satisfactory agreement with the experimentally observed electric field gradient at the Al-site. In particular, Schwarzenbach has shown that the assumption of spherically symmetric charge distributions is unrealistic in the case of $AlPO_4$ and that substantial contributions to the electric field arise from the dipole moments of the oxygen ions. The present discussion of the crystalline electric field problem follows closely the treatment of Schwarzenbach whose calculations of the electric field gradient were repeated and thus provided a partial check for the present calculations.

The electrostatic potential at $\vec{r}_A$ due to an ion whose nucleus is located at $\vec{r}_B$ is given by

$$V^{A,B} = \int \frac{\rho^B(\vec{R}) d^3R}{|\vec{r}_{A,B} + \vec{R}|} \qquad \text{(III-33)}$$

where $\vec{r}_{A,B} = \vec{r}_A - \vec{r}_B$, $\rho^B(\vec{R})$ is the charge distribution of ion B and $\vec{R}$ is measured from the site of the nucleus of B.

By expanding $\dfrac{1}{|\vec{r}_{A,B} + \vec{R}|}$ in a Taylor series up to second order in R and substituting into (III-33) one obtains

$$V^{A,B} = \int \frac{\rho^B(\vec{R}) d^3R}{|\vec{r}_{A,B}|} + \int \sum_{i=1}^{3} \rho^B(\vec{R}) \cdot R_i \frac{\partial}{\partial x_i} \left(\frac{1}{r}\right)_{r=r_{A,B}} d^3R$$

$$+ \frac{1}{2} \int \sum_{i,j=1}^{3} \rho^B(\vec{R}) R_i R_j \frac{\partial^2}{\partial x_i \partial x_j} \left(\frac{1}{r}\right)_{r=r_{A,B}} d^3R$$

$$= \frac{q^B}{|\vec{r}_{A,B}|} + \sum_{i=1}^{3} d_i^B \cdot \frac{\partial}{\partial x_i} \left(\frac{1}{r}\right)_{r_{A,B}} + \frac{1}{2} \sum_{i,j=1}^{3} Q_{ij}^B \cdot \frac{\partial^2}{\partial x_i \partial x_j} \left(\frac{1}{r}\right)_{r_{A,B}} \quad \text{(III-34)}$$

where $q^B = \int \rho^B(\vec{R}) d^3R$ is the monopole,

$$d_i^B = \int \rho^B(\vec{R}) \cdot R_i \, d^3R \text{ is the dipole moment,}$$

and $\quad Q_{ij}^B = \frac{1}{3} \int (3R_i R_j - \delta_{ij}|\vec{R}|^2)\rho^B(\vec{R}) d^3R$

is the component of the quadrupole moment of ion B. By summing $V^{A,B}$ over all ions B one obtains the potential at lattice site A in terms of the monopoles, dipoles, and quadrupoles of all the ions in the lattice.

The electric field at site A is obtained by calculating the negative gradient of the potential with respect to the coordinates of point A, or , equivalently, the positive gradient with respect to the coordinates of B, i.e.

$$\vec{E}^A = - \sum_B \nabla_A V^{A,B} = \sum_B \nabla_B V^{A,B} \quad . \qquad \text{(III-35)}$$

Explicitly the cartesian components of the electric field at site A are

$$E_k^A = \sum_B \left\{ q^B \frac{\partial}{\partial x_k} \left(\frac{1}{r}\right)_{r_{A,B}} + \sum_{i=1}^{3} d_i^B \left[\frac{\partial^2}{\partial x_k \partial x_i} \left(\frac{1}{r}\right)_{r_{AB}}\right] \right.$$

$$\left. + \frac{1}{2} \sum_{i,j=1}^{3} Q_{ij}^B \left[\frac{\partial^3}{\partial x_k \partial x_i \partial x_j} \left(\frac{1}{r}\right)_{r_{A,b}}\right] \right\}. \qquad \text{(III-36)}$$

Schwarzenbach's calculations indicate that the contribution
of the quadrupole moments to the electric field and field
gradient amount to less than 1% and hence the expansion (III-36)
can be terminated after the dipole term. Furthermore the
Al- and P-ions are assumed to have negligible dipole and
quadrupole moments compared to the O-ions on account of their
near tetrahedral environment.

The summation in (III-36) over all ions B can be written
in simplied form by collecting all dipole terms which are due
to symmetry related O-ions. The dipoles of two equivalent ions
B and B' are related by a linear transformation as follows

$$d_i^{B'} = \sum_{j=1}^{3} a_{ij} d_j^{B} \qquad (i = 1,2,3). \qquad \text{(III-37)}$$

Assuming that the dipole of the ion B is induced by the local
electric field one can write

$$d_i^{B} = \alpha^{B} E_i^{B} \qquad (i = 1,2,3) \qquad \text{(III-38)}$$

where α^{B} is the dipole polarizability which is assumed to be
scalar.

By substituting (III-38) into (III-37) and (III-37)
into (III-36) and dropping the quadrupolar term in (III-36) one
obtains the following set of simultaneous linear equations for
the components of the electric field at the sites of the two
inequivalent oxygen atoms O(1) and O(2) in the unit cell of
$AlPO_4$:

$$E_k^{O(1)} = E_k^{O(1)}(M) + \alpha^{O(1)} \sum_{i=1}^{3} H_{ki}^{O(1)O(1)} E_i^{O(1)} + \alpha^{O(2)} \sum_{i=1}^{3} H_{ki}^{O(1)O(2)} E_i^{O(2)}$$

$$E_k^{O(2)} = E_k^{O(2)}(M) + \alpha^{O(1)} \sum_{i=1}^{3} H_{ki}^{O(2)O(1)} E_i^{O(1)} + \alpha^{O(2)} \sum_{i=1}^{3} H_{ki}^{O(2)O(2)} E_i^{O(2)}$$

$$(III-39)$$

where

$$E_k^A(M) = - \sum_B \frac{q^B X_k^B}{r_{A,B}^3} \qquad (III-40)$$

is the k'th cartesian component of the monopole electric field at site A and the summation $\sum_B$ extends over all ions in the lattice and k = 1,2,3.

The tensors $(H_{ij}^{O(1)O(2)})$ and $(H_{ij}^{O(2)O(1)})$ are the transpose of one another

i.e. $(H_{ij}^{O(1)O(2)}) = (H_{ji}^{O(2)O(1)})$

which leaves the three independent tensors $(H_{ij}^{O(1)O(1)})$, $(H_{ij}^{O(1)O(2)})$, and $(H_{ij}^{O(2)O(2)})$ with (i,j = 1,2,3) to be calculated by lattice summation. One can now proceed to solve equations (III-39) for the self-consistent electric fields $\vec{E}^{O(1)}$ and $\vec{E}^{O(2)}$ and hence calculate the dipoles of the O(1) and O(2) ions using (III-38). The dipolar polarizability is known from Schwarzenbach's work.

7. Effects of Thermal Lattice Vibrations on the Spin-Hamiltonian Parameters.

In view of the strong temperature dependence of the thermal ellipsoid data observed in quartz (Young, 1962) one must examine to what extent the spin-Hamiltonian parameters b_n^m depend

on lattice vibrational effects. Assuming, as was done in the present case, that the zero-field splitting is adequately described by the Blume-Orbach mechanism, the b_n^m's are sensitive to the thermally generated fluctuations in interionic distances through the crystalline potential. One therefore expects that the spin-Hamiltonian parameters reflect the time dependence of the displacements of the ions from their equilibrium positions insofar as, at each instant in time, the appropriate b_n^m's correspond to a distorted lattice in which the ions are held fixed in their instantaneous positions. This picture is valid provided that the dynamic deviations of the ions from their lattice sites can be treated as if they were static distortions of the lattice (adiabatic approximation). This assumption is clearly justified since the wave functions used in calculating the b_n^m's differ in energy by several thousand cm^{-1} whereas typical phonon frequencies rarely exceed a few hundred cm^{-1} and therefore the electronic wave functions can be assumed to respond instantaneously to any lattice deformation. In the case of Mn^{2+} in MgO the maximum instantaneous variation of the zero-field splitting due to thermally generated fluctuations in interionic distances is estimated to be of the order of 1 cm^{-1} (Walsh et al, 1965). This however corresponds to typical Zeeman energies and the resulting E.P.R. spectrum would be smeared out over a magnetic field range which is of the order of typical observation fields and hence the spectrum would

become unobservable. The fact that spectra are nevertheless observed under such conditions is a result of motional narrowing. The condition for motional narrowing can be expressed in simplified form as

$$\tau < \frac{h}{\Delta E}$$

(Pake, 1962), where τ is the duration of the applied perturbation and ΔE is the resulting shift in the magnetic energy level. Since the perturbation in the present case consists of thermal fluctuations in the interionic distances which have frequencies of several hundred cm^{-1}, and ΔE, the resulting change in zero-field splitting, is only of the order of $1\ cm^{-1}$, motional narrowing is always present in solids.

The experimentally observed spin-Hamiltonian is therefore not the one which is appropriate for the rigid lattice but one which is obtained from the "instantaneous spin-Hamiltonian" by time-averaging over periods which are long compared to a lattice vibrational period. Furthermore, since the Blume-Orbach mechanism is linear in the crystalline potential, the time-averaging can be applied directly to the crystal field operator $V(\vec{R})$. Following the approach of Walsh, Jeener, and Bloembergen (1965) the crystal field operator is expanded to second order in the displacements $\vec{\delta r}(k) = [\delta x_1(k),\ \delta x_2(k),\ \delta x_3(k)]$ of the magnetic ion's Z effective neighbours at $\vec{r}(k)$ where $(k = 1, 2, 3 \ldots Z)$.

$$V(R) = V_o + \sum_{k=1}^{z} \sum_{i=1}^{3} \frac{\partial V}{\partial x_i(k)} \cdot \delta x_i(k)$$

$$+ \frac{1}{2} \sum_{k=1}^{z} \sum_{i,j=1}^{3} \frac{\partial^2 V}{\partial x_i(k) \partial x_j(k)} \delta x_i(k) \delta x_j(k) \qquad \text{(III-41)}$$

where $\vec{R}$ is the position vector of the magnetic ion, V_o is the potential of the rigid lattice, and such terms as $\frac{\partial^2 V}{\partial x_i(m) \partial x_j(n)}$ vanish. Strictly speaking, the expansion should be in terms of the deviations of the interionic distances, i.e. in terms of $\delta(\vec{r}(k)-\vec{R})$, and the derivatives should be taken with respect to the interionic distances $(\vec{r}(k)-\vec{R})$. However, in order to make use of the results of crystallographic structure refinements it is necessary to obtain an expression in terms of the mean square displacements of the ions from their equilibrium positions. Upon time-averaging (III-41) odd powers in the components of $\vec{\delta r}(k)$ drop out and the averaged crystalline potential becomes

$$\overline{V(\vec{R})} = V_o + \frac{1}{2} \sum_{k=1}^{z} \sum_{i,j=1}^{3} \frac{\partial^2 V}{\partial x_i(k) \partial x_j(k)} <\delta x_i(k) \, \delta x_j(k)>_t \quad \text{(III-42)}$$

where $< \, >_t$ denotes averaging with respect to time. By substituting

$$V(\vec{R}) = \sum_{k=1}^{z} \int \frac{\rho(\vec{r}(k)) d^3 r(k)}{|\vec{R}-\vec{r}(k)|}$$

into (III-42) and rewriting the second order terms to conform with standard quadrupolar notation one obtains

$$\overline{V(\vec{R})} = V_o + \frac{1}{2} \sum_{k=1}^{z} \sum_{i,j=1}^{3} Q_{ij}^t(k) \frac{\partial^2}{\partial x_i(k) \partial x_j(k)} \left(\frac{1}{r(k)}\right) \qquad \text{(III-43)}$$

where

$$Q_{ij}^t(k) = \frac{1}{3} \int \rho(\vec{r}(k)) d^3r(k) < 3\delta x_i(k) \delta x_j(k) - (\delta r(k))^2 >_t$$

$$= \frac{1}{3} \int \rho(\vec{r}(k)) d^3r(k) \int p(\vec{\delta}r(k)) [3\delta x_i(k) \delta x_j(k) - (\delta r(k))^2] d^3\delta r(k)$$

(III-44)

and $p(\vec{\delta}r(k))$ is the probability that the nucleus of the k'th ion is displaced from its equilibrium position by $\vec{\delta}r(k)$.

Since the quadrupole Q_{ij}^o in the expansion (III-34) of V_o has the same coefficient as Q_{ij}^t it is natural to combine the two quadrupolar terms and write

$$\overline{V(\vec{R})} = \sum_{k=1}^{z} [\frac{q_k}{r_o(k)} + \sum_{i=1}^{3} d_i(k) \frac{\partial}{\partial x_i(k)} (\frac{1}{r(k)})_{r=r_o}$$

$$+ \sum_{i,j=1}^{3} \{Q_{ij}^o(k) + Q_{ij}^t(k)\} \frac{\partial^2}{\partial x_i(k) \partial x_j(k)} (\frac{1}{r(k)})_{r=r_o}] \quad \text{(III-45)}$$

where q_k, $d(k)$ and $r_o(k)$ are the electronic charge, the electric dipole, and the equilibrium position respectively of the k'th ion. It is now apparent that the quadrupole moment of the k'th ion is made up of two components: one due to its non-spherical electronic charge distribution around the nucleus, and one due to the thermal motion of the nucleus around the equilibrium lattice site. Moreover, it can be shown (Schwarzenbach 1966) that the total quadrupole $Q_{ij}(k)$ can be written as

$$Q_{ij}(k) = \iint [3R_i(k)R_j(k)-R^2(k)]\rho(\vec{R}(k)-\vec{\delta}R(k))p(\delta\vec{R}(k))\cdot d^3R(k)d^3\delta R(k)$$

$$(III-46)$$

This expression states that Q_{ij} is the quadrupole due to a charge distribution which is described by the convolution of $\rho(\vec{R})$ with $p(\vec{R})$. This, however, is precisely the assumption which is made in carrying out a structure refinement in x-ray crystallography (Cochran, 1954). Moreover, in structure refinements with anisotropic temperature factors it is also assumed that $p(\vec{\delta}R)$ is a 3-dimensional Gaussian of the following form

$$p(\vec{\delta}R) = \frac{\exp(-\frac{1}{2}\sum\limits_{i=1}^{3}\frac{\delta R_i^2}{\overline{u_i^2}})}{\sqrt{(2\pi)^3\overline{u_1^2}\,\overline{u_2^2}\,\overline{u_3^2}}}$$

$$(III-47)$$

where $\vec{\delta}R = [\delta R_1, \delta R_2, \delta R_3]$ is the displacement of the nucleus from its equilibrium position along the three principal axes of the thermal ellipsoid and $\overline{u_i^2}$ are the mean square displacements along these directions. By substituting (III-47) into (III-46) the quadrupoles become (Schwarzenbach, 1966).

$$Q_{ij}(k) = Q_{ij}^O(k) + q(k)\,(\overline{u_i^2} - \frac{1}{3}\sum\limits_{i=1}^{3}\overline{u_i^2})\quad \text{for } i=j$$

$$= Q_{ij}^O(k)\qquad\qquad \text{for } i\neq j.\qquad (III-48)$$

By making use of the results of the structure refinement it is therefore possible to obtain the magnitude and orientation of the thermally generated quadrupoles. Each quadrupole can be

represented by point charges which are situated along the principal axes of the thermal ellipsoids. This procedure then allows direct use of the lattice summation formulas (III-5) which sum over all discrete charges in the lattice, in order to obtain the values of the crystal field coefficients $B_{\ell m}$.

CHAPTER IV

EXPERIMENTAL APPARATUS AND RESULTS

1. Spectrometer and Cavity Assembly

All E.P.R. measurements were carried out in the 8 mm microwave band using a Varian model V-4503 spectrometer. The spectrometer was of the balanced bridge type and could be operated to detect either the absorption or the dispersion signal. The klystron frequency was stabilized on the sample cavity by automatic frequency control (AFC) using a modulation frequency of 10 kHz. The E.P.R. signal was observed by employing 100 kHz magnetic field modulation and phase sensitive detection. The D.C. magnetic field was provided by a Varian 15" electromagnet which was mounted on a rotating base and was fed by a Varian Fieldial Mark II power supply. After initially calibrating the magnet power supply by nuclear magnetic resonance, the value of the magnetic field was read off the field selector dial to an accuracy of better than 0.1%. The magnet was capable of delivering a maximum field of approximately 23 kOe when a 2" air gap was used.

The use of high frequency magnetic field modulation meant that special techniques had to be employed to ensure that the magnetic field modulation could penetrate the cavity walls. At a frequency of 100 kHz the skin depth for good

55

Figure IV-0

    Heated cavity assembly used at 35 GHz.
(1) Stainless steel waveguide; (2) water-cooled
outer jacket; (3) alumina cylinder; (4) annular
slots in cavity walls; (5) bifilarly wound No. 18
Kanthal heater wire; (6) TE 011 copper cavity;
(7) refractory cement; (8) lock nut; (9) variable
frequency tuning plunger; (10) chromel/alumel thermo-
couple and 1/16" ceramic thermocouple insulation.

WATER
OUT

1

2

3

4

5

6

7

8

9

10

WATER IN
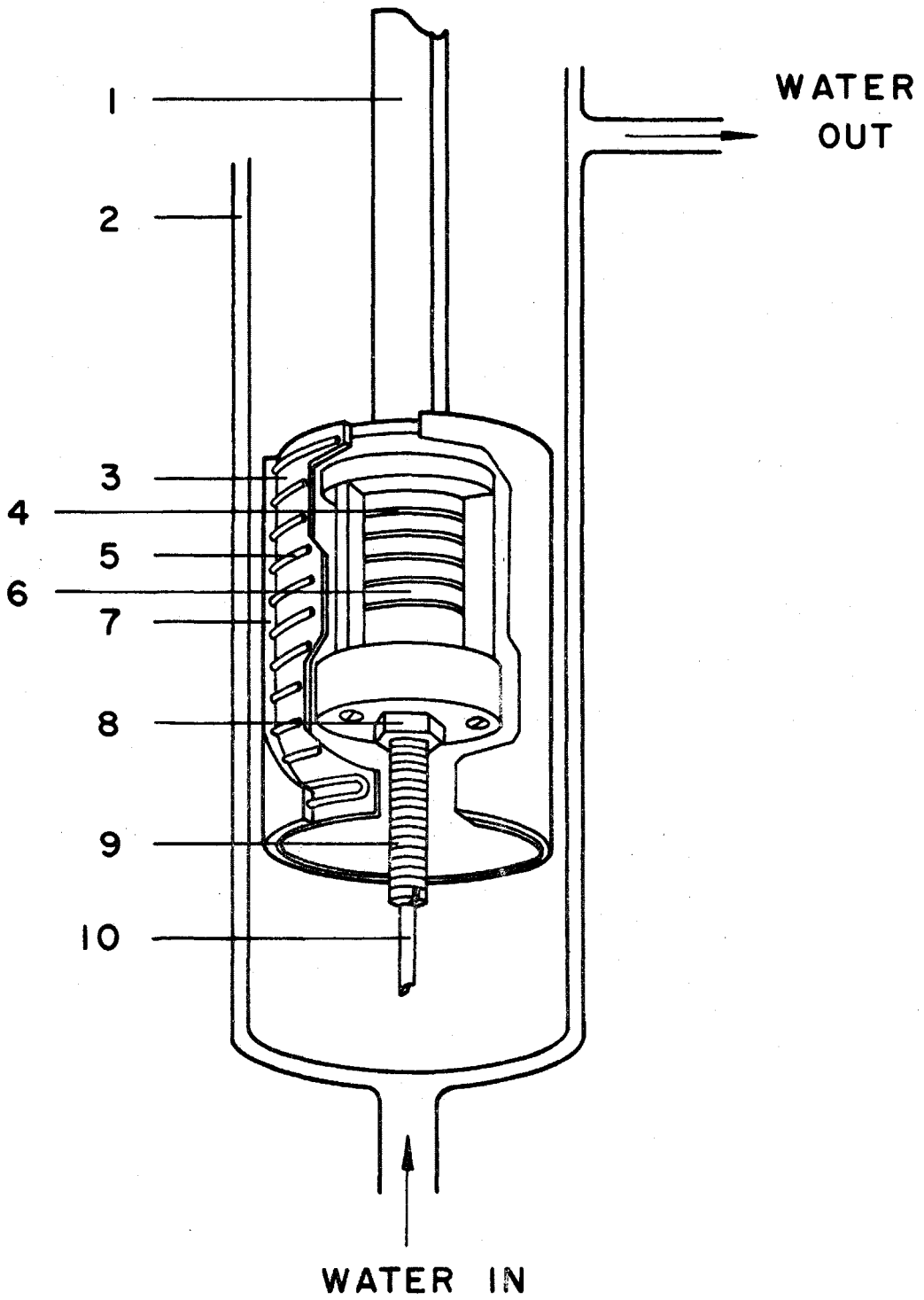
conductors is only a few tenths of a millimeter. For the low temperature E.P.R. measurements a silver-plated glass cavity was used. For the high temperature experiments a cylindrical TE 011 copper cavity was constructed. Annular slots of 0.5 mm width were machined into the cavity walls to permit entry of the 100 kHz modulation into the cavity. This configuration of the slots did not interfere with the microwave induced surface currents in the cavity walls and had the additional merit of suppressing the eddy currents in the cavity walls which were induced by the magnetic field modulation. Measurements of the 100 kHz modulation inside the cavity indicated that the modulation amplitude was attenuated by approximately a factor of two upon passage through the cavity walls. The cavity was continuously tunable, had an I.D. of 0.455" and an unloaded Q of approximately 7000.

The entire cavity was heated by a furnace consisting of a coil of non-inductively wound No. 18 Kanthal wire which was potted onto the outside of an alumina cylinder with refractory cement. The entire cavity assembly was inserted into a pyrex glass cylinder which was provided with a water cooled jacket at its lower end to protect the magnet pole pieces from the heat generated by the furnace. The glass cylinder was inserted into the 2" air gap between the pole pieces and evacuated to a pressure of approximately 10 microns in order to prevent oxidation of the copper cavity and to

eliminate thermal convection currents. The temperature of the sample was monitored with a No. 36 chromel/alumel thermocouple. The e.m.f. generated was measured with a Croyden potentiometer to a precision of 10 μ volts, which corresponded to 1/4°C. Uncalibrated thermocouples were used throughout because absolute temperature measurements in the presence of a variable magnetic field would have unduly complicated the experiments without yielding significant new information. The thermocouple was embedded in 1/16" O.D. ceramic thermocouple insulation and was inserted into the cavity through a central bore in the tuning plunger. The top end of the thermocouple served as the sample holder onto which oriented samples were mounted by use of a jig and held in place with Sauereisen cement. This arrangement ensured that the temperature was measured right at the sample. The cylindrical heater around the cavity was fed by a voltage/current regulated D.C. power supply and temperatures of up to 650°C could be obtained at a power output of 200 watts. The short term temperature stability at the sample was approximately 1/4°C at 600°C.

2. Samples

Doped single crystals of $AlPO_4$ were grown hydrothermally according to a method developed by Stanley (1954). The reagents were purified $AlPO_4$ powder supplied by Fischer Scientific Co., reagent grade phosphoric acid, and doubly distilled water. A solution was prepared by dissolving 55

grams of $AlPO_4$ in 160 ml of 56% (by weight) H_3PO_4 and by adding the appropriate amount of dopant in the form of $Fe(OH)_3$. The solution was then filtered through a fine Buchner type funnel and poured into 50 ml pyrex glass bottles which were sealed and placed in a steel autoclave. A small amount of water in the autoclave ensured equilization of vapour pressures inside and outside the glass bottles. Crystallization occurred as a result of the retrograde solubility curve of $AlPO_4$ in phosphoric acid. The autoclave was placed in a temperature regulated oven and heated to the crystallization temperature of 147°C. The temperature was increased linearly at a rate of 0.5°C per 24 hours. This was achieved by bucking the thermocouple voltage against a linearly swept reference voltage and using the difference voltage as an error signal. This error signal was fed into a Hewlett Packard null detector whose output was connected to an on/off relay which switched the power to the oven. After a period of up to 6 weeks clear, colourless crystals of a mean diameter of 2 to 8 mm were obtained. Undoped crystals showed only E.P.R. signals of negligible intensity near g = 2 whereas the E.P.R. signals from doped crystals indicated that concentrations of up to 5000 p.p.m. had been obtained.

After each high temperature experiment during which the sample temperature was raised to approximately 600°C it was noted that the specimens had turned milk white and com-

pletely opaque. It has been suggested by J. F. Scott
(private communication), and to some extent experimentally
verified, that this effect is due to nucleation of water
droplets which are estimated to be about 2000 $\overset{o}{A}$ in diameter.

All quartz samples used in this study were grown
hydrothermally by Sawyer Research Products Inc., East Lake,
Ohio, and contained up to 700 p.p.m. of iron. Other oriented
samples, also originating from the above source, were kindly
supplied by Dr. L. M. Matarrese of the U.S. National Bureau
of Standards, Boulder, Colorado. According to extensive
earlier work by Matarrese, Wells, and Peterson (1969) only
samples cut from brown regions of a larger crystal, which
consisted of regions varying in colour from green to yellow
and brown, gave rise to a predominant five-line spectrum of
well-behaved angular dependence. For this reason only specimens
of synthetic brown quartz were used in this study.

3. E.P.R. Spectra in $AlPO_4:Fe^{3+}$

E.P.R. measurements in $AlPO_4$ were carried out on
samples containing iron in concentrations of 1000 p.p.m. and
5000 p.p.m. At these concentrations dipolar broadening can
be expected to contribute significantly to the widths of the
resonance lines. However, in the present case, the observed
linewidths were the same for both the 1000 p.p.m. and the
5000 p.p.m. samples. It therefore appears that the observed

Figure IV-1

      Angular dependence of the resonant magnetic field values of the E.P.R. spectrum of Fe^{3+} in $AlPO_4$ in plane perpendicular to the c-axis.
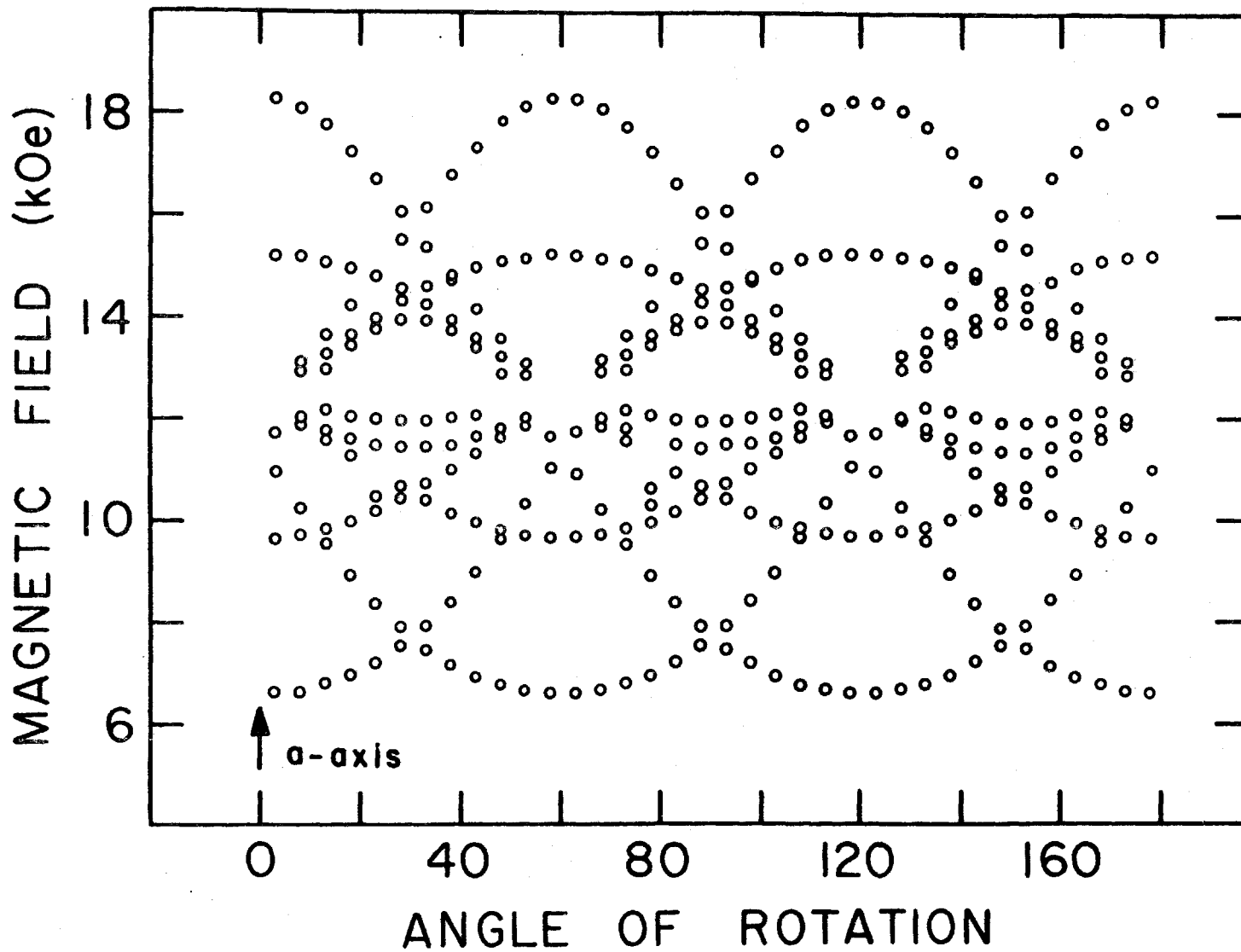
line width was primarily caused by inhomogeneities in the crystalline field rather than by the interaction between paramagnetic impurities. At room temperature the linewidths were 5, 8, and 10 Oe for the $-\frac{1}{2} \rightarrow +\frac{1}{2}$, $\pm\frac{3}{2} \leftrightarrow \pm\frac{1}{2}$, and the $\pm\frac{3}{2} \leftrightarrow \pm\frac{5}{2}$ transitions respectively. No evidence of hyperfine structure was detected.

When the magnetic field was rotated about the c-axis a spectrum of three equally intense sets of five lines was observed. Fig. (IV-1) shows the angular dependence of the spectrum. It can be seen that the spectrum repeats every 60 degrees and that the extrema in the resonant fields occur whenever $\vec{H}$ is parallel to one of the twofold axes a_1, a_2, a_3, where a_1 is the a-axis and a_2 and a_3 are generated from a_1 by the triad screw axis. The total spectrum thus appeared to be made up of three individual five-line spectra. Each five-line spectrum displayed an angular dependence that is typical of an Fe^{3+} ion in an orthorhombic field. It therefore appears that the iron impurities occupy three distinct lattice sites. For the purpose of describing the spectra it is convenient to denote the occupied sites as site I, II, and III. Apart from the five-line Fe^{3+} spectra there were also six narrow lines of moderate intensity which remained stationary near the magnetic field value corresponding to g = 2. These lines were attributed to the $-\frac{1}{2} \rightarrow \frac{1}{2}$ transition of Mn^{2+} and were of no consequence in the present study.

Figure IV-2

Angular dependence of the resonant magnetic field values for the $\pm 5/2 \longleftrightarrow \pm 3/2$ transitions of Fe^{3+} in $AlPO_4$ in the (c,a)-plane. The circles represent the spectrum due to site I and the dots represent the spectra due to sites II and III.
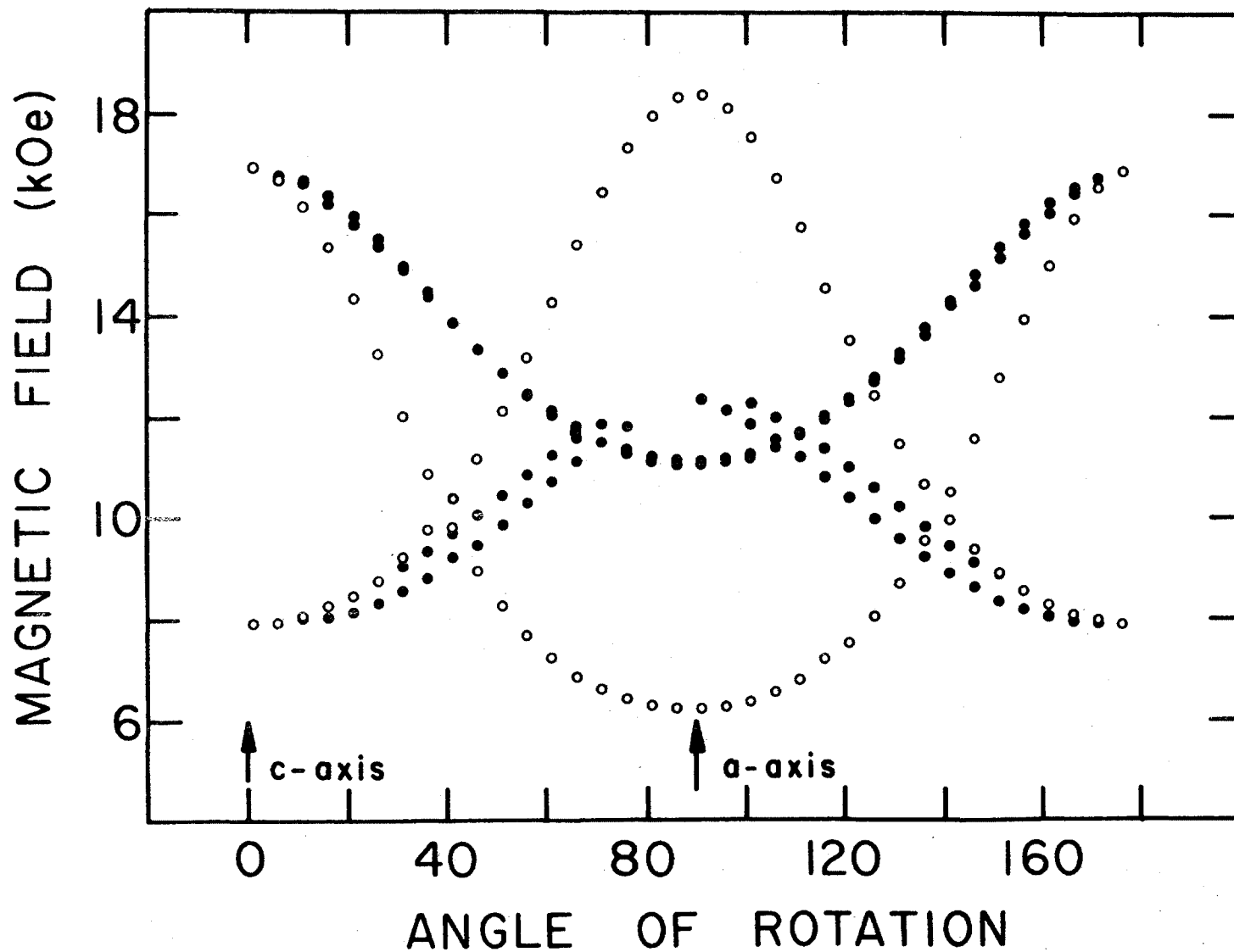
Figure IV-3

        Angular dependence of the resonant magnetic
field values for the $\pm 5/2 \longleftrightarrow \pm 3/2$ transitions of
Fe^{3+} in $AlPO_4$ in the plane perpendicular to the a-
axis. The circles and dots represent the spectrum
due to site I and the spectra due to sites II and
III respectively. The uncertainty of the sign of
the $\vec{c} \times \vec{a}$ direction arose because the direction of $\vec{a}$
was only known up to a sign.
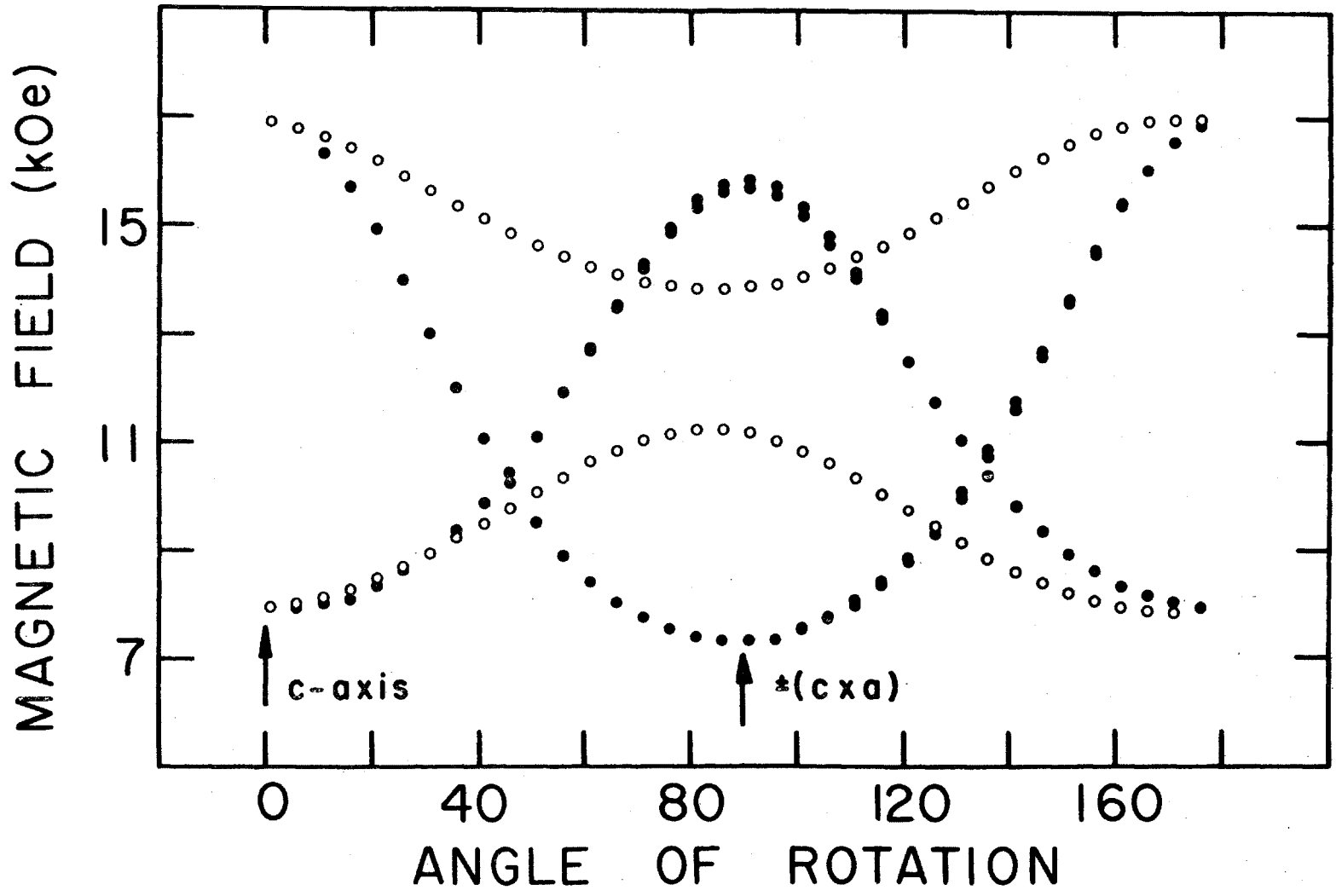
When $\vec{H}$ was rotated about the $\vec{a} \times \vec{c}$ axis the angular pattern shown in Fig. (IV-2) was obtained. It consists of the resonant field values for the $\pm \frac{5}{2} \longleftrightarrow \pm \frac{3}{2}$ transitions of Fe^{3+} at sites I, II, and III. It is noted that the extremal positions of the resonant field values for site I occur for $\vec{H}$ parallel to $\vec{a}$. Recalling that the extrema for the plane perpendicular to $\vec{c}$ occurred also for $\vec{H}$ parallel to $\vec{a}$ it follows that the twofold a-axis is a magnetic axis. The paramagnetic centers must therefore be located on the twofold a-axes a_1, a_2 and a_3. Moreover, since the three five-line spectra are related by a threefold rotation about the c-axis, the occupied sites on the twofold axes must be equivalent. This conclusion is also borne out by the fact that the three five-line spectra coincide for $\vec{H}$ parallel to $\vec{c}$. It is therefore sufficient to study only the Fe^{3+} spectrum of site I. Two of the three magnetic axes must lie in the plane perpendicular to $\vec{a}$ because the C_2 symmetry of the occupied site constrains one magnetic axis to lie along the a-axis. The angular dependences of the $\pm \frac{3}{2} \longleftrightarrow \pm \frac{5}{2}$ transitions in the plane perpendicular to $\vec{a}$ are shown in Fig. (IV-3). It is noted that the spectra for sites II and III are nearly superimposed in the entire 180-degree range of rotation. Close examination of the resonant field values in the region of the extremal positions of the spectrum for site I revealed that the maxima and minima for each of the five transitions occurred along slightly different directions. Moreover, the angle between the maximum and minimum positions

Figure IV-4

Angular dependence of the $-5/2 \rightarrow -3/2$ (bottom) and $3/2 \rightarrow 5/2$ (top) transitions of Fe^{3+} in $AlPO_4$ in the plane perpendicular to the a-axis for temperatures ranging from 11° to 551°C.
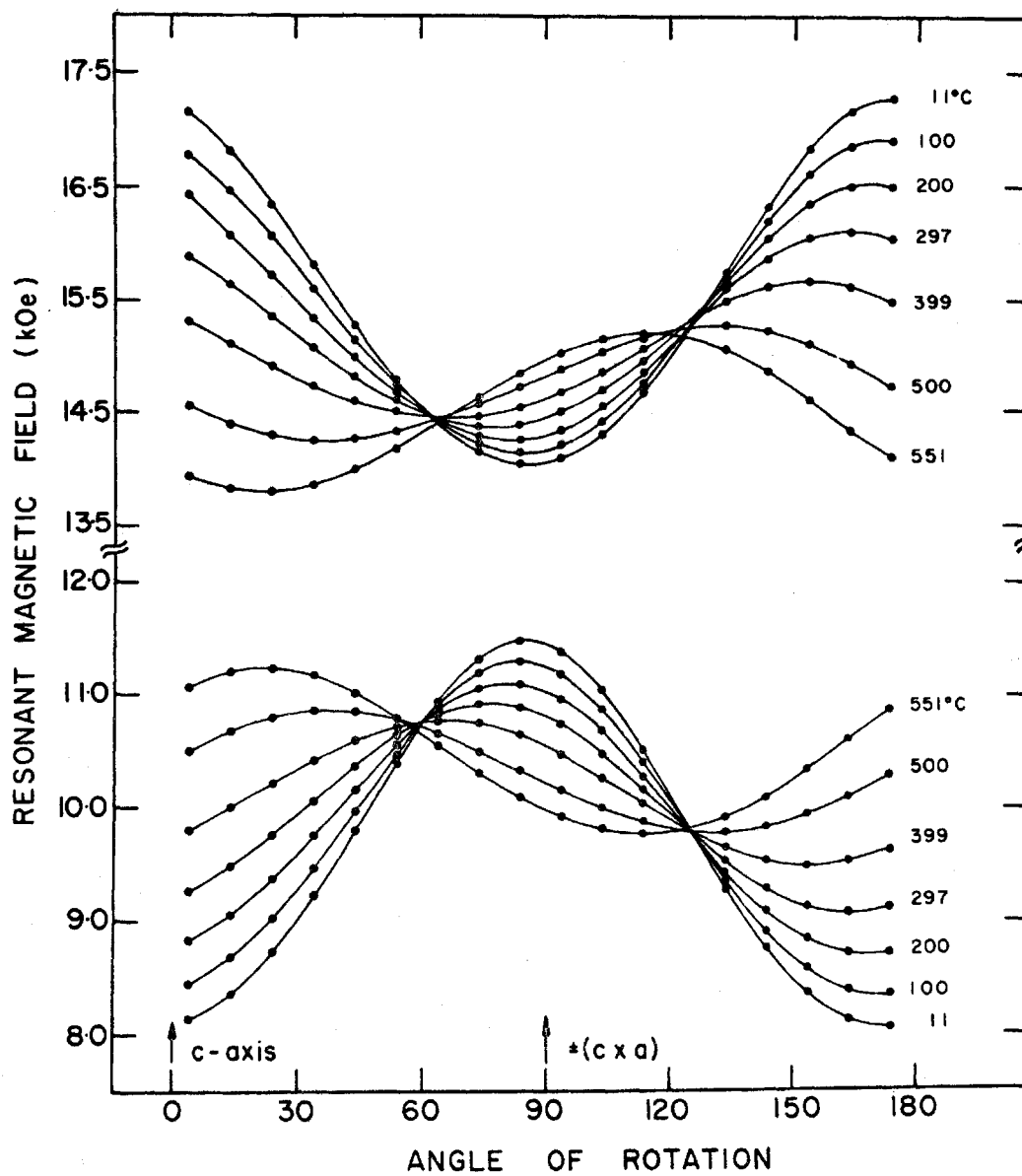
Figure IV-5

Angular dependence of the $-3/2 \leftarrow -1/2$ (bottom) and $1/2 \to 3/2$ (top) transitions of Fe^{3+} in $AlPO_4$ in the plane perpendicular to the a-axis for temperatures ranging from 11° to 551°C.
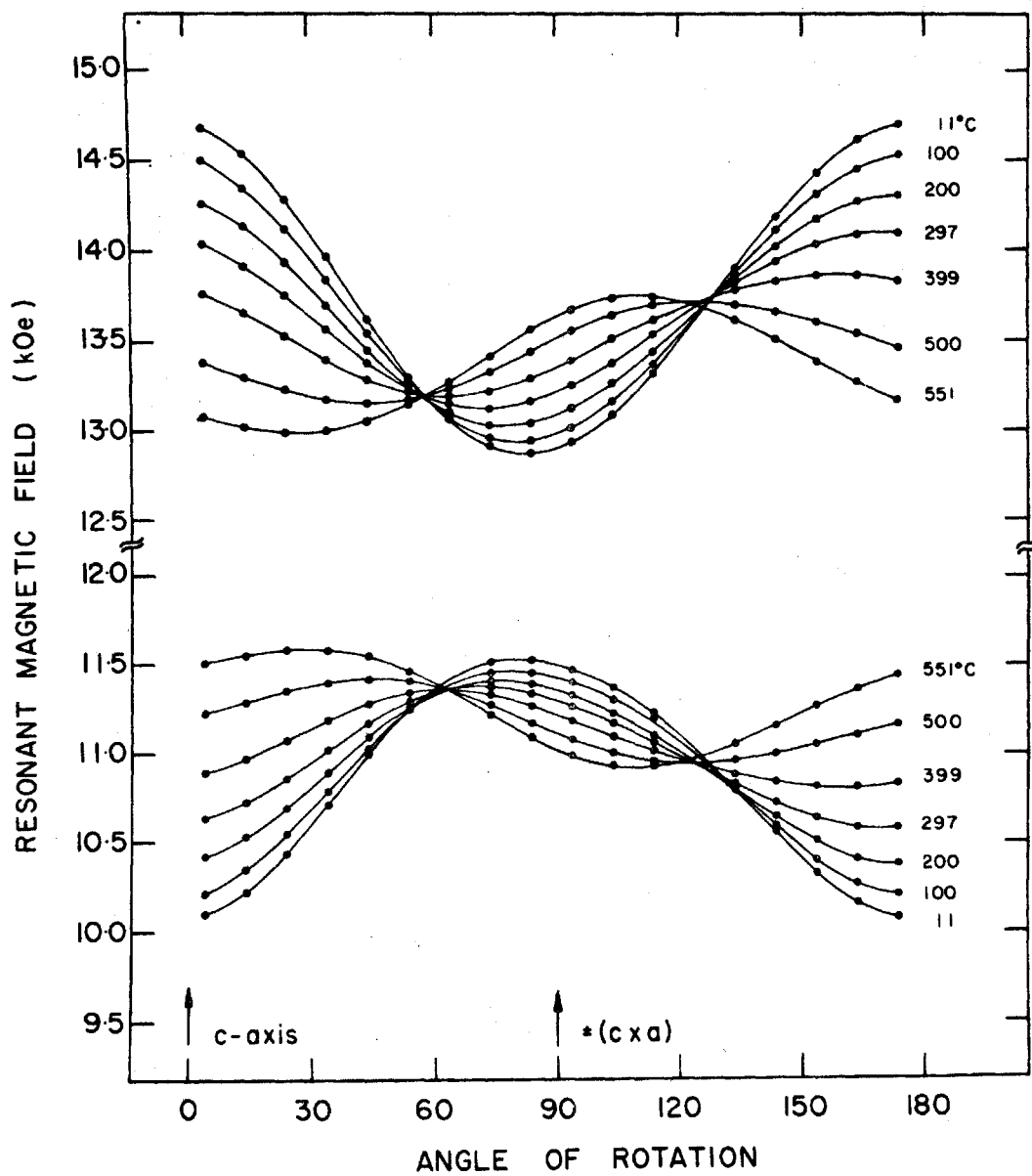
of the resonant fields for the same transition was slightly different from 90 degrees. The occurrence of such irregular "off-axis extrema" can be explained in terms of a generalized spin-Hamiltonian as discussed below (Section 5).

Temperature-dependent studies of the E.P.R. spectrum were carried out from 4.2° to 863°K. The data at 4.2°K were taken primarily for the purpose of determining the absolute signs of the spin-Hamiltonian parameters. The temperature variation of the angular dependence of the spectrum was investigated in the plane perpendicular to $\vec{a}$ and for $\vec{H}$ parallel to $\vec{a}$. The resonant field values of the $\pm \frac{5}{2} \longleftrightarrow \pm \frac{3}{2}$ transitions are shown in Fig. (IV-4) for temperatures in the range of 11° to 551 C. Fig. (IV-5) shows the resonant fields of the $\pm \frac{3}{2} \longleftrightarrow \pm \frac{1}{2}$ transitions for the same temperature range.

Above 550°C the onset of extensive line broadening resulted in severe loss of signal intensity so that the spectrum could no longer be observed in the entire 180-degree range of rotation. The angular range over which the line positions could be measured reliably became smaller as the phase transition was approached. Nevertheless it was possible to determine the spin-Hamiltonian parameters from the available data except in a region of 4 degrees above and below the transition temperature where it was not possible to take a sufficient number of measurements.

The temperature variation of the angular dependence of the spectrum in the plane perpendicular to $\vec{a}$ can be qualitatively

Figure IV-6

Temperature dependence of thé resonant
magnetic field values of Fe^{3+} in $AlPO_4$ for $\vec{H}$ parallel
to the a-axis.
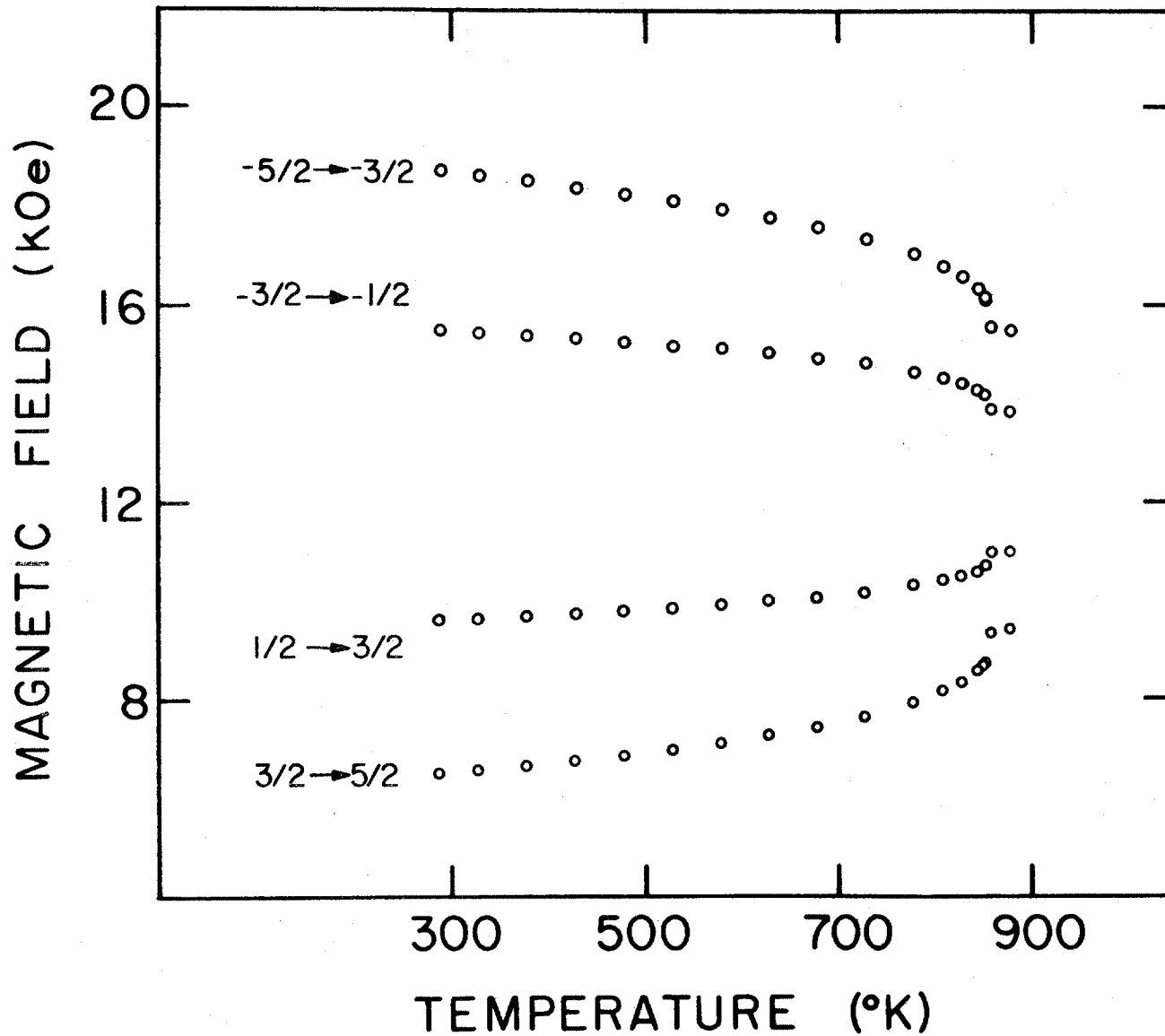
described as follows:

1. The difference between the maximum and the minimum reso-
   nant field values of a given transition shows an initial
   decrease, passes through a minimum near 750°K, and then
   rises sharply to its β-phase value. This difference is
   a rough measure of the spin-Hamiltonian parameter b_2^2.

2. The mean value of the resonant magnetic field of a given
   transition over the 180-degree range of rotation decreases
   at an increasing rate as the phase transformation is
   approached. This mean value is a rough measure of the
   spin-Hamiltonian parameter b_2^0.

3. The direction of the extremal positions of the resonant
   field values which roughly corresponds to the orientation
   of the second order rhombic component of the spin-Hamiltonian
   shows a rotation of approximately 85° between room tem-
   perature and the transition point.

The temperature dependence of the resonant field values for
the $\pm \frac{5}{2} \longleftrightarrow \pm \frac{3}{2}$ and the $\pm \frac{3}{2} \longleftrightarrow \pm \frac{1}{2}$ transitions for $\vec{H}$ parallel
to $\vec{a}$ are shown in Fig. (IV-6).

   A careful search for hysteresis effects was undertaken
in the immediate vicinity of the transition temperature T_o.
As the sample was allowed to drift through the temperature
region $T_o \pm 0.5°C$ the $\frac{1}{2} \rightarrow \frac{3}{2}$ transition could be observed in
both its α- and β-phase position. The temperature at which
both lines were equally intense was the same both on going

Figure IV-7

Room temperature resonant magnetic field
values of the $-5/2 \to -3/2$ transition of Fe^{3+} in a
specimen of $AlPO_4$ which was heated above the α-β
phase transformation temperature.
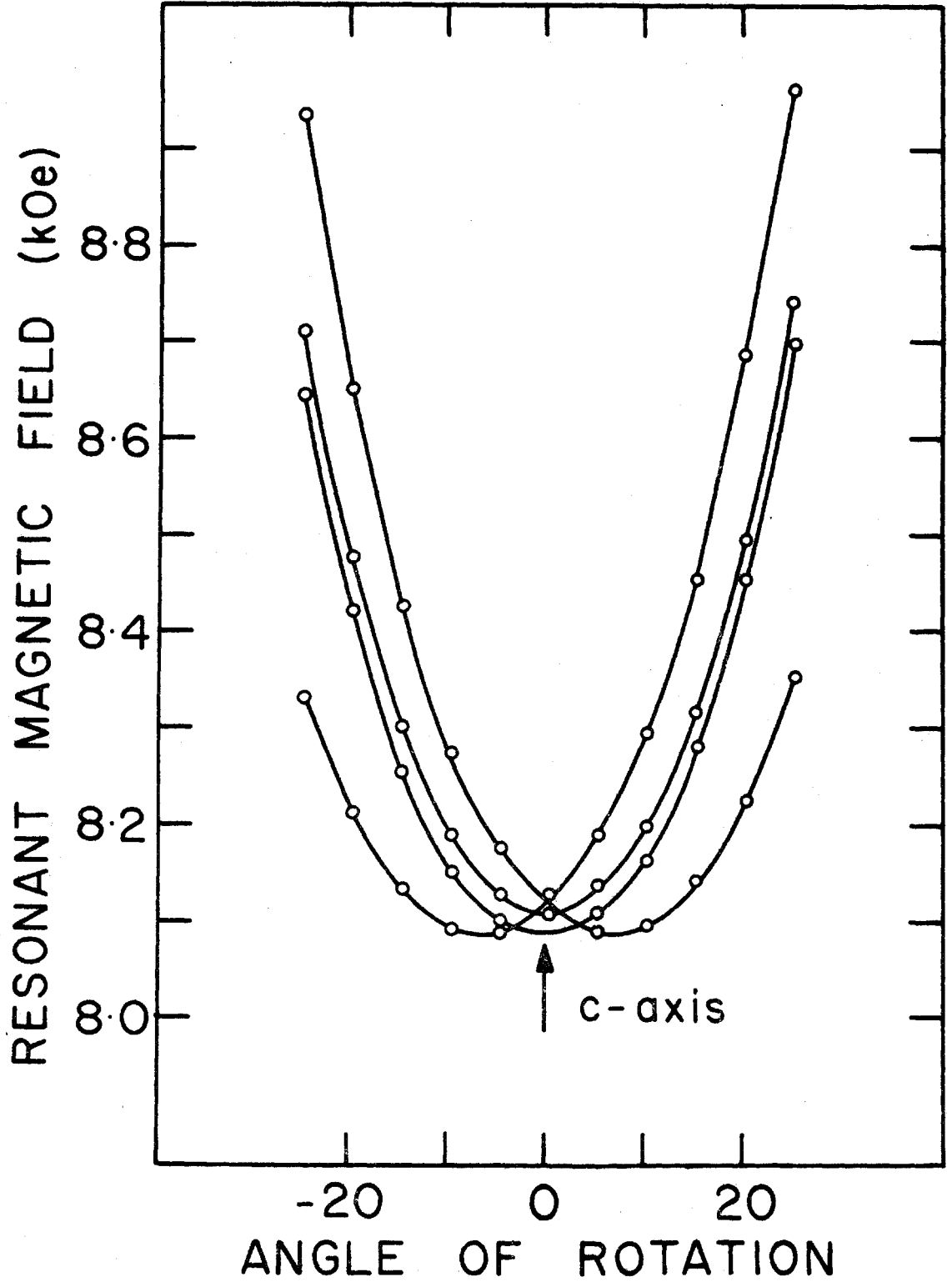
from the α- to the β-phase and vice versa. If this temperature

is taken as the transition temperature any hysteresis in the

transition temperature must have been smaller than 0.1°C

in order to remain undetected. 0.1°C is the precision of

the temperature measurements. The absence of a sizable tempera-

ture hysteresis is in contradicition with the findings of Troccaz

et al (1967) who reported a hysteresis of 7° ± 2°C for undoped

crystals of $AlPO_4$.

Several specimens were tested in order to determine

whether the E.P.R. spectra were reversible. The sample tempera-

ture was cycled over different ranges varying from a few de-

grees to several hundred degrees centigrade. It was found that

the spectral lines always appeared at the same resonant fields

with their original intensity. It can therefore be concluded

that the changes of the spin-Hamiltonian parameters as a

function of temperature as well as the intensity of the spec-

trum are reversible. However once a sample was heated above

the transition temperature it was irreversibly twinned.

Examination of the spectra in twinned specimens showed that

the number of spectra had doubled. Furthermore, the rotational

pattern of the three new five-line spectra was related to

that of the original spectra by a twofold rotation about the

c-axis. Fig. (IV-7) shows the resonant field values for

the $-\frac{5}{2} \rightarrow -\frac{3}{2}$ transition in the vicinity of the c-axis.

It is seen that the extremal positions are symmetrically

located about the c-axis. This indicates that the twinning

Figure IV-8

Angular dependence of the $-5/2 \rightarrow -3/2$
(bottom) and $3/2 \rightarrow 5/2$ (top) transitions of Fe^{3+}
in synthetic brown quartz in the plane perpendicular
to the a-axis for temperatures ranging from 13°
to 450°C.
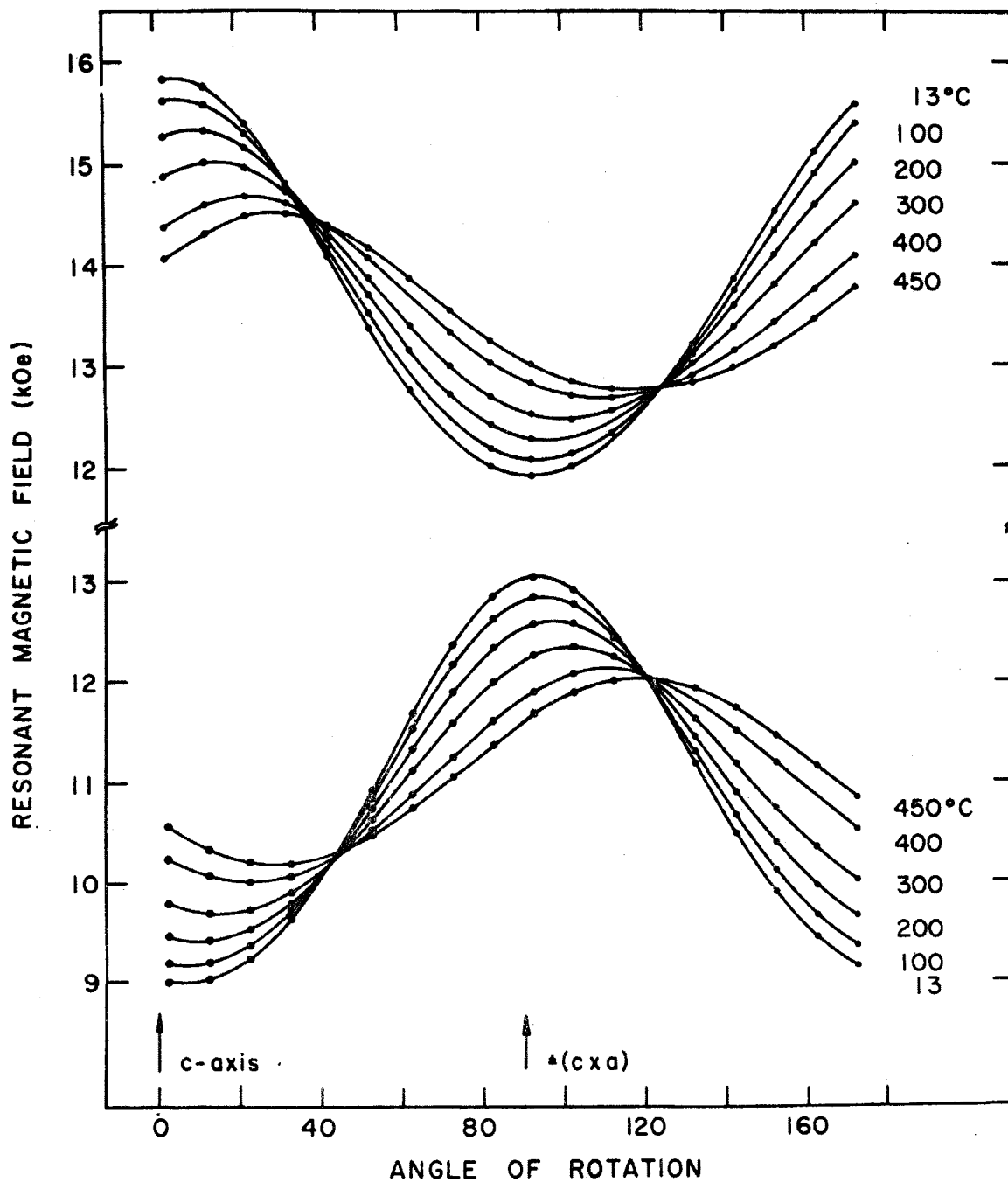
Figure IV-9

      Angular dependence of the $-3/2 \rightarrow -1/2$ (bottom)
and $1/2 \rightarrow 3/2$ (top) transitions of Fe^{3+} in synthetic
brown quartz in the plane perpendicular to the a-axis
for temperatures ranging from 13° to 450°C.
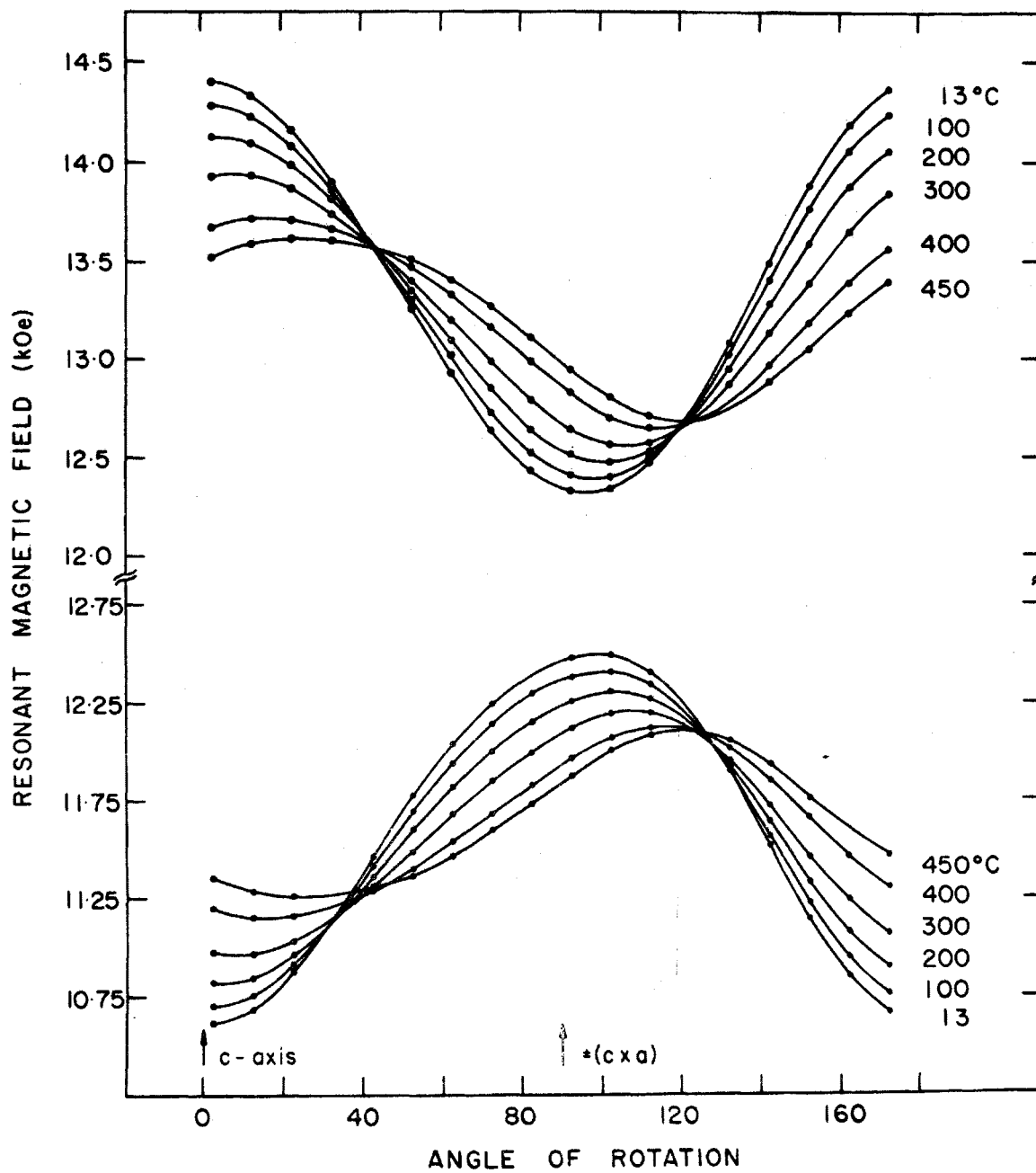
was of the Dauphiné type. A slight difference in intensity of the Dauphiné related spectra showed that the Dauphiné twin which was originally present predominated.

The width of the E.P.R. lines increased sharply as the phase transformation temperature T_o was approached from above and from below. Figure IV-17 shows the temperature dependence of the line width for the $\frac{1}{2} \to \frac{3}{2}$ transition for $\vec{H}||\vec{a}$. The peak itself has a half-width of approximately 3°C. The maximum line width occurred at the same temperature as the discontinuity in the resonant magnetic field. This discontinuity defines the transformation temperature. Unfortunately it was not possible to study the angular dependence of the line width because, near T_o, the $\pm\frac{1}{2} \longleftrightarrow \pm\frac{3}{2}$ transitions could only be observed over a small angular range of the magnetic field rotation on account of the decreasing signal intensity as $\vec{H}$ was rotated away from $\vec{a}$. The symmetric shape of the peak suggests that the same broadening mechanism is operative on either side of the transformation temperature. This observation appears to exclude Dauphiné twinning as a possible cause of the line broadening because the distinction between the two Dauphiné twin configurations is lost at the transformation temperature. One is therefore led to attribute the line broadening to short range disorder within a domain of a given Dauphiné configuration as discussed in section VI-3.

4. E.P.R. Spectra in Iron-doped Synthetic Brown Quartz

E.P.R. measurements in synthetic brown quartz were
carried out between room temperature and 450°C. There was no
need to take low temperature data because the absolute signs
of the spin-Hamiltonian parameters were already known from
previous work by Matarrese, Wells and Peterson (1969). These
authors made a detailed study of the room temperature spec-
trum of Fe^{3+} in synthetic brown quartz. The spectrum is
qualitatively the same as in $AlPO_4$. It follows from the
observed symmetry of the angular patterns that the Fe^{3+} ions
occupy three equivalent sites. These sites are located on
twofold axes which are parallel to the a_1, a_2, and a_3 axes.

Temperature-dependent measurements were taken in the
plane perpendicular to $\vec{a}$. The resonant field values for the
$\pm\frac{5}{2} \longleftrightarrow \pm\frac{3}{2}$ transitions and the $\pm\frac{3}{2} \longleftrightarrow \pm\frac{1}{2}$ transitions are
shown in Fig. (IV-8) and Fig. (IV-9) respectively for tempera-
tures ranging from 13° to 450°C. It is evident that the tem-
perature variation of the angular dependence of the spectra
in the plane perpendicular to $\vec{a}$ strongly resembles that of Fe^{3+}
in $AlPO_4$. Using the same terminology as was employed in the
case of $AlPO_4$, this temperature variation can be described as
follows: At 450°C the difference between the maximum and minimum

resonant field values for a given transition reached approximately half its room temperature value. The mean value of the resonant fields decreased as the transition temperature was approached. The directions of the extremal positions of the resonant field values at 450°C showed a rotation of 20 degrees from their room temperature directions.

Unlike the Fe^{3+} spectrum in $AlPO_4$, the spectrum in quartz began to decrease rapidly in signal intensity at temperatures above 400°C and all but the $-\frac{1}{2} \rightarrow \frac{1}{2}$ transition disappeared at approximately 480°C. On further heating the sample to a final temperature of 620°C it was found that the $-\frac{1}{2} \rightarrow \frac{1}{2}$ transition disappeared at 550°C, i.e. 23° below the transition temperature, and did not reappear in the β-phase. It has been suggested that the destruction of the E.P.R. spectra on heating is caused by the crystallization of nuclei of ferrous silicate (Lehmann and Moore, 1966). On cooling the sample to room temperature the Fe^{3+} spectra reappeared with all lines at their original magnetic field positions but reduced in signal intensity by approximately a factor of 40. The reappearance of the spectra is very likely a result of the decrease in line width on lowering the temperature rather than a partial restoration of the original paramagnetic centers. The disappearance of the E.P.R. spectra on heating is therefore irreversible whereas the changes in the spin-Hamiltonian parameters are reversible. Although several crystals were

heated beyond the transition temperature, no evidence of a new set of spectra was detected which might have been attributed to Dauphiné twinning.

5. Analysis of the E.P.R. Data

The spin-Hamiltonian which describes the magnetic energy levels of an Fe^{3+} ion in a crystalline environment of C_2 symmetry can be written in the following from (Vinokurov et al, 1964):

$$H = \mu_B g \vec{H} \cdot \vec{S} + \frac{1}{3} b_2^0 O_2^0 + \frac{1}{3} b_2^2 O_2^2 + \frac{1}{60} b_4^0 O_4^0 + \frac{1}{60} b_4^2 O_4^2 + \frac{1}{60} b_4^4 O_4^4 \quad (IV-1)$$

where $\vec{S} = [S_x, S_y, S_z]$ is the electronic spin operator, μ_B is the Bohr magneton, g is the isotropic "g-factor", and $\vec{H}$ is the applied magnetic field. The Z-axis of the coordinate system is parallel to the twofold axis. The O_n^m's are operator equivalents involving powers of S_x, S_y and S_z. The explicit form of the operator equivalents is given by Orbach (1961). The coefficients b_2^0, b_2^2, b_4^0, b_4^2 and b_4^4 are the spin-Hamiltonian parameters which are determined by experiment.

The choice of the twofold axis as a coordinate axis for the spin-Hamiltonian is natural because it represents a magnetic axis of the paramagnetic center insofar as all E.P.R. lines of site I have extrema along its direction. The assignment of the X and Y axes in the plane perpendicular to $\vec{a}$ is less unique because the extrema of the different magnetic resonance lines for site I do not occur along the same direc-

tion . This occurrence of irregular "off-axis extrema" indicates that the principal axes of the non-axial components of the spin-Hamiltonian do not coincide. This is not surprising because the C_2 symmetry of the occupied site constrains these extrema only to the extent that they must lie in the plane perpendicular to $\vec{a}$. A proper description of the E.P.R. spectra therefore requires a generalized spin-Hamiltonian in which the orientation of the various non-axial components is left unspecified. An analysis of the room temperature E.P.R. spectrum of Fe^{3+} in synthetic brown quartz in terms of such a generalized spin-Hamiltonian has been carried out by Matarrese, Wells, and Peterson (1969). Since the symmetry of the occupied site is the same in both quartz and $AlPO_4$ the results derived by the above authors apply also in the case of $AlPO_4$. In particular, it can be shown that the spectra for sites II and III are degenerate in the plane perpendicular to $\vec{a}$ and hence the spectra for the two sites should be superimposed for all directions of $\vec{H}$ in this plane. The small splitting which is nevertheless observed (see Fig. (IV-3)) is therefore caused by a misalignment of the sample.

In the present study the primary goal was the measurement of the temperature dependence rather than a precision determination of the spin-Hamiltonian parameters. It was therefore considered sufficient to allow only for a possible rotation of the cubic component of the form $\dfrac{C_4^o}{60} (O_4^o + 5\, O_4^4)$

with respect to the rhombic component $b_2^2 O_2^2$. To do so the cubic component was split off the remainder of the spin-Hamiltonian and referred to a coordinate system which was rotated from the principal axes of the rhombic component O_2^2. Thus the modified spin-Hamiltonian becomes:

$$H = \mu_B g\vec{H}\cdot\vec{S} + \frac{1}{3} b_2^O O_2^O + \frac{1}{3} b_2^2 O_2^2$$

$$+ \frac{1}{60} b_4^{O'} O_4^O + \frac{1}{60} b_4^2 O_4^2 + \frac{1}{60} c_4^O (O_4^O + 5\ O_4^4); \quad (IV-2)$$

where the "unbalanced" axial coefficient $b_4^{O'} = b_4^O - c_4^O$ and $c_4^O = \frac{b_4^4}{5}$.

A completely general spin-Hamiltonian would also have to allow for a possible rotation of $b_4^2 O_4^2$ with respect to $b_2^2 O_2^2$. However, in the present case it was extremely doubtful whether the orientation of $b_4^2 O_4^2$ could have been determined with any certainty because the parameter b_4^2 turned out to be of the same order of magnitude as the experimental error in the magnetic field measurements, i.e. approximately 10 Oe. For this reason it was felt that the results of the data analysis were not significantly affected by the assumption that the principal axes of O_4^2 and O_2^2 were coincident.

The coordinate axes X and Y were chosen to lie along the principal axes of O_2^2 because this component dominated all other non-axial terms. The axis triplet (X,Y,Z) was therefore orthogonal.

The analysis of the E.P.R. spectrum is greatly facilitated if one can use the magnetic quantum number M to label the magnetic energy levels and resonance transitions. To be able to do so the Zeeman term must dominate all other terms in the spin-Hamiltonian. It is evident from the regular rotational pattern of the E.P.R. spectrum that the Zeeman term is indeed predominant. The Zeeman term is diagonal with respect to the representation $|SM>$ if the Z-axis is parallel to the applied magnetic field. For a general magnetic field direction the coordinate system is therefore different from the one in which the operators O_n^m in (IV-2) have been defined. The form of the spin-Hamiltonian in the rotated coordinate system will therefore be different. From the transformation properties of the operator equivalents O_n^m, which are given by Vinokurov (1964), the spin-Hamiltonian for rotations of $\vec{H}$ about the a-axis can be shown to be

$$H = \mu_B gHS_z + \frac{1}{3}[a_2^0 O_2^0 + a_2^1 O_2^1 + a_2^2 O_2^2]$$

$$+ \frac{1}{60}[a_4^0 O_4^0 + a_4^1 O_4^1 + a_4^2 O_4^2 + a_4^3 O_4^3 + a_4^4 O_4^4]$$

$$+ \frac{1}{60}[d_4^0 O_4^4 + d_4^1 O_4^1 + d_4^2 O_4^2 + d_4^3 O_4^3 + d_4^4 O_4^4] \qquad (IV-3)$$

where
$$a_2^0 = \frac{1}{2}(b_2^2 \cos 2\phi - b_2^0)$$

$$a_2^1 = \mp 2ib_2^2 \sin 2\phi$$

$$a_2^2 = \frac{1}{2}(3b_2^0 + b_2^2 \cos 2\phi)$$

$$a_4^0 = \frac{1}{8}(3b_4^0 - b_4^2 \cos 2\phi)$$

$$a_4^1 = \pm \frac{i}{2} b_4^2 \sin 2\phi$$

$$a_4^2 = \frac{1}{2}(b_4^2 \cos 2\phi - 5b_4^0)$$

$$a_4^3 = \mp \frac{7}{2} i b_4^2 \sin 2\phi$$

$$a_4^4 = \frac{7}{8}(b_4^2 \cos 2\phi + 5b_4^0)$$

$$d_4^0 = \frac{c_4^0}{8} [3 + 5 \cos 4(\phi-\gamma)]$$

$$d_4^1 = \mp 5i\, c_4^0 \sin 4(\phi-\gamma)$$

$$d_4^2 = \frac{5}{2} c_4^0 [\cos 4(\phi-\gamma)-1]$$

$$d_4^3 = \mp 5i\, c_4^0 \sin 4(\phi-\gamma)$$

$$d_4^4 = \frac{5}{8} c_4^0 [7 + \cos 4(\phi-\gamma)]$$

$$(IV-4)$$

ϕ is the angle between the applied magnetic field and the X axis, and γ is the angle between the extrema of the cubic component $(O_4^0 + 5O_4^4)$ and the X axis. The upper and lower signs are taken respectively when computing the matrix elements $\langle M|O_n^m|M\pm m\rangle$.

Matrix elements of H were calculated between the magnetic substates of the $S = \frac{5}{2}$ manifold using the known matrix elements $\langle M|O_n^m|M\pm m\rangle$, which are related to the 3-j symbols. The resulting 6×6 Hermitian matrix was diagonalized to find the magnetic energy levels for a given applied magnetic field as a function of the seven parameters g, b_2^0, b_2^2, $b_4^{0'}$, b_4^2, c_4^0, and γ. Since the Zeeman term is the predominant term in the spin-

Hamiltonian the magnetic energy levels are ordered according
to the magnetic quantum number M such that

$$E(M,\vec{H}) > E(M-1,\vec{H})$$

where $E(M,\vec{H})$ is the eigenvalue of H for an applied magnetic
field $\vec{H}$ and M is a half-integer in the range $-\frac{3}{2} \le M \le \frac{5}{2}$.
This property of the eigenvalues enables one to identify the
pair of eigenvalues of H which are associated with a given
resonance line of the experimentally observed E.P.R. spectrum.
The values of the six spin-Hamiltonian parameters and the
angle γ were determined by minimizing the following function
in seven-dimensional parameter space:

$$F = \sum_{M=-\frac{3}{2}}^{M=\frac{5}{2}} \sum_{i} \{h\nu - [E(M,H(\theta_i,\phi_i,M)) - E(M-1,H(\theta_i,\phi_i,M))]\}^2 \quad (IV-5)$$

where $h\nu$ is the energy of the microwave quantum of frequency
ν and $H(\theta_i,\phi_i,M)$ is the resonant field value for the transition
$M-1 \to M$ which is observed in a direction defined by the polar
angles θ_i,ϕ_i.   The summation $\sum_i$ extends over all directions
θ_i,ϕ_i in which measurements were carried out.

A computer program was written to find the minimum
of the function F in parameter space. Use was made of the
subroutine FMCG of the IBM Scientific Subroutine Package.
This subroutine performed the calculation of an unrestrained
minimum of a function of several variables using conjugate
gradients. An initial estimate of the spin-Hamiltonian para-

meters had to be supplied as well as subprograms for calcu-
lating the value of F and the gradient of F at a given point
in parameter space. The initial estimates of the spin-
Hamiltonian parameters were found by using the first order per-
turbation formulas for the resonant magnetic field values.
The computer program for calculating F was broken down into
subprograms for carrying out the following functions:

1. Determination of the X and Y axes in the plane perpendicular
   to $\vec{a}$ by performing a Fourier analysis of the resonant mag-
   netic field values $H(90°, \phi_i, M)$ for $M = \pm \frac{5}{2}$ and $\pm \frac{3}{2}$. The
   rhombic components $b_2^2 O_2^2$ and $b_4^2 O_4^2$ are the only terms in the
   spin-Hamiltonian which give rise to a $\cos 2\phi$ component in
   the angular pattern of the E.P.R. spectrum. Since b_2^2 was
   two orders of magnitude larger than b_4^2 the angular position
   of the $\cos 2\phi$ component corresponded very nearly to the
   principal axes directions of the $b_2^2 O_2^2$ component which, in
   turn, determine the directions of the X and Y axes, as
   discussed above.

2. Calculation of the transformed spin-Hamiltonian in the
   rotated coordinate system in which the Z axis is parallel
   to the applied magnetic field.

3. Calculation of the energy matrix of the transformed spin-
   Hamiltonian between the magnetic substates of the $S = \frac{5}{2}$
   manifold.

Temperature °K	g	b_2^0(kOe)	b_2^2(kOe)	b_4^0(kOe)	b_4^2(kOe)	c_4^0(koe)	Rhombic angle	Cubic angle
4.2	2.008	1.611	1.084	0.029	−0.008	−0.011	86.6°	−29.9°
193	2.009	1.556	0.937	0.030	−0.004	−0.012	85.1°	−29.9°
256	2.008	1.529	0.868	0.027	−0.007	−0.011	84.4°	−30.4°
284	2.004	1.517	0.837	0.028	−0.007	−0.011	84.6°	−30.6°
324	2.003	1.497	0.787	0.028	−0.002	−0.011	84.2°	−30.6°
374	2.003	1.470	0.722	0.028	0.004	−0.011	83.3°	−30.7°
427	2.002	1.440	0.653	0.026	0.000	−0.010	81.9°	−30.6°
474	2.002	1.411	0.587	0.025	−0.008	−0.010	80.3°	−30.6°
522	2.002	1.378	0.517	0.026	−0.009	−0.010	78.4°	−31.2°
570	2.005	1.342	0.449	0.026	−0.004	−0.010	75.7°	−31.2°
622	2.008	1.300	0.377	0.026	0.002	−0.010	71.7°	−30.6
672	2.008	1.255	0.311	0.025	−0.001	−0.010	65.3°	−
724	2.008	1.200	0.261	0.025	−0.007	−0.009	54.4°	−
773	2.009	1.134	0.261	0.025	−0.006	−0.009	39.6°	−
803	2.009	1.079	0.302	0.024	−0.009	−0.009	29.2°	−
824	2.007	1.031	0.359	0.024	−0.007	−0.009	24.0°	−

(continued next page)

Temperature °K	g	b_2^0(kOe)	b_2^2(kOe)	b_4^0(kOe)	b_4^2(kOe)	c_4^0(kOe)	Rhombic angle	Cubic angle
843	2.008	0.957	0.455	0.026	−0.005	−0.011	16.4°	−
848	2.008	0.930	0.490	0.022	0.002	−0.009	14.4°	−
850	2.008	0.912	0.515	0.024	0.002	−0.009	13.3°	−
854	2.008	0.773	0.690	0.015	0.021	−0.005	0.0°	−
858	2.007	0.762	0.707	0.022	−0.007	−0.008	0.0°	−
863	2.007	0.758	0.713	0.022	−0.008	−0.008	0.3°	−

Table IV-1. The spin-Hamiltonian parameters as a function of temperature for Fe^{3+} in $AlPO_4$. The experimental errors are ±0.005 kOe. The rhombic angle is measured from the principal axis of $b_2^2 O_2^2$ (X-axis) to the c-axis. The cubic angle is measured from the principal axis of $c_4^0 O_4^4$ to the c-axis. Above 650°K the quality of the data fit to the spin-Hamiltonian parameters was no longer sensitive to changes in the cubic angle.

Temperature °C	g	b_2^0(kOe)	b_2^2(kOe)	b_4^0(kOe)	b_4^2(kOe)	c_4^0(kOe)	Rhombic angle	Cubic angle
12	2.003	0.737	1.000	0.035	−0.005	−0.017	86.5°	−15.7°
51	2.001	0.734	0.960	0.035	−0.002	−0.016	85.9°	−15.5°
100	2.003	0.730	0.904	0.035	0.002	−0.016	84.8°	−15.3°
150	2.004	0.724	0.845	0.034	−0.003	−0.016	83.6°	−15.2°
200	2.003	0.717	0.782	0.034	−0.002	−0.016	82.0°	−14.5°
250	2.003	0.708	0.718	0.033	0.004	−0.015	79.9°	−14.6°
300	2.004	0.696	0.651	0.033	−0.003	−0.015	77.4°	−15.1°
350	2.004	0.680	0.582	0.033	−0.005	−0.016	74.0°	−15.1°
400	2.007	0.661	0.512	0.032	0.000	−0.016	69.3°	−13.7°
450	2.000	0.637	0.451	0.033	0.002	−0.016	62.2°	−13.5°

Table IV-2. The spin-Hamiltonian parameters as a function of temperature for Fe^{3+} in quartz. The experimental errors are ±0.005 kOe. The rhombic angle is measured from the principal axis of $b_2^2 O_2^2$ (X-axis) to the c-axis. The cubic angle is measured from the principal axis of $c_4^0 O_4^4$ to the c-axis.
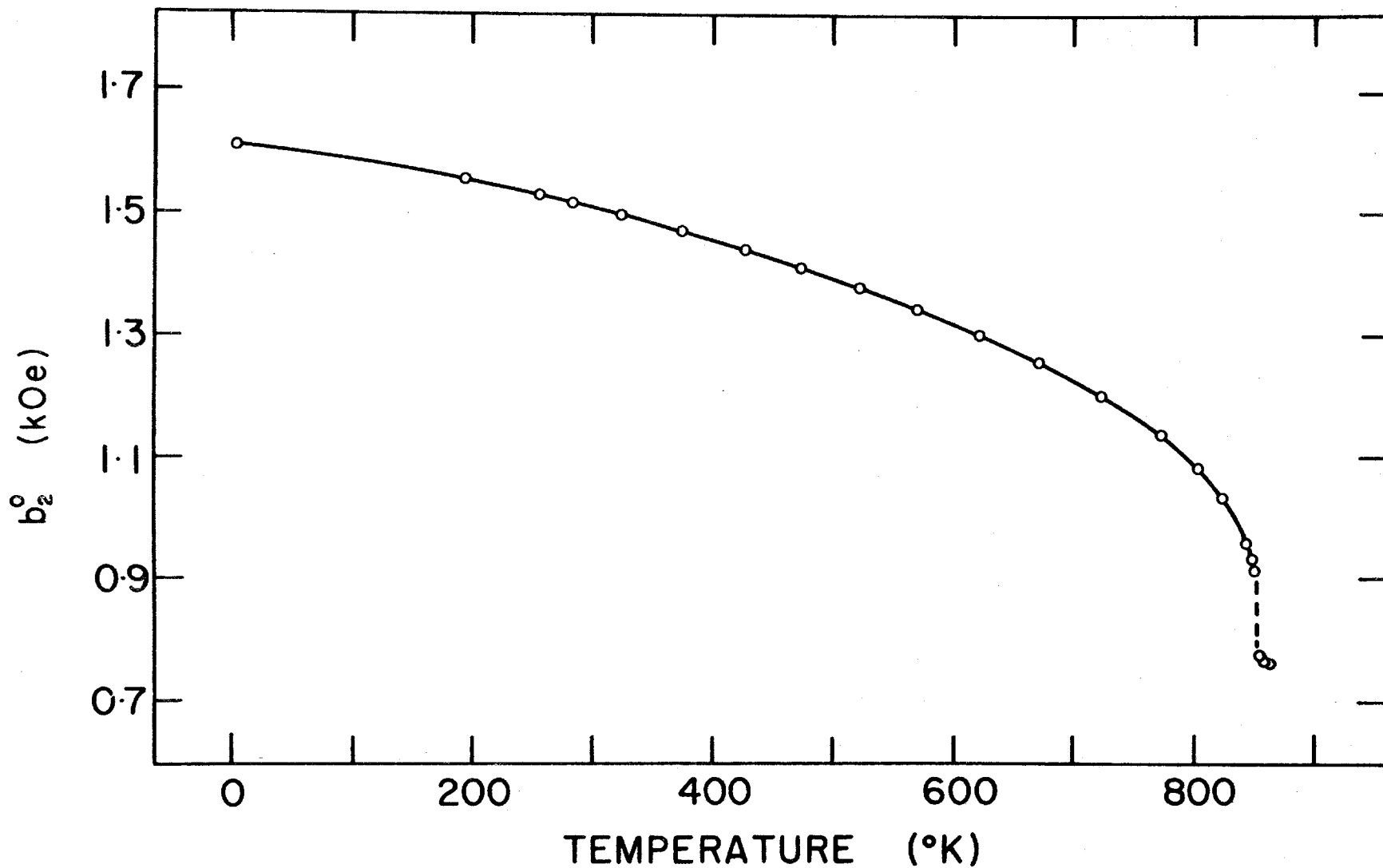
Figure IV-10. Axial splitting parameter b_2^o versus temperature for Fe^{3+} in $AlPO_4$
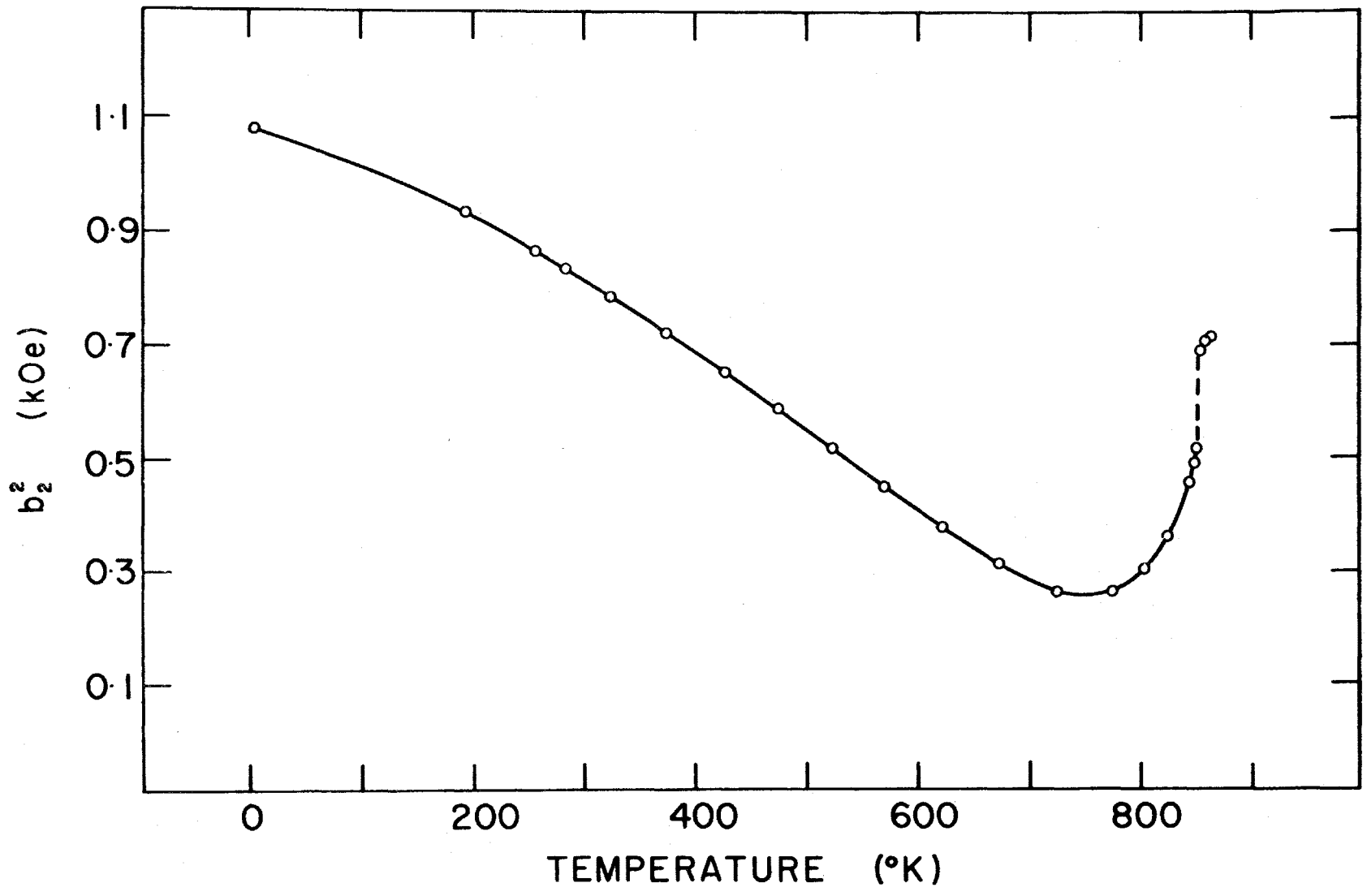
Figure IV-11. Rhombic splitting parameter b_2^2 versus temperature for Fe^{3+} in $AlPO_4$

Figure IV-12

Temperature dependence of the angle between the principal axis (X-axis) of $b_2^2 O_2^2$ and the c-axis for Fe^{3+} in $AlPO_4$.
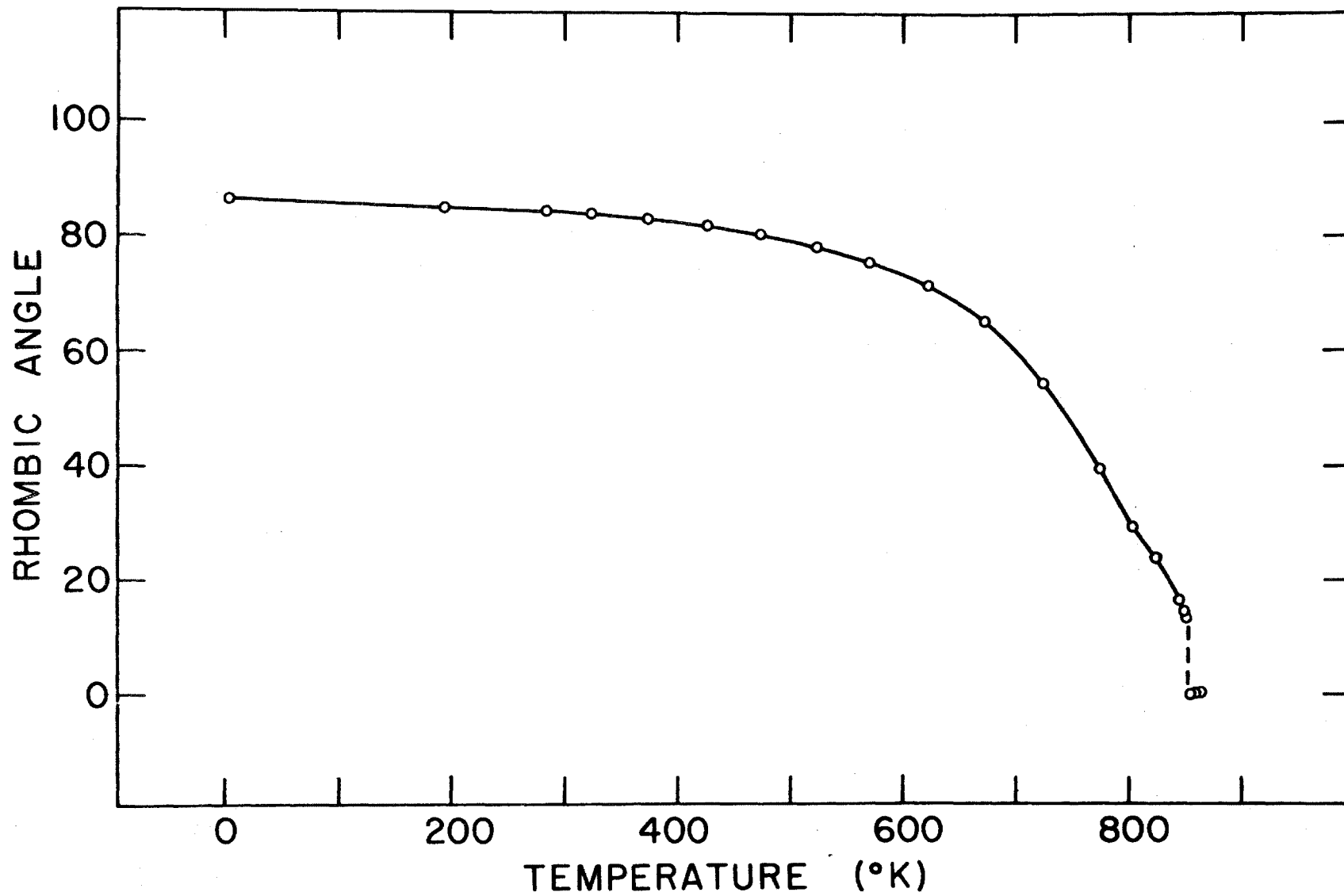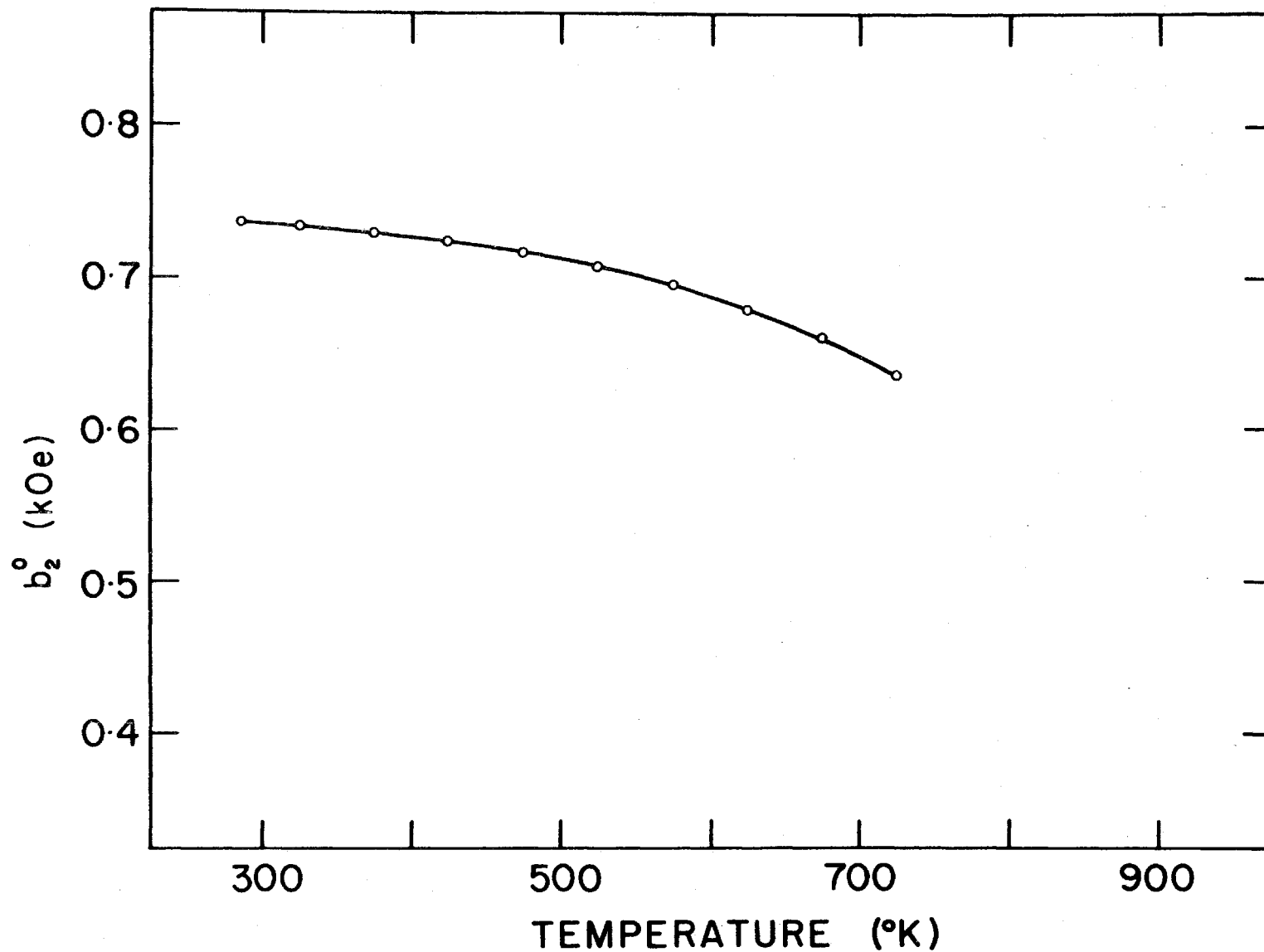
Figure IV-13. Axial splitting parameter b_2^0 versus temperature for Fe^{3+} in synthetic brown quartz
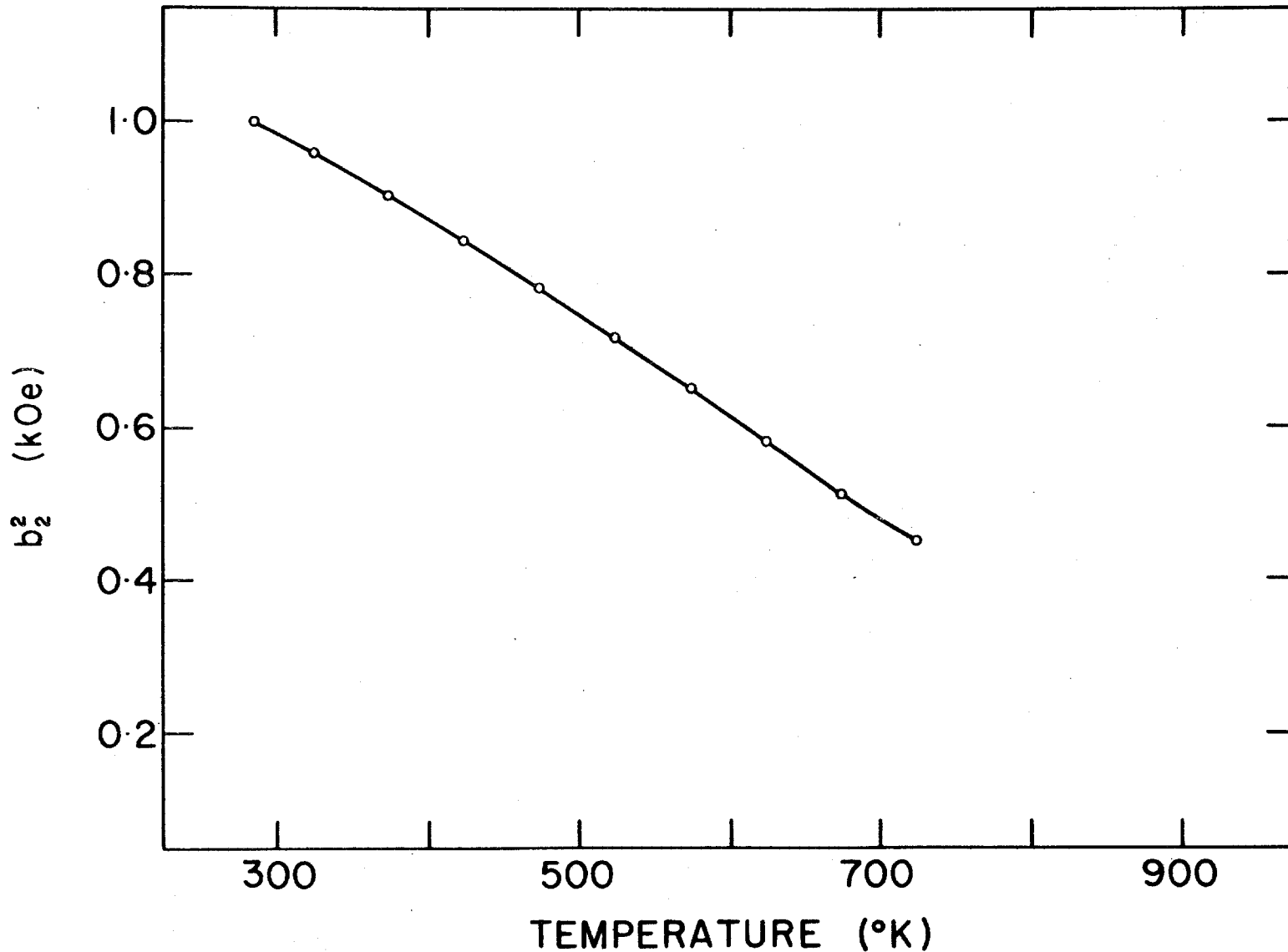
Figure IV-14.   Rhombic splitting parameter b_2^2 versus temperature for Fe^{3+} in synthetic brown quartz

Figure IV-15

Temperature dependence of the angle between the principal axis (X-axis) of $b_2^2 O_2^2$ and the c-axis for Fe^{3+} in synthetic brown quartz.
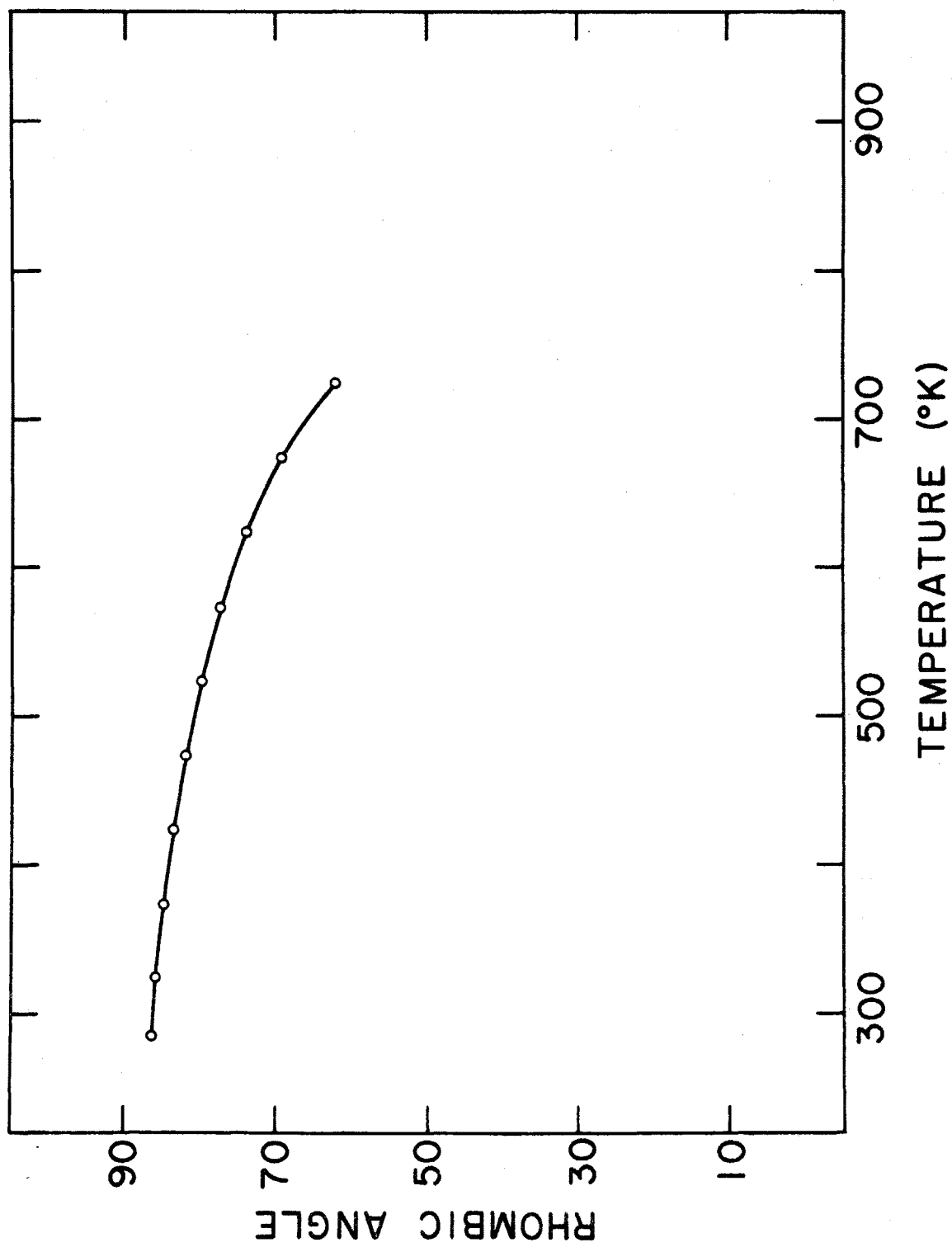
Figure IV-16

　　Calculated energy levels of Fe^{3+} in $AlPO_4$ at room temperature. The dashed lines indicate the $\Delta M = \pm 1$ transitions.
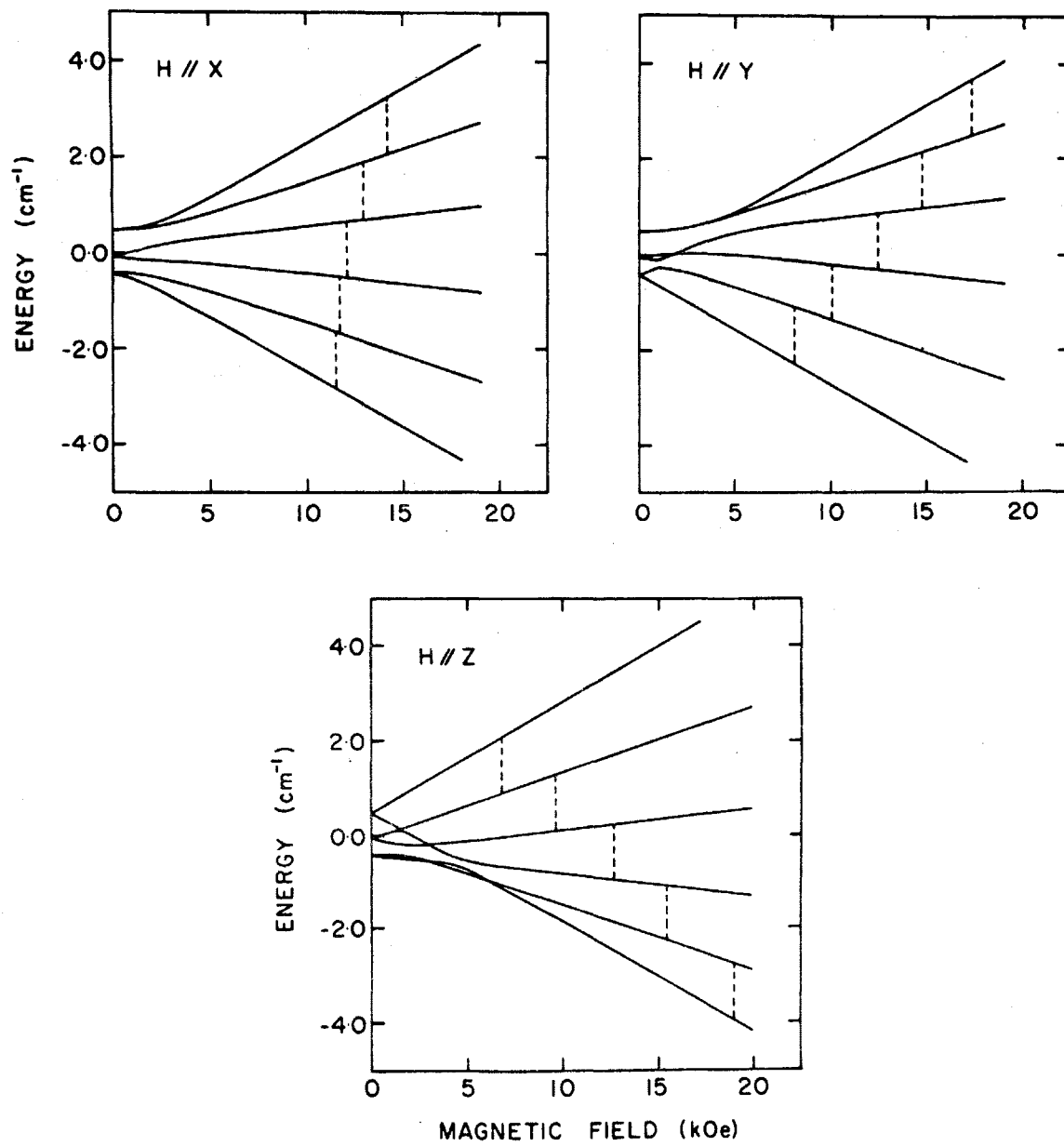
4. Calculation of the eigenvalues of the energy matrix by diagonalization.

5. Substitution of the eigenvalues into (IV-5) and evaluation of F.

The calculation of the gradient of F required no additional subprograms because the partial derivatives can be approximated by finite differences which only involve the evaluation of F.

Separate data fits were carried out for each temperature. A measure of the quality of the fit was provided by the value of the r.m.s. deviation which is defined as $\sigma \equiv \sqrt{\frac{F}{N}}$ where N is the number of data points. The value of σ was typically 5 Oe but never exceeded 10 Oe and occasionally was as low as 2 Oe. The values of the temperature-dependent parameters obtained in this way for $AlPO_4$ and quartz are shown in Tables (IV-1) and (IV-2) respectively. Plots of the values of b_2^0, b_2^2 and the angle between the X axis and the crystalline c-axis as a function of temperature are shown in Figures (IV-10) to (IV-15) for both $AlPO_4$ and quartz.

The experimentally determined room temperature values of the spin-Hamiltonian parameters for Fe^{3+} in $AlPO_4$ were substituted into the spin-Hamiltonian (IV-2) and the magnetic energy levels were calculated as a function of $\vec{H}$. The results for $\vec{H}||X$, $\vec{H}||Y$, and $\vec{H}||Z$ are shown in Fig. (IV-16). The dashed lines indicate the strong $\Delta M = \pm 1$ transitions. The zero field splittings were 0.544 and 0.360 cm^{-1}.
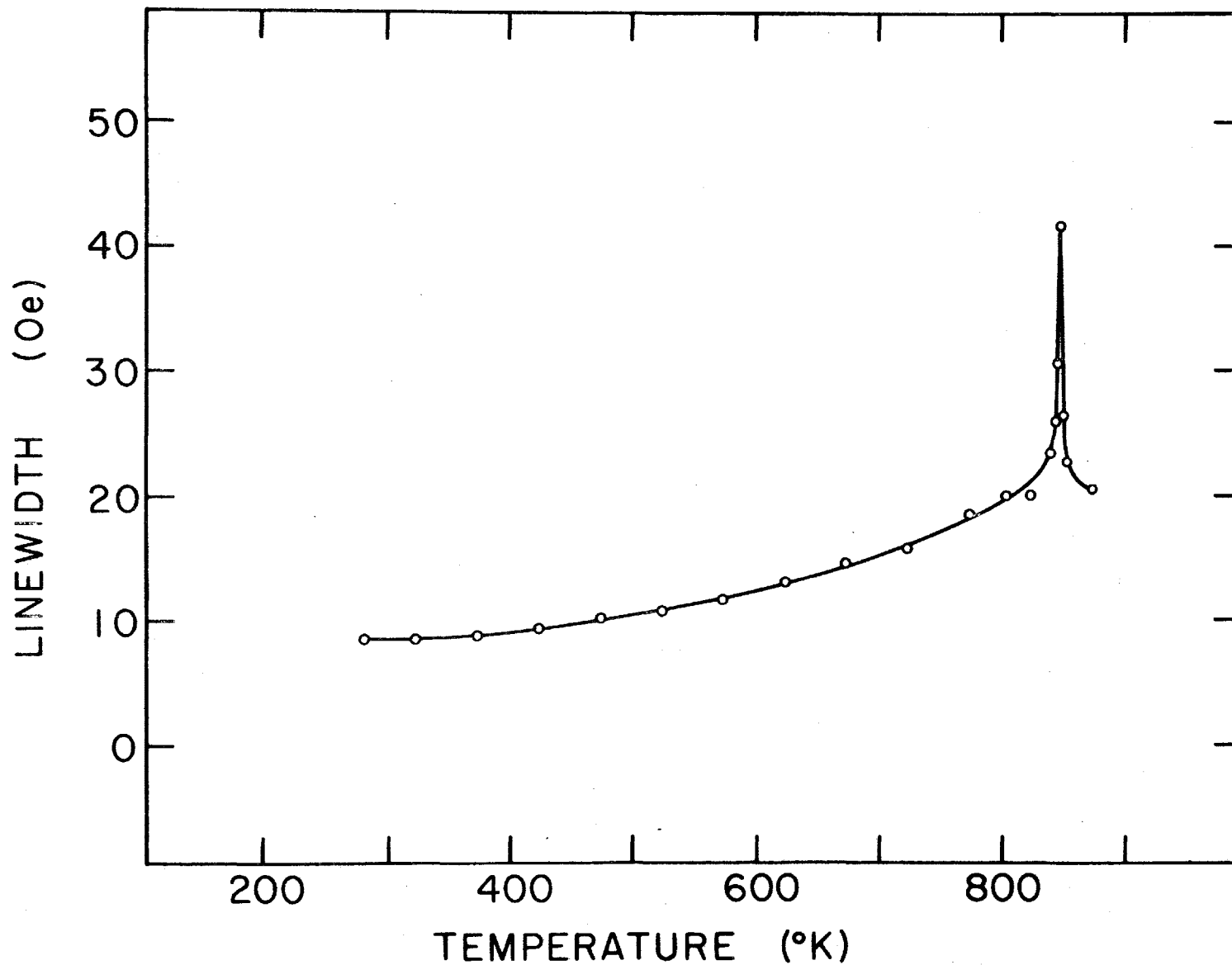
Figure IV-17. Linewidth versus temperature of the $1/2 \rightarrow 3/2$ transition of Fe^{3+} in $AlPO_4$
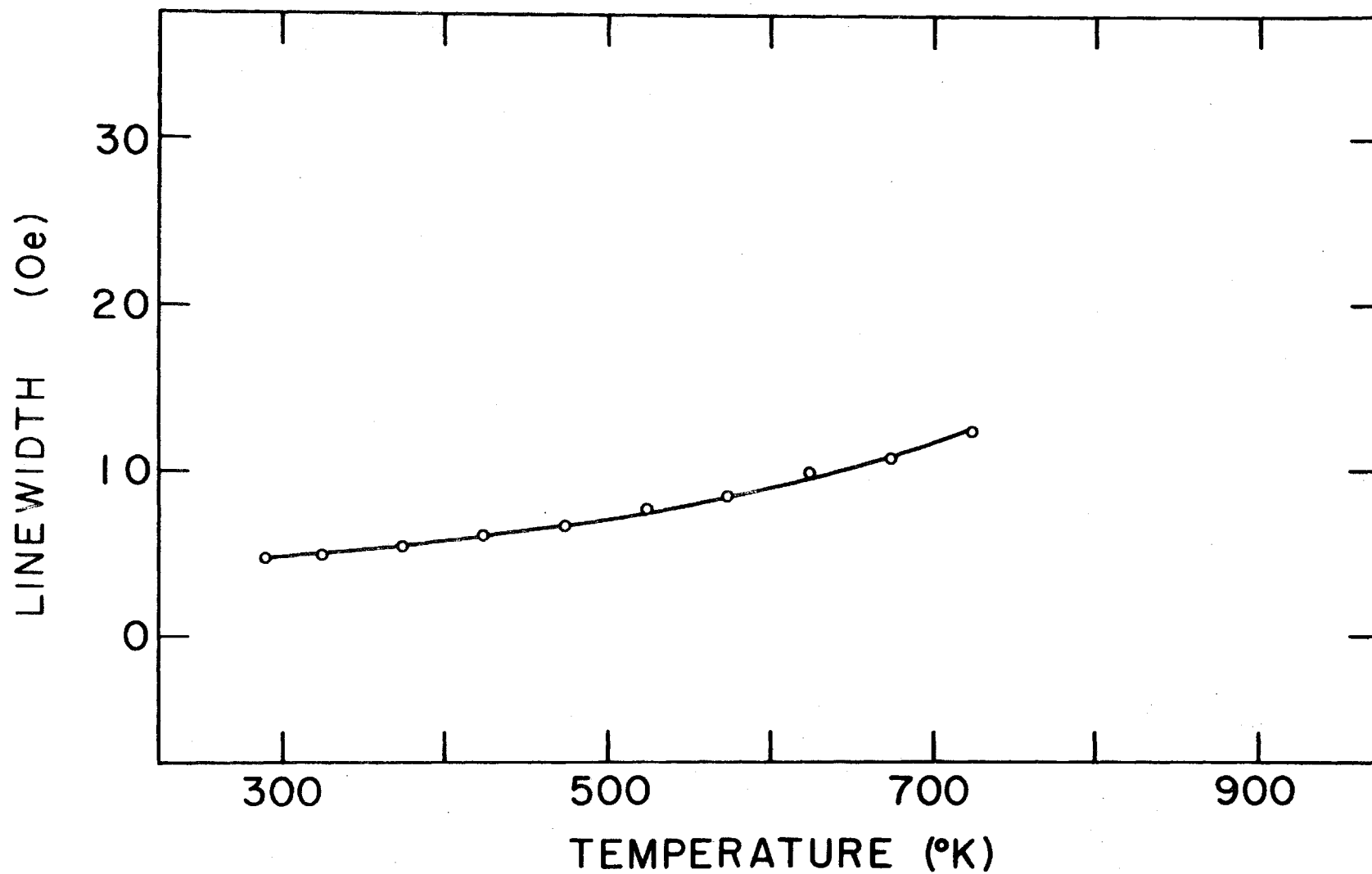
Figure IV-18. Linewidth versus temperature of the $1/2 \rightarrow 3/2$ transition of Fe^{3+}
in synthetic brown quartz

CHAPTER V

CALCULATION OF THE SPIN-HAMILTONIAN PARAMETERS

The theory presented in Chapter III was used to calculate the spin-Hamiltonian parameters of Fe^{3+} at the Al-site in $AlPO_4$. In particular, the D-tensor was calculated using the epxressions (III-26) to (III-29). The spin-Hamiltonian parameters b_2^0 and b_2^2 as well as the orientation of the second order rhombic component O_2^2 were obtained by diagonalization of the D-tensor as indicated in section (III-5).

1. The Point-Multipole Model

The major portion of this work dealt with the calculation of the crystal field coefficients at the Al-site. In previous crystal field calculations by Schwarzenbach (1966) it was shown that higher order multipoles of the O-ions contribute significantly to the electric field gradient at the Al-site. In particular, the contribution of the electric dipoles of the O-ions to the electric field gradient was larger than the contribution of the monopoles. The contribution of the quadrupoles of the stationary O-ions was considerably less than that of the monopoles and dipoles. It was therefore neglected in the present calculations. However, the quadrupolar contribution of the O-ions due to

their thermal motion became significant at higher temperatures and could not be neglected.

The crystal field coefficients are defined by equation (III-5) and were computed by direct lattice summation over discrete point charges. The following point-multipole model of the crystal lattice was constructed for the calculation of the crystal field coefficients as a function of temperature:

1. The monopole charges were assumed to be 3+ for the Al-ions, 5+ for the P-ions, and 2- for the O-ions. This assumption was based on the results of the structure refinement of $AlPO_4$ by Schwarzenbach (1966).

2. The electric dipoles of the O-ions were represented by two equal and opposite point charges which were located at two slightly separated positions along the oxygen metal-ion bonds. The magnitude of the dipoles was assumed to be temperature independent.

3. The thermally generated quadrupoles of the O-ions were represented by six point charges. Two point charges were placed on each of the three principal axes of the thermal ellipsoid, one on either side of the equilibrium oxygen position. The magnitude of the quadrupoles was calculated from the thermal ellipsoid data of quartz and was varied by changing the displacements of the point charges from the equilibrium oxygen sites.

The fractional co-ordinates of the atoms in the unit cell were calculated as a function of temperature using the temperature-dependent values of $\vec{\delta}$ and $\vec{\gamma}$ for quartz. The vector $\vec{\delta}(T)$ is the fractional displacement of each of the two inequivalent oxygen atoms from the midpoint between their two Dauphiné-related oxygen sites. Similarly, the vector $\vec{\gamma}(T)$ is the fractional displacement of the Al- and P-atoms from the midpoints between their respective Dauphiné-related sites. The absolute co-ordinates were obtained by multiplying the fractional co-ordinates with the temperature-dependent values of the lattice parameters $\underline{a}$ and $\underline{c}$ for $AlPO_4$ which were measured by Troccaz et al (1967).

2. Calculation of the Induced Electric Dipoles of the Oxygen Ions

The self-consistent electric fields $\vec{E}^{O(1)}$ and $\vec{E}^{O(2)}$ at the sites of the oxygen ions O(1) and O(2) respectively were calculated by solving the set of simultaneous linear equations (III-39). The coefficients of these equations consist of the components of the tensors $H^{O(1)O(1)}$, $H^{O(1)O(2)}$, and $H^{O(2)O(2)}$ and the vector components of the monopole electric fields $\vec{E}^{O(1)}(M)$ and $\vec{E}^{O(2)}(M)$. The H-tensors were computed by summing over oxygen atoms which were located inside a sphere of radius R about a given oxygen site. The convergence of the H-tensors was tested by carrying out the summations over spheres of successively increasing radii. R R was increased from 50 $\overset{\circ}{A}$ to 70 $\overset{\circ}{A}$ in steps of 2 $\overset{\circ}{A}$. The r.m.s.

fluctuations of the tensor components were less than 1% about their mean values. The following mean values were obtained:

$$H^{O(1)O(1)} = \begin{pmatrix} 52.773 & -20.923 & 56.640 \\ -20.927 & -49.597 & 57.381 \\ 56.652 & -57.380 & -46.785 \end{pmatrix} \times 10^{-3} \; \overset{\circ}{A}{}^3$$

$$H^{O(1)O(2)} = \begin{pmatrix} -40.297 & -99.771 & 0.259 \\ -155.537 & 182.220 & 47.421 \\ -70.273 & 65.514 & 89.517 \end{pmatrix} \times 10^{-3} \; \overset{\circ}{A}{}^3$$

$$H^{O(2)O(2)} = \begin{pmatrix} 25.622 & -9.151 & 32.679 \\ -9.151 & -90.635 & -75.990 \\ 32.679 & -75.990 & 16.527 \end{pmatrix} \times 10^{-3} \; \overset{\circ}{A}{}^3$$

The monopole electric fields $\vec{E}^{O(1)}(M)$ and $\vec{E}^{O(2)}(M)$ were calculated by direct lattice summation over all monopoles inside a sphere of radius R about an O(1)-site and an O(2)-site respectively, using equation (III-40). The electric fields were calculated for values of R which were successively increased from 70 $\overset{\circ}{A}$ to 90 $\overset{\circ}{A}$ in steps of 2 $\overset{\circ}{A}$. The r.m.s. deviation of the magnitude of the electric fields was approximately 2%. The results are listed in Table (V-1). Equations (III-39) were solved using the value $\alpha^{O(1)} = \alpha^{O(2)} = 0.33 \; \overset{\circ}{A}{}^3$. This value of the dipolar polarizability of the O-ions was reported by Schwarzenbach (1966). The

values of the self-consistent electric fields $\vec{E}^{O(1)}$ and $\vec{E}^{O(2)}$

are shown in Table (V-1).

Lattice Site	$E_1(M)$	$E_2(M)$	$E_3(M)$	$|\vec{E}(M)|$
O(1)	-1.595	-2.908	-3.907	5.468
O(2)	-4.095	3.102	0.518	5.550
	E_1	E_2	E_3	$|\vec{E}|$
O(1)	-1.719	-2.411	-3.677	4.721
O(2)	-3.902	2.854	0.260	4.841

Table (V-1): The components and magnitudes of the monopole
electric fields $\vec{E}(M)$ and the self-consistent
fields $\vec{E}$ at the lattice sites O(1) and O(2)
in units of 10^6 c.g.s. The co-ordinate axes
(1,2,3) are parallel to the axes $\vec{a}$, $\vec{c}\times\vec{a}$, and $\vec{c}$
respectively.

The self-consistent electric fields $\vec{E}^{O(1)}$ and $\vec{E}^{O(2)}$ turned

out to lie in the bonding planes defined by the bonds P-O(1)-Al

and P-O(2)-Al respectively. The deviation out of these bon-

ding planes was not more than 1°. It was therefore possible

to decompose the electric fields and hence the dipoles

vectorially along the directions of the oxygen metal-ion bonds

and to picture the deformation of the oxygen ion charge

cloud as a covalent bond. Equations (III-38) express the re-

lationship between the electric dipoles and the self-consistent electric fields at the oxygen sites. The electric dipoles were represented by equal and opposite point charges of magnitude Q. These point charges were placed along the O-Al and O-P bonds at distances $\pm\delta r_{O-Al}$ and $\pm\delta r_{O-P}$ from the equilibrium oxygen sites.

$$\delta r_{O-Al} = \frac{\alpha E_{O-Al}}{2\,Q} \quad \text{and} \quad \delta r_{O-P} = \frac{\alpha E_{O-P}}{2\,Q}$$

where E_{O-Al} and E_{O-P} are the components of the electric fields along the O-Al and O-P bond directions respectively and $\alpha = 0.33 \overset{\circ}{A}{}^3$. The value of Q had to be chosen large enough to ensure that the dipoles were sufficiently good approximations of point dipoles which are defined by $\vec{d} = \lim_{\substack{Q\to\infty \\ \delta r\to 0}} Q\cdot\vec{\delta}r$.

Clearly the values of the crystal field coefficients should not depend on the particular values chosen for Q and $|\vec{\delta}r|$ but only on their product. Successive evaluations of the crystal field coefficients for increasing values of Q showed that this situation obtained for $Q>3|e|$ and corresponding values of $|\vec{\delta}r| < \frac{1}{30} \overset{\circ}{A}$.

3. The Quadrupoles of the Oxygen Ions Due to Their Thermal Motion

An ion at a particular lattice site acquires, as a result of its thermal motion, an effective quadrupole moment $Q_{ii} = Z|e|(\overline{u_i^2} - \frac{1}{3} \sum_{k=1}^{3} \overline{u_k^2})$ where $i = 1,2,3$, Z is the ionic

charge in units of one electron charge $|e|$, and $\overline{u_1^2}$, $\overline{u_2^2}$, and $\overline{u_3^2}$ are the mean square displacements of the ion along the three principal axes of the thermal ellipsoid. The aggregate of point charges which was used to represent the charge distribution of an ion of monopole $Z|e|$ and thermal quadrupole Q_{ii} must satisfy the following conditions

$$\sum_k q(k) = Z|e| \qquad\qquad (V-1)$$

and

$$\sum_k q(k) [R_i^2(k) - \tfrac{1}{3}|\vec{R}(k)|^2] = Q_{ii} \qquad\qquad (V-2)$$

where the summation over k extends over all point charges of the aggregate and $q(k)$ and $\vec{R}(k) = [R_1(k), R_2(k), R_3(k)]$ are the charge and position vector of the k'th point charge of the aggregate. Equations (V-1) and (V-2) ensure that the aggregate of point charges has the correct monopole and quadrupole moments respectively. In the case of the O-ions $Z = 2$ and the values of $q(k)$ and $\vec{R}(k)$ which satisfied the conditions were as follows:

$$q(k) = -\tfrac{1}{3}|e| \quad ; \quad k = 1,2,\ldots.6$$

$$\vec{R}(1) = (\sqrt{3u_1^2},0,0) \quad ; \quad \vec{R}(4) = -(0,\sqrt{3u_2^2},0)$$

$$\vec{R}(2) = -(\sqrt{3u_1^2},0,0) \quad ; \quad \vec{R}(5) = (0,0,\sqrt{3u_3^2})$$

$$\vec{R}(3) = (0,\sqrt{3u_2^2},0) \quad ; \quad \vec{R}(6) = -(0,0,\sqrt{3u_3^2})$$

The position vectors $\vec{R}(k)$ are referred to the axes triplet

(p,q,r) and $\overline{u_1^2}$, $\overline{u_2^2}$, and $\overline{u_3^2}$ are the mean square amplitudes of the thermal vibrations of the O-atoms along the directions p, q, and r respectively

4. Calculation of the Crystal Field Coefficients

The crystal field coefficients B_{40}, B_{42} and B_{44} were calculated by substituting into equation (III-5) and summing over all point charges inside a sphere of radius 57 Å about a particular Al-site. The co-ordinates of the ions were expressed with respect to the co-ordinate axes (X,Y,Z), where Z was parallel to the a-axis, Y was parallel to the c-axis, and X was along the $\vec{c} \times \vec{a}$ direction. For each temperature at which the crystal field coefficients were evaluated, the atomic positions in the unit cell and the thermal quadrupoles of the O-ions were calculated before carrying out the lattice summation. The electric dipoles changed only insofar as the directions of the oxygen metal-ion bonds changed.

The convergence of the crystal field coefficients can be tested by calculating their values for several different radii. This, however, was not practical in the present case because of the long execution time of the computer program. In one case, however, the radius was increased from 57 Å to 59 Å and the resulting change in the values of the crystal field coefficients was about 2%. The values of the crystal field coefficients for different temperatures are shown in

Table (V-2).

Temp. °K	B_{40}	B_{42}	B_{44}	Angle Between Extremal Axis of B_{42} and X-Axis (Degrees)	Angle Between Extremal Axis of B_{44} and X-Axis (Degrees)
325	0.2218	0.024	0.2019	33.1	57.6
450	0.2179	0.023	0.1984	34.8	56.9
575	0.2149	0.023	0.1943	38.3	55.9
690	0.2133	0.021	0.1894	43.5	54.8
750	0.2112	0.020	0.1863	47.9	54.0
800	0.2111	0.018	0.1840	54.0	53.1
825	0.2107	0.017	0.1821	58.7	52.4
850	0.2089	0.017	0.1782	68.0	51.2
854	0.2030	0.025	0.1629	86.6	45.0

Table (V-2): Calculated values of the crystal field coefficients in units of $e^2/2a^5$ and the orientation of the B_{42} and B_{44} components in the (XY) plane.

5. The Spin-Hamiltonian Parameters by the Blume-Orbach Mechanism

The quantities $p_{\alpha\alpha}$, $p_{\alpha\beta}$, and $p_{\alpha\gamma}$ were calculated according to the expressions (III-30) by substituting the eigenvectors $(\alpha_i, \beta_i, \gamma_i)$ and the eigenvalues Δ_i of the matrix (III-14). The eigenvectors and eigenvalues are listed in Table (V-3) for $D_q = -900$, -1200, and -1600 cm^{-1}.

i	α_i	β_i	γ_i	$\Delta_i (cm^{-1})$ measured from $E(^6S)$
		$D_q = -900\ cm^{-1}$		
1	0.1006	0.9694	-0.2240	53030
2	0.7791	0.2168	0.5882	41180
3	0.6188	0.1154	0.7770	24990
		$D_q = -1200\ cm^{-1}$		
1	0.1804	0.9314	-0.3163	53920
2	0.7537	0.3375	0.5640	43130
3	0.6320	0.1367	0.7628	22150
		$D_q = -1600\ cm^{-1}$		
1	0.3021	0.8474	-0.4366	55790
2	0.7064	0.5065	0.4944	45120
3	0.6401	0.1591	0.7516	18300

Table (V-3): Values of α_i, β_i, γ_i, and Δ_i for Fe^{3+}

The expressions (III-26), (III-27), and (III-28) were evaluated using the values $\lambda = 440\ cm^{-1}$ (Kotani, 1949) and $<r^4> = 2.7894$ atomic units (Rado and Suhl, 1965). λ_{42} is the angle between the extremal axes of B_{42} and B_{44} and was
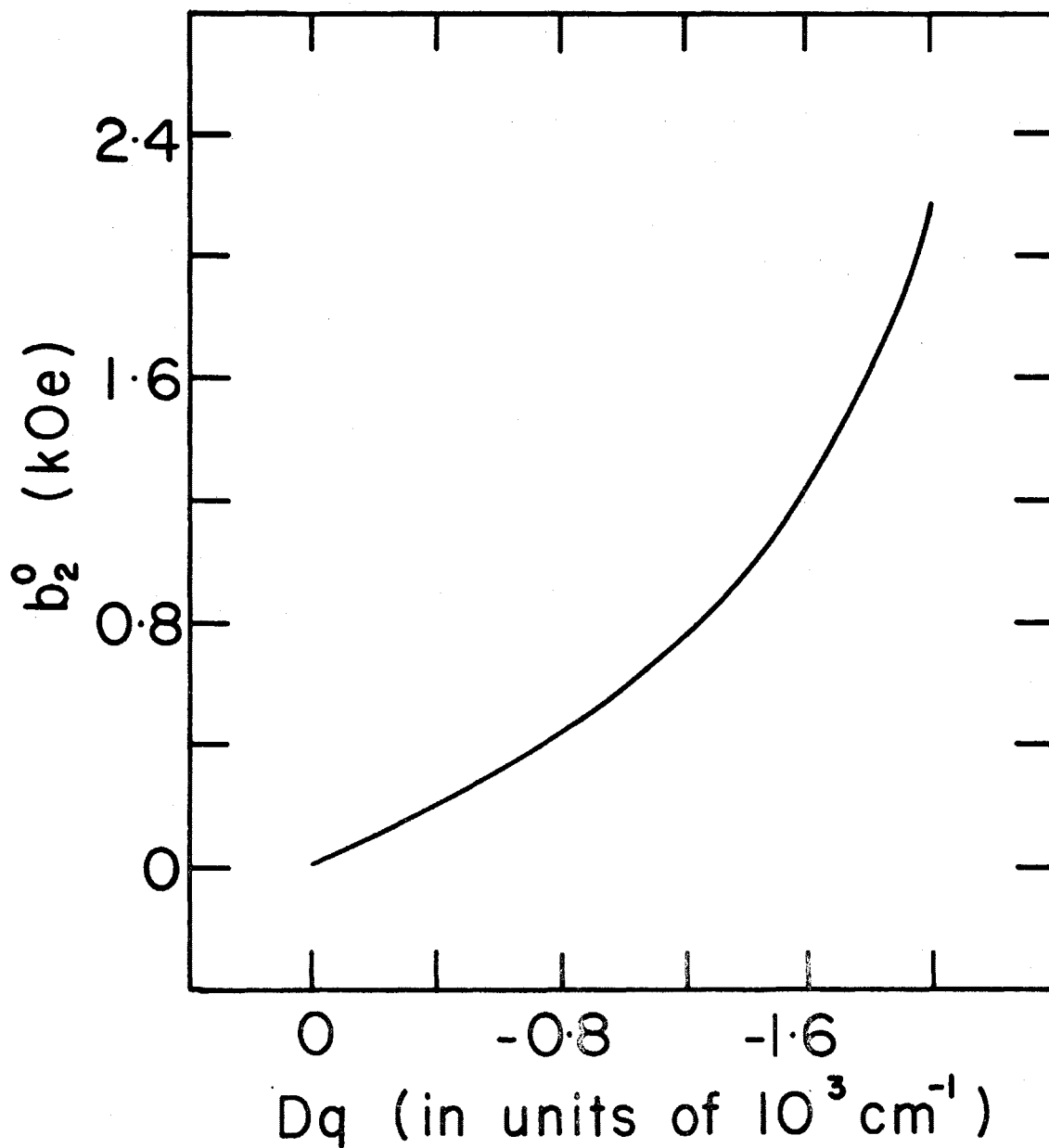
Figure V-1. Calculated axial parameter b_2^0 as a function of Dq
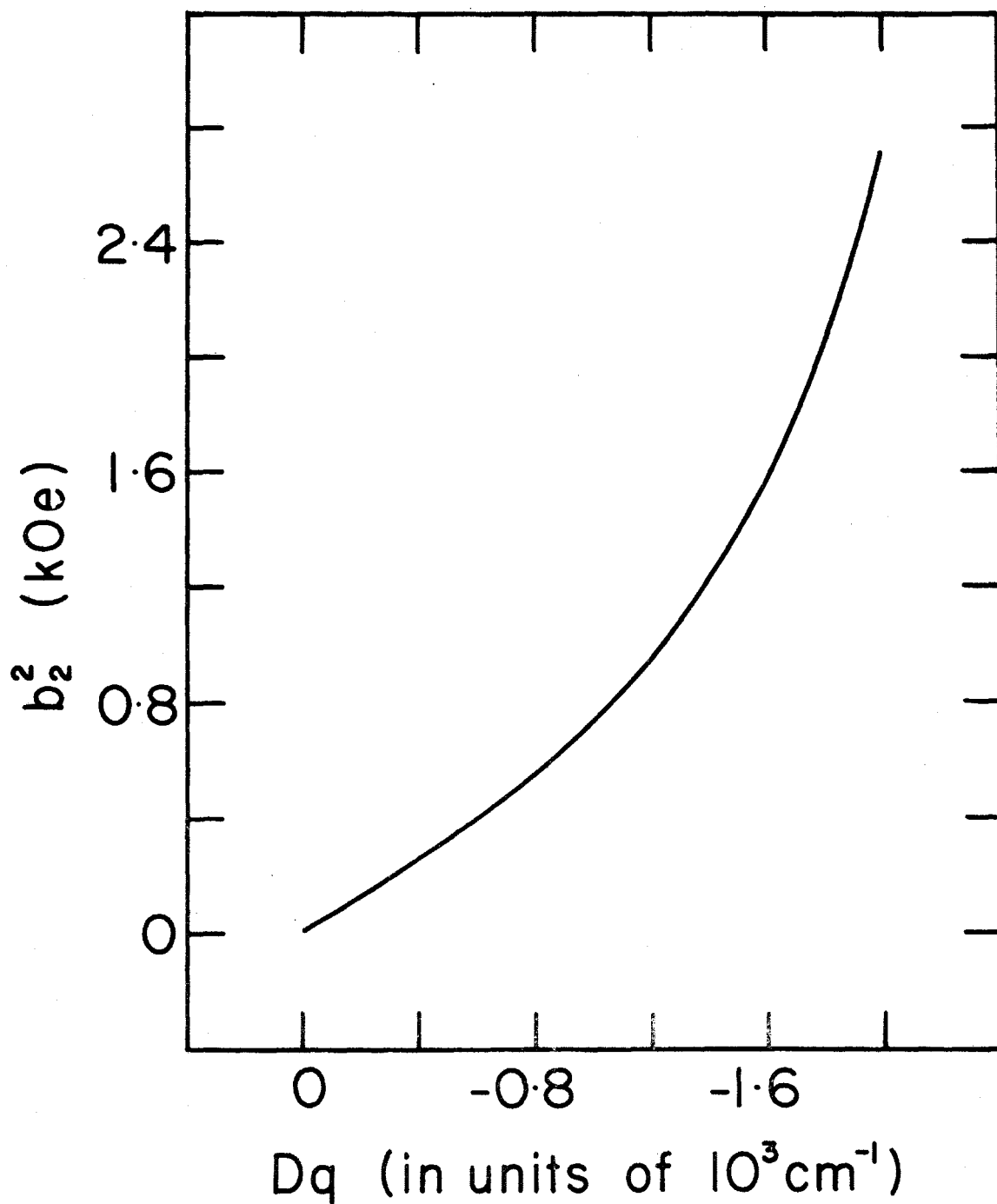
Figure V-2. Calculated rhombic parameter b_2^2 as a function of Dq

Figure V-3

Calculated and experimental values of
the axial parameter b_2^0 versus temperature for
Fe^{3+} in $AlPO_4$.
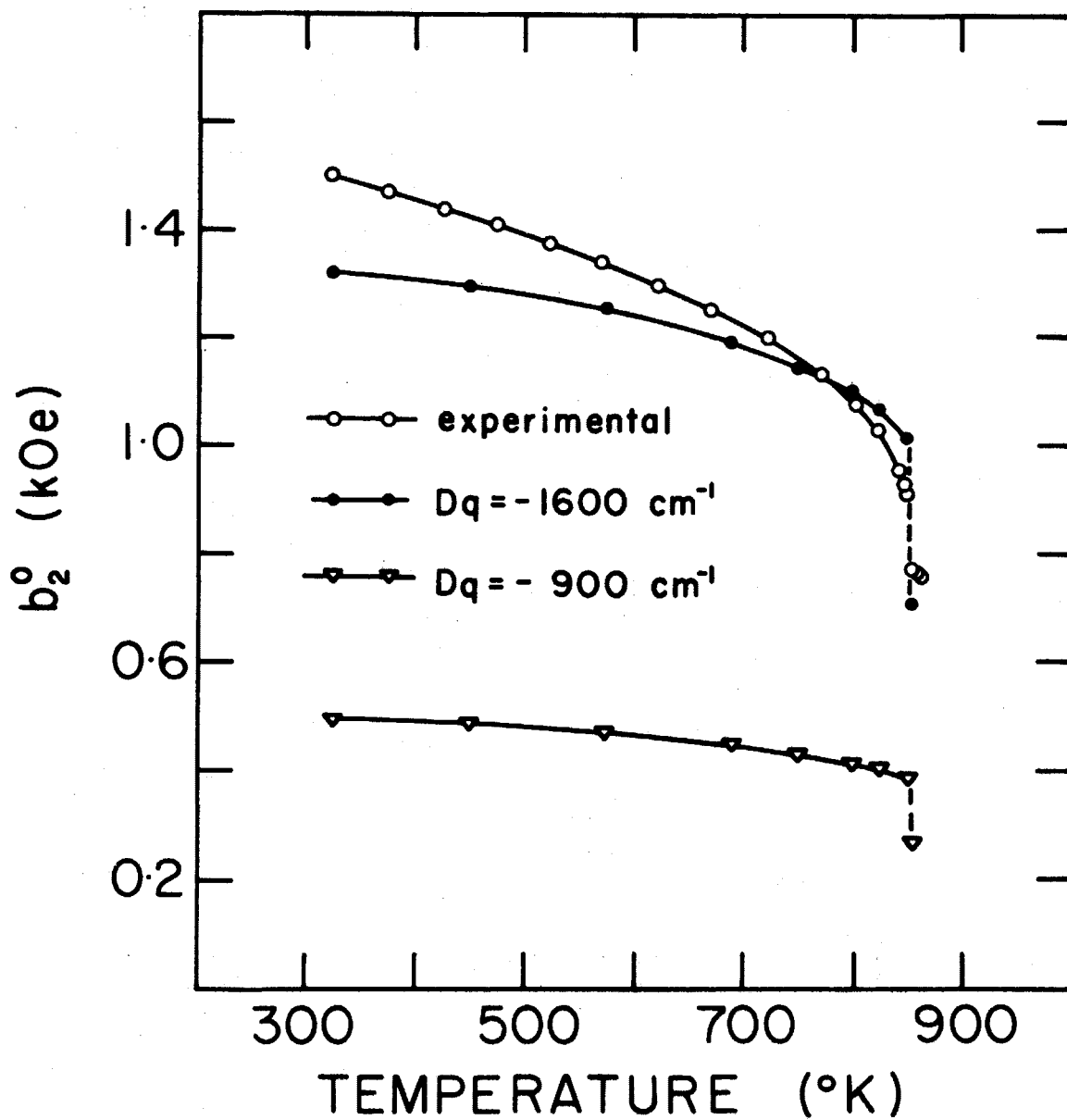
Figure V-4

Calculated and experimental values of
the rhombic parameter b_2^2 versus temperature for
Fe^{3+} in $AlPO_4$.
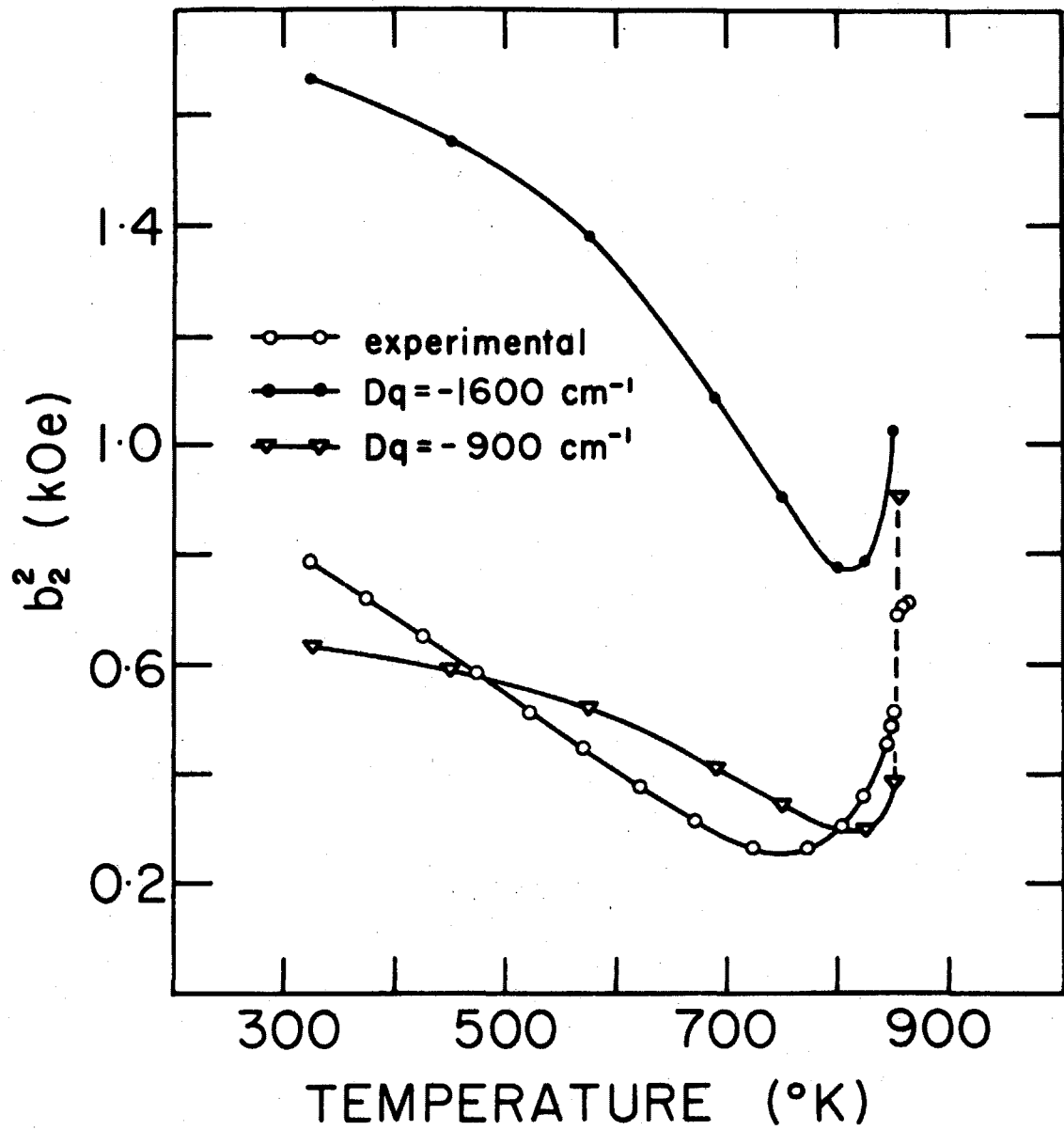
Figure V-5

Calculated angle between the principal axis (X-axis) of the rhombic component $b_2^2 O_2^2$ and the c-axis versus temperature for Fe^{3+} in $AlPO_4$.
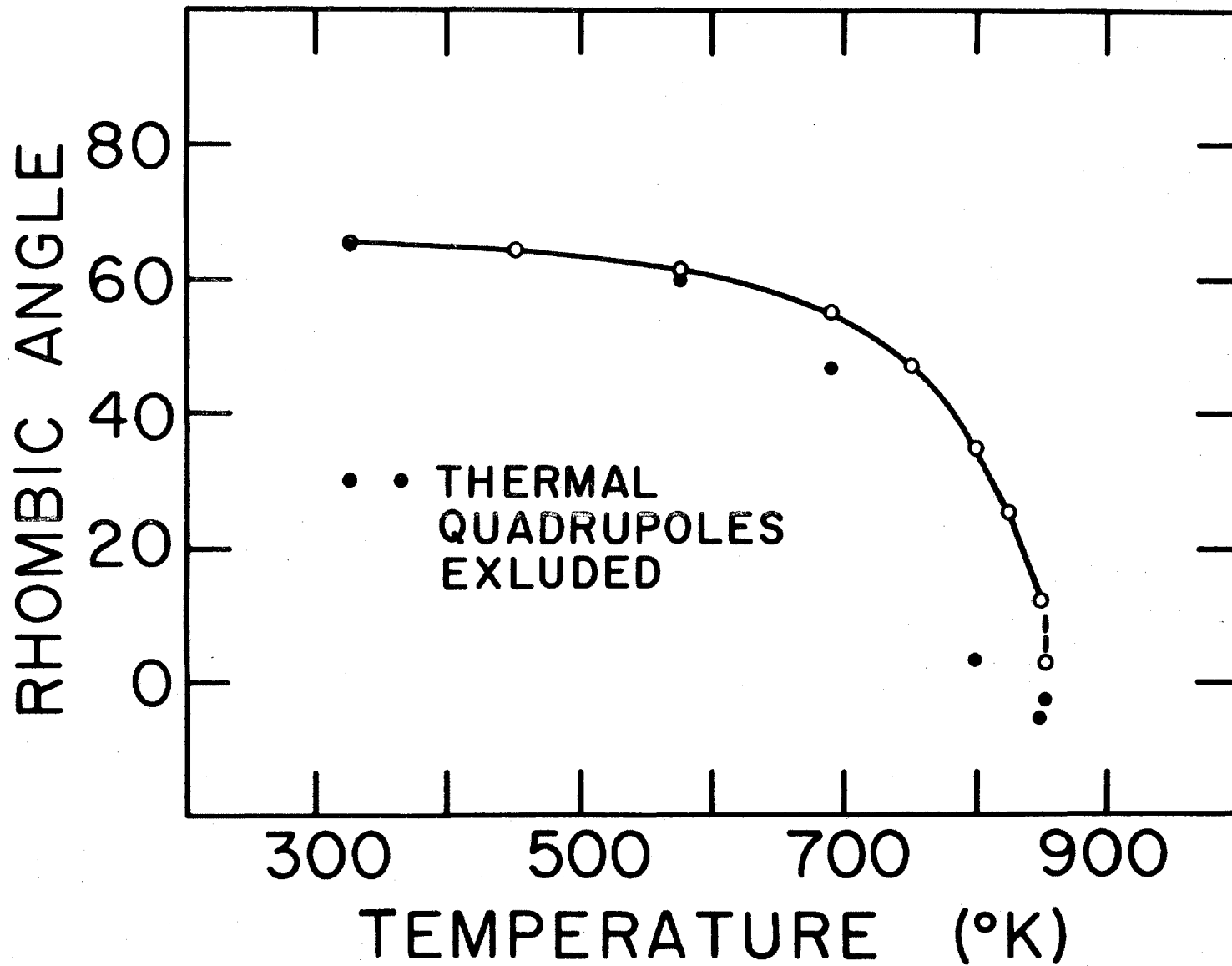
calculated from the values listed in Table (V-2). The D-tensor was diagonalized and the spin-Hamiltonian parameters were evaluated according to equations (III-31) and (III-32). The directions of the eigenvectors of the D-tensor define the extremal positions of the rhombic component $b_2^2 O_2^2$. Figures (V-1) and (V-2) show the values of b_2^0 and b_2^2 as a function of D_q. For this calculation the crystal field coefficients for T = 352°K were used. The orientation of the rhombic component $b_2^2 O_2^2$ showed no dependence on D_q.

By using the temperature-dependent values of the crystal field coefficients listed in Table (V-2) the parameters b_2^0 and b_2^2 and the orientation of O_2^2 in the (XY) plane were calculated as a function of temperature. Figures (V-3), (V-4), and (V-5) show the results for D_q = -900 and -1600 cm^{-1}. It is noted that an increase in $|D_q|$ does not only increase the values of b_2^0 and b_2^2 but also enhances their temperature variation.

It was found that there was no single value of D_q for which the experimental and calculated values of both b_2^0 and b_2^2 were in good quantitative agreement. If the value of D_q was chosen to give agreement with b_2^0, the resulting calculated value of b_2^2 turned out to be too large by approximately a factor of two. If, on the other hand, the value of D_q was chosen to give agreement with b_2^2, the calculated

Figure V-6

     Calculated axial parameter b_2^o versus
temperature for Fe^{3+} in $AlPO_4$. The solid and
dashed curves represent calculations with and
without the effects of thermal lattice vibrations
of the oxygen ions.
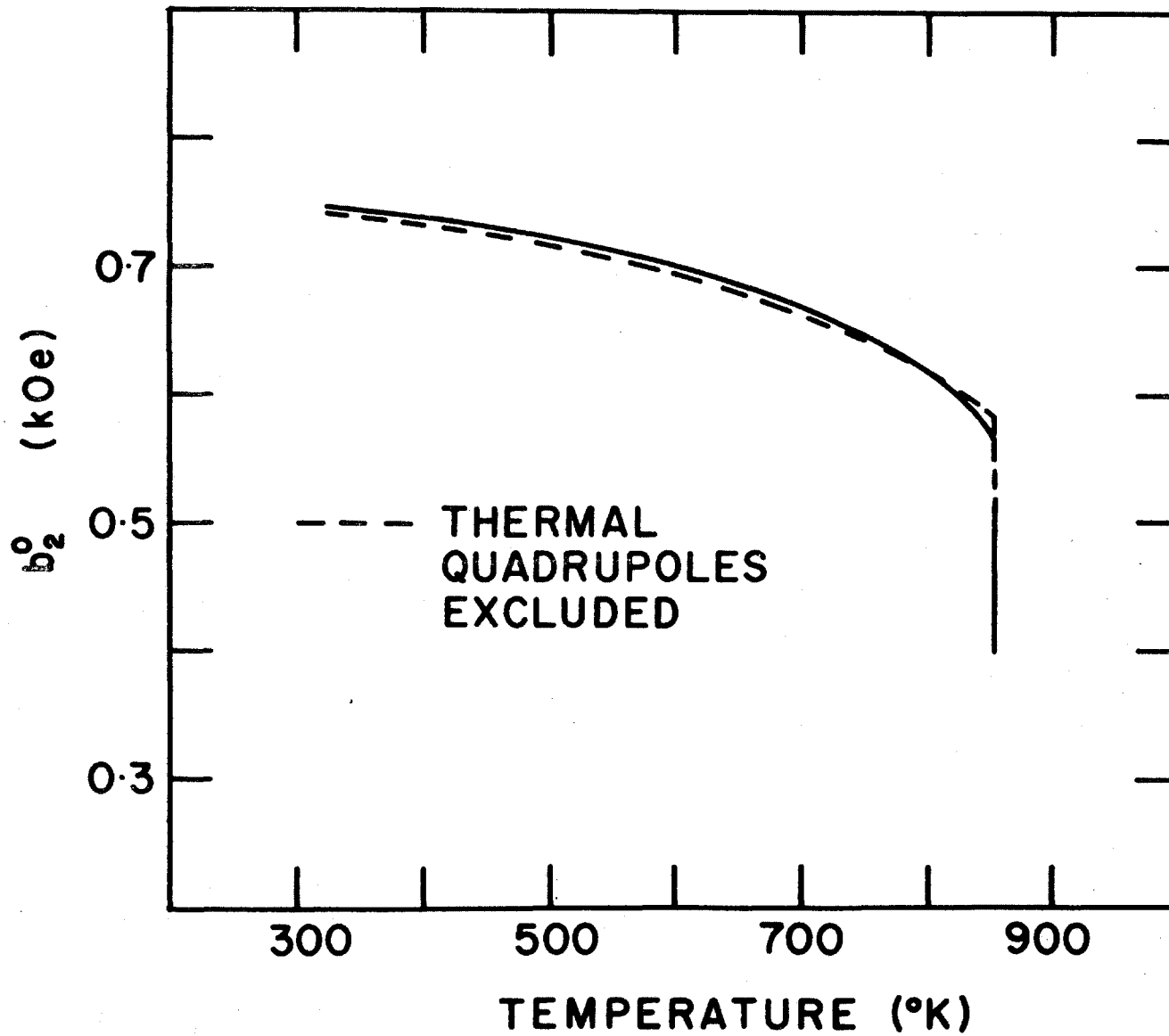
Figure V-7

    Calculated rhombic parameter b_2^2 versus temperature for Fe^{3+} in $AlPO_4$. The solid and dashed curves represent calculations with and without the effects of thermal lattice vibrations of the oxygen ions.
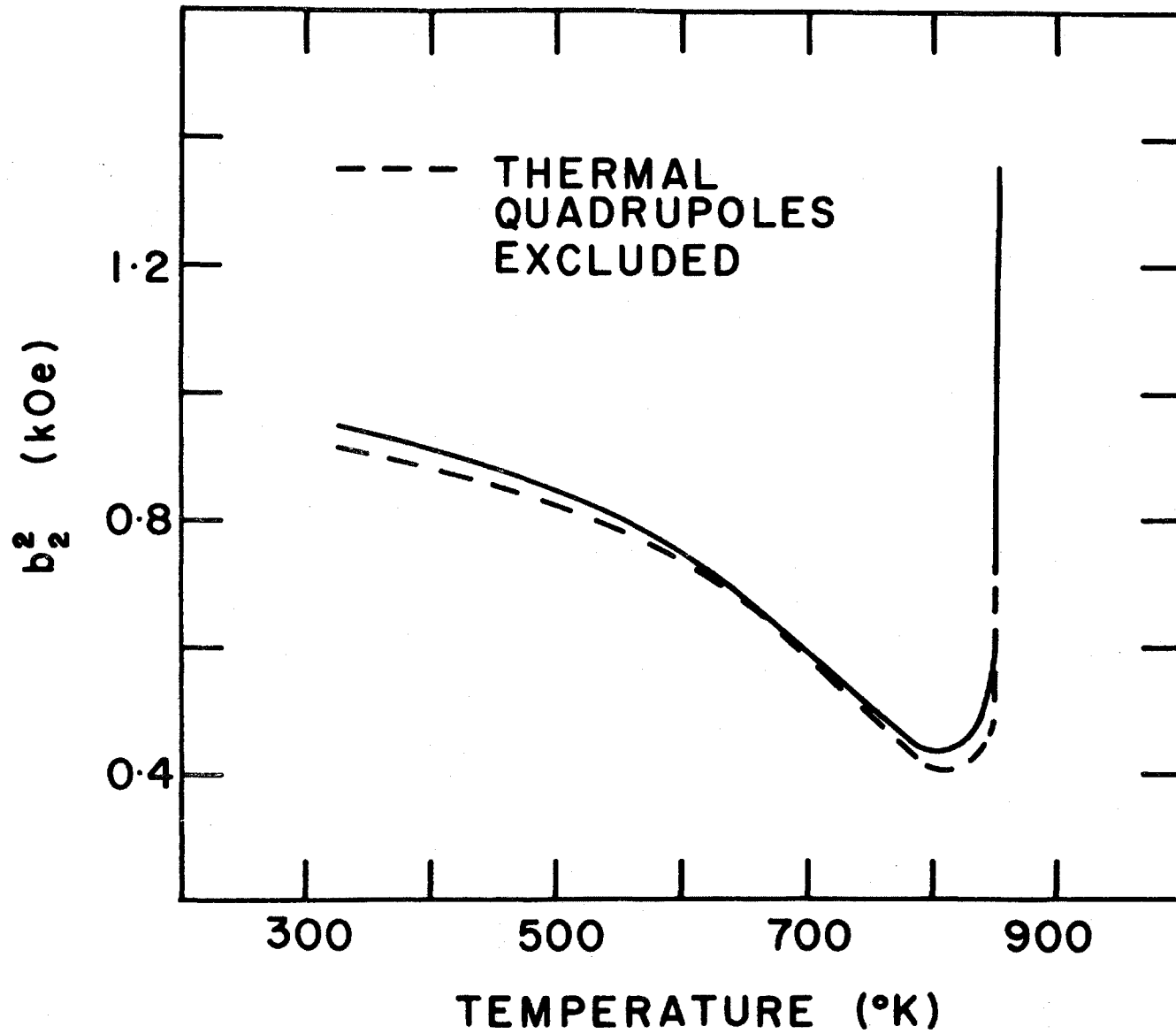
value of b_2^0 turned out to be too small by approximately a factor of two. For this reason the selection of the best value of D_q, solely on the basis of giving the optimum fit to the experimental data, was somewhat arbitrary.

The point-multipole model of the crystal lattice contained three temperature-dependent sets of quantities: The positions of the atoms in the unit cell, the size of the unit cell as expressed by the lattice parameters $\underline{a}$ and $\underline{c}$, and the size and orientation of the thermal quadrupoles of the O-ions. In discussions of the temperature dependence of the spin-Hamiltonian parameters it is customary to distinguish between implicit or thermal expansion effects and explicit or lattice vibrational effects. To obtain an estimate of the extent of explicit effects in the present calculations, the parameters b_2^0 and b_2^2 and the orientation of the extremal axes of the rhombic component $b_2^2 O_2^2$ were calculated as before except for setting the r.m.s. amplitudes identically equal to zero. The results of this calculation are shown in Figures (V-5), (V-6) and (V-7). It is evident that the calculated values of b_2^0 and b_2^2 are virtually unaffected by explicit effects except at the transition temperature. The orientation of the rhombic component $b_2^2 O_2^2$, however, is already markedly affected at temperatures 150°C below the transition.

6. Calculations of the Crystal Field Coefficients on the Basis of an Order-Disorder Model.

An order-disorder model was constructed in which the crystal lattice was made up of a statistical mixture of Dauphiné-related unit cells. The degree of disorder was specified by the value of the order parameter η,

$$\eta = \frac{W(\alpha_1) - W(\alpha_2)}{W(\alpha_1) + W(\alpha_2)}$$

where $W(\alpha_1)$ and $W(\alpha_2)$ are the probabilities that a unit cell was of Dauphiné type α_1 and α_2 respectively. As the value of η changes from 0 to 1 the lattice changes from a state of complete disorder, in which both types of unit cells occur with equal probability, to a state of complete order, in which each unit cell is of type α_1.

The crystal field coefficients B_{40}, B_{42} and B_{44} were calculated for six different values of η which ranged from 1.0 to 0.58. In this interval of η the values of the crystal field coefficients B'_{40} and B_{42} changed by approximately 20%. However, these changes appeared to be occasioned by random fluctuations due to the statistical nature of the disorder model, rather than by a variation in the order parameter η. Similarly, the angular position of the fourth order rhombic component B_{42} changed by approximately 3° in an apparently random fashion. An estimate of the statistical fluctuations

was obtained by evaluating the crystal field coefficients for constant η but for differently disordered lattices. Again, typical changes of approximately 20% were obtained for the crystal field coefficients. The rhombic angle, in one case, changed by 2.5°.

In summary, it may be concluded that any changes in the crystal field coefficients, whether they were caused by random fluctuations or by variations of η, were too small to reproduce the experimentally observed temperature variation. This is true in particular of the observed rotation of the rhombic component of the crystal field. Calculations based on an order-disorder model were therefore not pursued in more detail.

CHAPTER VI

DISCUSSION OF RESULTS

1. The Fe^{3+} Center in $AlPO_4$ and in Synthetic Brown Quartz

It was concluded above, on the basis of the observed symmetry of the rotational pattern of the E.P.R. spectra, that the Fe^{3+} ions in $AlPO_4$ occupy three crystallographically equivalent lattice sites. In the α-phase, these three sites must have the point symmetry C_2 and the twofold axis must be parallel to $\vec{a}$. In the β-phase, the point symmetry of the three occupied sites is D_2. This is evident from the fact that the magnetic axes in the plane perpendicular to the a-axis are pallel to $\vec{c}$ and $\vec{a} \times \vec{c}$ respectively. However, this information alone is not sufficient to make an unambiguous assignment of the occupied site. If one rules out the P-site on account of the pentavalency of P, there are still three possible sites left which could be occupied by the Fe^{3+} ions. These sites are the substitutional Al-site, the interstitial site on the twofold axis between two equivalent Al-atoms on the same a-axis, and the interstitial site on the twofold axis between two equivalent P-atoms on the same a-axis. Both interstitial sites lie near the 3_1 axis of the structure. If the separation between the interstitial site and the neigh-

bouring cation sites is to be maximized due to electrostatic repulsion, the maximum separation between the ferric ion at the interstitial site and the nearest Al^{3+} or P^{5+} will be $\frac{a}{2}$ ($= 2.47 \overset{\circ}{A}$). This separation is less than the sum of the metallic radii of aluminum and iron. One would therefore expect some metallic bonding between the Fe^{3+} and Al^{3+}. This would result in a serious deviation of the "ionic" state of Fe^{3+} from the assumed $^6S_{5/2}$ state. A further argument in favour of assigning the Fe^{3+} center to the substitutional Al-site can be made by applying a rule which has been formulated by Pauling (1948) and which is applicable to a large body of structures, particularly minerals. It states that "in a crystal containing different cations those with large valence and small coordination number tend not to share polyhedron elements with each other". If Fe^{3+} entered the interstitial site it would share a tetrahedral edge with an AlO_4 group whereas in the substitutional Al-site it would only share a corner. As for the interstitial site between two P-atoms, it would be even less favoured because of the larger formal charge on the P-ion.

The assignment of the substitutional Al-site is further supported by the considerable agreement between the experimental and theoretical temperature dependence of the second order orthorhombic component of the spin-Hamiltonian. This agreement was obtained for the substitutional Al-site.

Calculations of the crystal field coefficients as a function of temperature for the interstitial site between two equivalent Al-sites on the a-axis failed to give satisfactory agreement. In particular, the value obtained for B_{40} had the wrong sign and was larger by two orders of magnitude than the value obtained for the substitutional Al-site. The value of B_{42} was larger by one order of magnitude. The rotation of the rhombic component B_{42} between room temperature and the transition was less than 10° as compared to the observed value of 85°.

In the case of quartz the conclusions which can be drawn from the symmetry of the rotational pattern of the room temperature E.P.R. spectra are analogous to $AlPO_4$. The three occupied sites are equivalent and have point symmetry C_2 in the α-phase. There are three different sites in the quartz structure to which the Fe^{3+} center could be assigned. One of the interstitial sites in quartz is different from the interstitial sites in $AlPO_4$. It is the site on the two-fold axis between two equivalent Si-atoms on the same c-axis. The second interstitial site lies on the twofold axis between two equivalent Si-atoms on the same a-axis. The striking similarity between the rotational pattern of the E.P.R. spectra in quartz and in $AlPO_4$ strongly supports the view that the occupied sites in each system must correspond to one another structurally. This similarity is particularly apparent

with regard to the orientations of the principal axes.
Moreover, the temperature dependences of the spin-Hamiltonian
parameters as well as the rotation of the rhombic component
in the (XY) plane are qualitatively the same as in $AlPO_4$,
between room temperature and 450°C. If Fe^{3+} enters substitutionally into the Si-site a local charge compensator is
required. It must be displaced relative to the Fe^{3+} ion along
the a-axis, if this axis is to be preserved as a magnetic
axis, or it must be too far removed from the Fe^{3+} ion to
affect the E.P.R. spectrum.

2.   Mechanism of the α-β Phase Transformation

The experimentally observed temperature variation of
the spin-Hamiltonian parameters in $AlPO_4$ between room temperature and the transition temperature T_o include a rotation of
the second order rhombic component by 85° about the a-axis,
and a decrease of the axial parameter b_2^0 by a factor of two from
its room temperature value of 1.5 kOe to 0.77 kOe at T_o.
The rhombic parameter b_2^2 decreased from 0.8 kOe to a minimum
value of 0.25 kOe at 490°C and then increased again to a value
of 0.7 kOe at T_o.

It is interesting to compare these experimental results with the results of the calculations which were obtained
on the basis of the temperature-dependent point-multipole
model. Between room temperature and T_o the calculated angle

of rotation of the rhombic component about the a-axis was 63°.
The values of the spin-Hamiltonian parameters b_2^0 and b_2^2 de-
pended strongly on the particular choice of the value D_q. As
pointed out above, this choice is somewhat arbitrary insofar
as the value of D_q of -1600 cm^{-1} yielded good agreement for
b_2^0 but gave a value of b_2^2 which was approximately twice as
large as the experimental value. For D_q = -900 cm^{-1}, on
the other hand, reasonable agreement was obtained for b_2^2 but
the values of b_2^0 were only one third as large as the experi-
mental values. Typical values of D_q for trivalent ions of
the first transition series are 1700 cm^{-1} for octahedral co-
ordination (McClure, 1959). For tetrahedral co-ordination
the values are generally found to be half as large and of the
opposite sign. One therefore expects that D_q = -900 cm^{-1}
is a more reasonable value than D_q = -1600 cm^{-1}. For D_q = -900
cm^{-1} the axial parameter b_2^0 was found to decrease by a factor
of two from its room temperature value of 0.5 kOe to a value
of 0.27 kOe at T_o. The rhombic parameter b_2^2 decreased from
0.64 kOe at room temperature to a minimum value of 0.3 kOe
at 540°C and then rose sharply to a value of 0.9 kOe at T_o.

The large discrepancy between the experimental and
theoretical value of b_2^0 can be accounted for more easily than
a similar discrepancy in the value of b_2^2. The axial parameter
b_2^0 is determined to a large extent by the unbalanced axial field
coefficient $B_{40}' = B_{40} - \sqrt{\frac{14}{5}} B_{44}$. For an undistorted tetra-

hedral environment the terms B_{40} and $\sqrt{\frac{14}{5}} B_{44}$ are equal and B_{40}' vanishes. A finite value of B_{40}' can be regarded as a measure of the deviation from cubic point symmetry. In the case of the Al-site in $AlPO_4$ the nearest neighbour O-ions form a distorted tetrahedron. Additional distortion is introduced by the substitution of the Al^{3+} ion by Fe^{3+} since their ionic radii are 0.51 and 0.64 $\overset{o}{A}$ respectively. If the atomic co-ordinates of the undistorted lattice are used to calculate B_{40}', as was done in this work, a large error in the value of B_{40}' could result. Apart from this discrepancy, however, the temperature-dependent point multipole model reproduces the essential features of the experimentally observed temperature dependence of the second order orthorhombic component of the spin-Hamiltonian. This can be regarded as evidence that the Blume-Orbach mechanism is indeed predominant in the zero-field splitting of Fe^{3+} in $AlPO_4$.

Let us now examine to what extent the results of this E.P.R. study support the model of the α-β phase transformation proposed by Young, on the basis of x-ray studies. According to Young's description, all the atoms in the α-phase structure of quartz move in double minimum potentials. The positions of the minima are displaced from the high symmetry β-phase sites by ±δ(T) in the case of the oxygen atoms and by ±γ(T) in the case of the silicon atoms. The (+) and (-) signs refer to the two possible Dauphiné-twin configurations. Due to the

cooperative interaction in the α-phase the shape of the double
potential is strongly asymmetric. The ions of a particular
domain of the crystal therefore tend to be on the same side
of the double well, thus constituting one type of Dauphiné
twin. As the temperature is increased the values of $|\vec{\delta}|$ and
$|\vec{\gamma}|$ decrease continuously and reach approximately half their
room temperature values at a few degrees below T_o. At this
temperature a sharp increase in the oxygen thermal vibrational
amplitude perpendicular to the Si-O-Si plane occurs. As the
r.m.s. vibrational amplitude of the oxygen vibration along
the line joining the two Dauphiné-twin related sites (this
line is approximately perpendicular to the Si-O-Si plane)
exceeds the distance from the α-phase position to the β-phase
position, the α-β phase transformation takes place. At this
point the values of $|\vec{\delta}|$ and $|\vec{\gamma}|$ change discontinuously to
zero and the distinction between the twins is lost. The dis-
continuity of $|\vec{\delta}|$ and $|\vec{\gamma}|$ at the transition temperature
indicates that the transition is of first order. The double
minimum in the α-phase is replaced by a single minimum in the
β-phase. If the double minimum existed in the β-phase
the atoms would have to be statistically distributed between
the two minima for the structure to be consistent with the
β-phase space group $P6_2 22$. However, this situation would
imply an order-disorder phase transition which has been ruled
out by Young on the basis of temperature-dependent intensity

measurements of particular x-ray reflections.

The temperature-dependent measurements in $AlPO_4$ of b_2^0, b_2^2, and the principal axes directions of O_2^2 show a slight discontinuity at T_O. This discontinuity is most pronounced in the case of the principal axes rotation and is barely noticeable in the case of b_2^0 and b_2^2. However, there is no doubt that the spin-Hamiltonian parameters undergo a discontinuous change at T_O, because a jump in the resonant field of the $\frac{1}{2} \rightarrow \frac{3}{2}$ transition, which amounted to 300 Oe for $H||\vec{a}$, was observed at the transition temperature. The α-β phase transformation in $AlPO_4$ is therefore a first order transformation.

Information about the temperature dependence of the positions of the atoms in the unit cell can only be gained indirectly via the temperature-dependent calculations of the spin-Hamiltonian parameters. The temperature dependence of the calculated values of b_2^0 and b_2^2 is almost solely the result of changing the positions of the atoms. Agreement between the theoretical and experimental temperature dependence therefore confirms that the atoms in the $AlPO_4$ lattice move toward their β-phase positions approximately as described by the temperature-dependent vectors $\vec{\delta}(T)$ and $\vec{\gamma}(T)$. It therefore follows that the results of this study are consistent with Young's conclusion that the atoms in the β-phase occupy single minimum potentials.

Unfortunately the present study does not provide
any conclusive evidence about the role of the temperature-
dependent r.m.s. amplitudes of the thermal vibrations of the
O-atoms in the phase transition. However, it is evident from
Fig. (V-5) that significant improvement between the calculated
and experimentally observed rotation of the principal axes
was obtained when the thermal quadrupoles of the O-atoms were
taken into account.

3. Temperature Dependence of the Linewidth

The width of the E.P.R. lines shows a sharp increase
in the vicinity of the transition temperature. The linewidth
is generally attributed to either inhomogeneous or life-time
broadening. Although it was not possible to distinguish
between the two mechanisms experimentally, one can propose
a phenomenological model to explain the temperature dependence
of the linewidth in terms of inhomogeneous broadening.

The configurational potential energy of the crystal as
a whole has the shape of a double minimum in the α-phase. As
the transition temperature is approached the separation between
the two potential minima decreases in accordance with the
experimentally measured values of $|\vec{\delta}|$ and $|\vec{\gamma}|$. This leads
necessarily to a reshaping of the double minimum potential:
The height of the barrier separating the two minima decreases
and the curvature of the minima is substantially reduced.

This manifests itself in the gradual shift of the 207 cm^{-1} Raman line and several zone-center accoustic modes to lower frequencies (Shapiro and Cummins, 1968).

The associated increase in anharmonicity reveals itself in the sharp increase of the lattice parameters (Troccaz et al, 1967). The equilibrium positions of the atoms become less sharply defined and spacial fluctuations of the equilibrium sites are likely to occur. These fluctuations consist of small static displacements of the atoms from their mean equilibrium positions. These displacements occur along the line joining two Dauphiné-related sites but remain on one side of the double minimum potential. Instead of a well-defined crystal field at each site occupied by an Fe^{3+} ion there is now a distribution of space-fluctuating crystal fields which give rise to inhomogeneous broadening. This line broadening is therefore a measure of the short range disorder within a domain of a given Dauphiné configuration. At the transition temperature the two minima coalesce and a single minimum is formed. The single minimum quickly loses its anharmonic character and decreases in width. The equilibrium sites become sharply defined and the inhomogeneous broadening disappears. This interpretation is consistent with the sharp increase in the frequencies of the Brillouin lines observed by Shapiro and Cummins in quartz.

If the increase in linewidth is to be explained in terms of life-time broadening one has to propose a mechanism which leads to a sharp increase in the rate of transition

between the magnetic substates. This would most likely involve a Raman process because at high temperatures the Raman process dominates the direct or one-phonon relaxation process. The increase in the relaxation rate could be the result of an increase in the phonon density of states at a point where the energy difference between two branches of the phonon spectrum is of the order of Larmor frequency which in this case is approximately one wave number.

CHAPTER VII

SUMMARY OF RESULTS AND CONCLUSIONS

The second order orthorhombic component of the spin-Hamiltonian of Fe^{3+} in $AlPO_4$ was found to be strongly temperature-dependent, particularly in the region of the α-β phase transformation. Between $4.2°K$ and the transformation temperature of $854°K$ the axial parameter b_2^0 decreased from 1.611 ± 0.005 kOe to 0.773 ± 0.005 kOe. In the same temperature interval the principal axes of the rhombic component $b_2^2O_2^2$ rotated by $87°$ about the a-axis bringing the principal axes in the high temperature β-phase into coincidence with $\vec{c}$ and $\pm(\vec{c}\times\vec{a})$ respectively. The spin-Hamiltonian analysis was carried out in a co-ordinate system in which the X and Y axes coincided with the principal axes of $b_2^2O_2^2$ at all temperatures. In this co-ordinate system the rhombic parameter b_2^2 decreased from 1.084 ± 0.005 kOe at $4.2°K$ to a minimum value of 0.250 ± 0.005 kOe at $450°C$ and then increased to 0.690 ± 0.005 kOe in the β-phase. The temperature variation of the second order orthorhombic component was continuous up to the transformation temperature. At this temperature the parameters b_2^0 and b_2^2, and the principal axes of the rhombic component underwent a discontinuous change. This indicates that the α-β phase transformation in $AlPO_4$ is of first order with

130

the transformation temperature close to the critical
temperature.

It follows from the high symmetry directions of the
magnetic axes in the β-phase that the time-averaged positions
of the atoms are the high-symmetry β-phase sites. The
picture of a statically disordered β-phase structure, con-
sisting of a statistical distribution of the atoms among
Dauphiné twin-related sites, must therefore be ruled out.
However, the E.P.R. results are consistent with a dynamically
disordered structure in which rapid tunnelling between
Dauphiné twin-related sites takes place. In this case the
sharp drop in line width just above the transformation tem-
perature has to be attributed to motional narrowing.

More definitive conclusions about the transformation
mechanism can only be drawn from the conbined results of
experiment and a theoretical calculation of the second order
orthorhombic component of the spin-Hamiltonian of Fe^{3+} in $AlPO_4$.
This calculation was based on a temperature-dependent point-
multipole model in which use was made of the results of a
temperature-dependent x-ray study by Young of the α-β phase
transformation in quartz. Thus, the assumption was made that
the temperature dependences of the fractional co-ordinates
and r.m.s. amplitudes of the thermal vibrations of the atoms
in $AlPO_4$ were essentially the same as in quartz. The validity

of this assumption has yet to be checked by x-ray experiments. The theoretical values of the parameters b_2^o and b_2^2 as well as the angular position of the rhombic axes were in satisfactory agreement with experiment. One is therefore led to conclude that the temperature-dependent point multipole model represents a reasonable approximation of the actual phase transformation mechanism. In particular, the atoms are gradually displaced towards the high symmetry β-phase positions and the final portion of the displacement occurs discontinuously. Furthermore, the occupied site of the Fe^{3+} center, which cannot be assigned on the basis of the symmetry of the Fe^{3+} spectrum alone, is most likely the Al-site. The assumption that the zero field splitting of Fe^{3+} in $AlPO_4$ was predominantly due to the Blume-Orbach mechanism was also borne out.

Further experimental work to check the validity of the point-multipole model would be desirable. In particular, the electric field gradient at the Al-site in $AlPO_4$ could be measured as a function of temperature using the nuclear magnetic resonance of Al^{27}. At present only room temperature measurements of the electric field gradient are available (Schwarzenbach, 1966).

The temperature variation of the spin-Hamiltonian parameters were reversible but irreversible Dauphiné twinning occurred when the temperature of the specimen was raised

above the transformation temperature. A hysteresis in the transformation temperature, which was reported by Troccaz et al (1967), was absent in the present study.

The width of the E.P.R. lines as a function of temperature showed a sharp peak which was centered at the transformation temperature. Although possible mechanisms for this increase in line width were proposed, further experimental work is needed to determine whether inhomogeneous or life-time broadening is responsible.

The temperature-dependent measurements in iron-doped synthetic brown quartz are less conclusive than the $AlPO_4$ measurements because the Fe^{3+} center becomes unstable at higher temperatures so that reliable measurements could only be taken up to 450°C. The irreversible destruction of the Fe^{3+} center is believed to be due to the formation of ferrous silicate in which the oxidation state of Fe^{3+} changes to Fe^{2+} (Lehmann and Moore, 1965). The temperature dependence of the Fe^{3+} spectrum in synthetic brown quartz can be accounted for in terms of the temperature-dependent changes of the second order orthorhombic component of the spin-Hamiltonian. The temperature dependence of this component was remarkably similar to the temperature dependence observed in $AlPO_4$. One is therefore led to conclude that a displacive type mechanism is also operative in the α-β phase transformation in quartz. Moreover, the analogous orientation of the magnetic axes of the Fe^{3+} center

in both systems suggests that the Fe^{3+} ions enter the
Si-site substitutionally.

BIBLIOGRAPHY

Amit, D. J., J. Phys. Chem. Solids 31, 1099 (1970).

Arnold,H., Z.Kristallogr. 121, 145 (1965).

Axe, J.D. and Shirane, G., Phys. Rev. B 1, 342 (1970).

Blume, M. and Orbach, R.,Phys. Rev. 127, 1587 (1962).

Brumberger, H., Claffey, W., Alexandropoulos, N.G. and
   Hakim, D., Phys. Rev. Letters 22, 537 (1969).

Cady, W. G., Piezoelectricity (McGraw Hill, New York, 1946).

Chambers, J.G., Datars, W.R. and CAlvo, C., J. Chem. Phys.
   41, 806 (1964).

Cochran, W., Acta Cryst. 7, 503 (1954).

Cochran, W.,Advanc. Phys. 9, 387 (1960).

Corbridge, D.E.C., Pearson, M.S. and Walling, C. Topics in
   Phosphorous Chemistry, Vol. 3 (Interscience Publishers,
   New York, 1966), p. 195.

Cowley, R. A., Phil. Mag. 11, 673 (1965).

Frondel, C., Am. Mineralogist 30, 447 (1945).

Ginzburg, V. L., Soviet Physics - Solid State 2, 1824 (1960).

Heller, P., Rep. Prog. Phys. 30, 731 (1967).

Henning, J.C.M., Liebertz, J. and van Stapele, R.P., J.
   Phys. Chem. Solids 28, 1109 (1967).

Ishida, K. and Honjo, G., J. Phys. Soc. Japan 26, 1558 (1969).

Kleinman, D. A. and Spitzer, W. G., Phys. Rev. 125, 16 (1962).

Kotani, M., J. Phys.Soc. Japan $\underline{4}$, 293 (1949).

Landau, L.D. and Lifshitz, E.M. Statistical Physics (Pergamon Press Ltd., London, 1958).

Lehmann, G. and Moore, W.J., J. Chem. Phys. $\underline{44}$, 1741 (1966).

Matarrese, L. M., Wells, J.S. and Peterson, R.L., J. Chem. Phys. $\underline{50}$, 2350 (1969).

McClure, D.S., Solid State Physics, Vol. 9 (Academic Press Inc., New York, 1959).

Moore, C.E., Atomic Energy Levels (U.S. Dept. of Commerce, National Bureau of Standards, 1962).

Mosesman, M.A. and Pitzer, K.S., Am. Chem. Soc. J. $\underline{63}$, 2348 (1941).

Mueller, K.A., Berlinger, W. and Waldner, F., Phys. Rev. Letters $\underline{21}$, 814 (1968).

O'Leary, G.P. and Wheeler, R.G., Phys. Rev. B $\underline{1}$, 4409 (1970).

Orbach, R., Proc. Roy. Soc. (London) $\underline{A264}$, 458 (1961).

Pake, G.E., Paramagnetic Resonance (W. A. Benjamin Inc., New York, 1962).

Pauling, L., The Nature of the Chemical Bond, 2nd Edition (Cornell University Press, Ithaca, N.Y. 1948).

Rado, G. T. and Suhl, H., Magnetism, Vol. II, Part A (Academic Press, New York, 1965) p. 291.

Schwarzenbach, D., Z. Kristallogr. $\underline{123}$, 11 (1966).

Schwarzenbach, D., Z. Kristallogr. $\underline{123}$, 422 (1966).

Scott, J.F., Phys. Rev. Letters $\underline{21}$, 907 (1968).

Scott, J.F., Phys. Rev. Letters 24, 1107 (1970).

Shafer, E.C. and Roy, R. Z., Z. Phys. Chem. N.F., 11, 30 (1957).

Shapiro, S. M., O'Shea, D.C. and Cummins, H.Z., Phys. Rev. Letters 19, 361 (1957).

Shapiro, S.M. and Cummins, H.Z., Phys. Rev. Letters 21, 1578 (1968).

Shapiro, S.M., Ph.D. Thesis, John Hopkins University, Baltimore, Md., 1969.

Sharma, R. R., Das, T.P. and Orbach, R., Phys. Rev. 149, 257 (1966).

Sharma, R.R., Das, T.P. and Orbach, R., Phys. Rev. 155, 338 (1967).

Sharma, R. R., Das, T.P. and Orbach, R., Phys. Rev. 171, 378 (1968).

Sinel'nikov, N.N., Doklady Akad. Nauk SSSR 92, 369 (1953).

Smith, G.S. and Alexander, L.E., Acta Cryst. 16, 462 (1963).

Stanley, J.M., Ind. Engng. Chem. 46, 1684 (1954).

Troccaz, M., Berger, C., Richard, M. and Eyraud, L., Bull. Soc. Chim. de France 11, 4256 (1967).

Vinokurov, V.M., Zaripov, M.M. and Stepanov, V.G., Soviet Physics - Solid State, 6, 870 (1964).

Walsh, W.M. Jr., Jeener, J. and Bloembergen, N., Phys. Rev. 139, A1338 (1965).

Wannier, G. H., Elements of Solid State Theory (Cambridge
    University Press, 1960).

Watanabe, H., Operator Methods in Ligand Field Theory
    (Prentice-Hall, Inc., Englewood Cliffs, N.J.,1966).

Young, R.A., Mechanism of the Phase Transition in Quartz,
    Solid State Sciences Division, Air Force Office of
    Scientific Research, Washington 25, D.C. (1962).